RHODES UNIVERSITY
Where leaders learn

Development of Styrene based Imprinted Sorbents for Selective Clean-up of Metalloporphyrins in Organic Media

A thesis submitted to Rhodes University in fulfilment of the requirements for the degree of Doctor of Philosophy (Science)

Kehinde Nurudeen Awokoya

Supervised by

Professor Nelson Torto

Co-supervised by

Professor Zenixole Tshentu

November 2013

Dedication

There ain't nobody deserving this dedication but the Almighty God- I AM WHO I AM.

Acknowledgements

This thesis would not have been possible without the guidance and kind assistance of several individuals who have in one way or another contributed and rendered their precious guidance in carrying out and completion of the research work.

My outmost gratitude to the Boss, Prof. Nelson Torto. He not only gives me the motivation and drive to persevere during the years of this PhD course but also acts as a father to share my deep down feelings. I would like to acknowledge his invaluable assistance as well as his patience, encouragement, guidance, and enthusiasm throughout the course of this project. I could not have wished for better supervisor who supported me throughout this very costly educational trip.

I would also like to thank my co-supervisor, Dr Zenixole Tshentu, Associate Professor, Department of Chemistry, Nelson Mandela Metapolitan University for his assistance and input into this project. Your contributions, detailed comments and insight have been of great value to me.

Special thanks to Prof. Aderemi Ogunfowokan for recommending me to the Boss.

Dr Kevin Lobb your support and guidance with molecular modelling is highly appreciated.

Let me extend my gratitude to the staff of Rhodes University for their support in particular, the Chemistry Department, the other chemistry research groups, Benita, Barbara, Sibu, Sindi, technicians and everyone else. You have been awesome!

A special word of thanks to my colleagues in F12 (Prof. Nelson Torto research group), Dr Chigome, Yolanda, Boitumelo, Nokthula, Mamello, Bella, Pablo, Williams and Noor. I further

would like to mention my mentor, Dr Bareki Shimma Batlokwa for his support and friendship. Thanks, to all the other past postgrads colleagues, with who I shared my time, for their friendship and encouragement. I am indebted to Prof. and Mrs Olubomehin, thanks for being there when the going got tough.

I will not fail to mention pastors and members of the Redeemed Christian Church of God, Grahamstown, Alice, and Port Elizabeth, Pastor Adedeji, Okewole, Tella, Pastor (Mrs) Adedeji, Deaconess Okoh, Dr and Mrs Agbedayin, Bro. Sesan, Gerald, Thomos, Emeka, Emmanuel, Shan, Sis. Bukky, Ronke, Treasure, Judith, Dr Raphael, Mr and Mrs Zelalem, Mawumo, Paul, Elu, Queen,and Ifeoluwa.

I am extremely grateful to my dearest wife for her constant support and love which kept me sane always, and our lovely children Aduragbemi, Aduramigba, and Adurafimihan who have been great sources of inspiration in my life. I am thankful to my parents, brothers, sisters and in-laws.

Finally, special thanks are due to Olabisi Onabanjo University for granting me study leave, African Network for Analytical Chemists (SEANAC), South African Coal and Oil Ltd (Sasol (Pty) Ltd), and Water Research Commission (WRC) South Africa for funding.

Abstract

Most crude oils contain traces of vanadium and nickel complex with porphyrins (VTPP and NTPP) within their asphaltene fraction. Although these metals are only present in trace quantities, they have a significant and detrimental impact on the refining process by degrading the quality of intermediate and end products. Therefore, their selective removal is highly desirable. This thesis presents the development of nickel porphyrin, nickel vanadyl porphyrin imprinted nanofibers and vanadyl porphyrin imprinted polymer (MIP) particles for application as selective sorbents. Computational model based on the combination of molecular dynamics simulations and quantum mechanics was successfully applied to the styrene functional monomer selection. The particle was prepared by bulk polymerization and the nanofibers by a novel approach combining molecular imprinting and electrospinning technology. The morphologies, thermal stabilities and porosities of the imprinted sorbents were studied using SEM, TGA, and BET nitrogen gas adsorption. Chloroform was found to swell the polymer particles to a higher degree than methanol and acetonitrile. The adsorption characteristics of the imprinted sorbents best fitted with Freundlich isotherm model. The imprinted sorbents recorded high extraction efficiencies (EEs) of > 99 % in selectively extracting the metalloporphyrins. The impact of the template on the affinity of recognition for NTPP was evaluated. The results showed that the NTPP adsorption capacity increased as the molar ratio of NTPP to styrene was increased from 1:1 to 3:1. The optimal ratio of template to functional monomer which yielded the best specific affinity and highest recovery (99.9 %) was 3:1. The effects of trifluoroacetic acid (TFA), dichloromethane (DCM), dimethyl sulphoxide (DMSO), pentane (PEN) on electro-spinnability of the polymer solutions and the morphological appearance of the nanofibers were investigated. The imprinted

nanofibers exhibited the same selectivity specialism for both NTPP and VTPP. A remarkable stability in relation to reusability was observed when imprinted nanofibers were used, as they could be reused nine times without incurring any significant loss in removal efficiency. The results were validated by analysing a certified reference material. The imprinted sorbents were therefore found to be selective sorbents that are well suited for handling trace metals in organic media.

Contents

List of papers and conference

Parts of the research reported in this thesis have been published and the details are as follows:

Paper 1

Kehinde N. Awokoya, Bareki S. Batlokwa, Bridget A. Moronkola, Samuel Chigome. Dezzeline A. Ondigo, Zenixole Tshentu, Nelson Torto (2014) Development of a styrene based molecularly imprinted polymer and its molecular recognition properties of vanadyl tetraphenyporphyrin in organic media. *International Journal of Polymeric Materials and Biomaterials, 63: 107–113.*

Paper 2

Kehinde N. Awokoya, Bridget A. Moronkola, Samuel Chigome. Dezzeline A. Ondigo, Zenixole Tshentu, Nelson Torto (2013) Molecularly imprinted electrospun nanofibers for adsorption of nickel-5,10,15,20-tetraphenyporphine (NTPP) in organic media. *Journal of Polymer Research, 20: 148.*

Paper 3

Kehinde N. Awokoya, Zenixole Tshentu, Nelson Torto (2013) Fabrication and evaluation of multiply templated cross-linked molecularly imprinted electrospun nanofibers for selective extraction of nickel and vanadyl tetraphenylporphyrins from organic media. (Under review).

Paper 4

Kehinde N. Awokoya, Kevin A. Lobb, Zenixole Tshentu, Nelson Torto (2013) Anatomy of a successful imprint: A computational study on monomer suitability towards the template in molecularly imprinted polymer (In preparation).

Conference

4TH SEANAC International Conference, Titled "Analytical Chemistry for the Environment, Health and Water" held in Maputo, Mozambique between 8TH – 11TH July, 2012. (Oral presentation).

List of abbreviations

AA	Acrylic acid
AAPD	Azobis (methylpropionamide)dihydrochloride
ACC	Azobis-(cyclohexanecarbonitrile)
ACM	Acrylamide
ACN	Acrylonitrile
AFM	Atomic force microscopy
AIBN	Azobisisobutyronitrile
ASAP	Accelerated Surface Area and Porosimetry System
BET	Brunaure Emmett and Teller
BP	Bisacryloyl piperazine
BPO	Benzoylperoxide
CRM	Certified reference material
DAO	Deasphalted oil
DCM	Dichloromethane
DFT	Density functional theory
DMSO	Dimethyl sulphoxide
DPEP	Deoxophyllocrythroetioporphyrin
DSC	Differential Scanning Calorimetry
DVB	Divinylbenzene
EDX	Energy dispersive X-ray spectroscopy
EGDMA	Ethyleneglycol dimethacrylate
FTIR	Fourier transform infrared
HA	Hyaluronic acid
HDM	Hydrodemetallization

HEMA	2-Hydroxyethylmethacrylate
ICP-OES	Inductively coupled plasma-optical emission spectroscopy
L-PEI	Linear-polyethylenimine
LPG	Liquid petroleum gases
MAA	Methacrylic acid
MD	Molecular dynamics
MIN	Molecularly imprinted electrospun nanofiber
MIP	Molecularly imprinted polymer
n	Number of functional monomers
NIN	Non-imprinted electrospun nanofiber
NIP	Non-imprinted polymer
NIST	National Institute of Standards and Technology
NMR	Nuclear magnetic resonance
NNMB	N, N'-Methylene-bisacrylamide
NTPP	Nickel tetraphenylporphyrins
NVMIN	Nickel vanadyl molecularly imprinted electrospun nanofiber
NVP	N-vinylpyrrolidone
OEP	Octaethylporphyrin
PCL	Polycaprolactone
PD	Phenylene-diacrylamide
PDO	Polydioxanone
PEN	Pentane
PEO	Polyethylene oxide
PET	Poly(ethylene terephthalate)
PF	Pre-flash tower
PGA	Polyglycolic acid

PGA-co-TMC	Poly(glycolide-co-tromethylene carbonate)
PLA	Polylactic acid
PPY	Polypyrrole
PS	Polystyrene
PU	Polyurethane
S	Styrene
SARA	Saturates, aromatics, resins, and asphaltenes
SDA	Solvent deasphalting unit
Sr	Swelling ratio
SRM	Standard reference material
TEM	Transmission electron microscopy
TFMAA	Trifluoromethacrylic acid
TFA	Trifluoroacetic acid
TGA	Thermogravimetric analysis
TPP	Tetraphenylporphyrin
TRIM	Trimethylolpropane trimethacrylate
USA	United States of America
UV	Ultraviolet
VBA	Vinylbenzoic acid
VID	Vinylimidazole
VPY	Vinylpyridine
VTPP	Vanadyl tetraphenylporphyrin
Vc	Critical value
H	Air-gap
L	Length
R	Radius

wt%	Weight percent
α	Recognition coefficients
σ	Electrical conductivity
γ	Surface tension
ρ	Density

List of figures

List of tables

1

Introduction

1.1 Crude Oil

From a chemical viewpoint, crude oil is a complex mixture of hydrocarbon compounds. Crude oil constitutes an important part of primary fossil fuels [1-2]. A plural rather than a collective singular is a much more accurate designation of crude oils. Indeed crude oils encompass substances of considerable heterogeneity that vary widely in their appearance, composition, viscosity, flammability, quality, as well as economic value.

Crude oils originate from the decomposition of organic material that undergoes sedimentation and is subsequently degraded under the influence of heat, pressure, bacteria and catalysts during millions of years. The composition of the mixture depends on its location. Two adjacent wells may produce quite different crudes and even within a well the composition may vary significantly with depth [3].

1.1.1 Crude oil composition

The appearance of crude oils ranges from light, gasoline-like, highly mobile liquids to heavier reddish-brown fluids to highly viscous, tarry black materials. Crude oils are not individual chemical compounds (hence it is impossible to define them by a singular chemical structure)- they are a complex mixture of scores of hydrocarbons and other minor ingredients. The elements contained in crude oil include carbon (83-87 wt.%), hydrogen (11-15 wt.%), sulphur (0.05-7 wt.%), nitrogen (0.1-2 wt.%), oxygen (0.05-1.83 wt.%), and metals (0.01-0.14 wt.%) [4].

The saturates, aromatics, resins, and the asphaltenes (SARA) method is one example of an approach to separate crude oil into four major fractions or chemical classes based on the

difference in solubility and polarity. The four fractions are the saturates **(S)**, aromatics **(A)**, resins **(R)**, and asphaltenes **(A)**. The schematic outlining the SARA method is shown in Fig 1.1.1 [5].
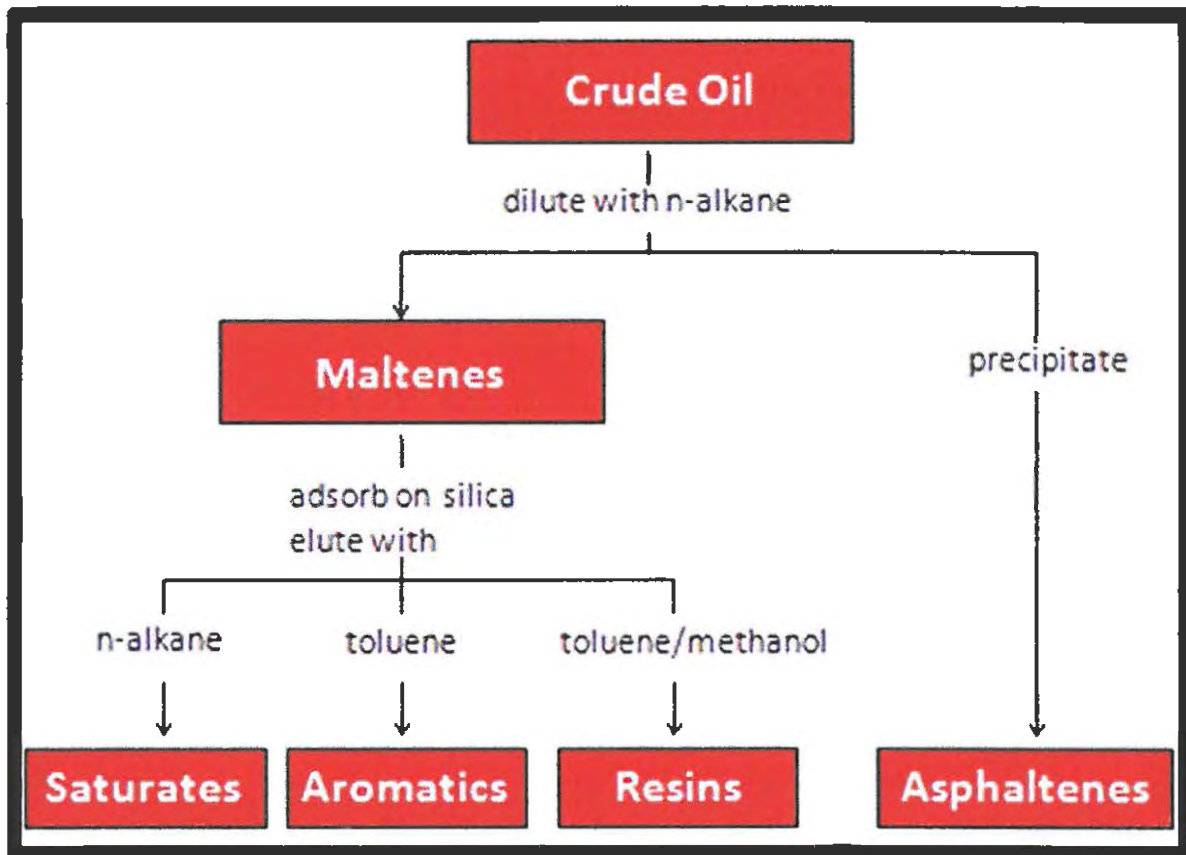
Figure 1.1.1: SARA separation scheme [5].

The asphaltene content of crude oil varies from 0.1% to more than 20% depending on the production field. Asphaltenes contain high concentrations of heteroatoms, such as sulphur and nitrogen, as well as metals, such as vanadium and nickel. Due to the heavy nature of the asphaltenes, their characterisation is mostly done by techniques used in polymer analysis,

such as size exclusion chromatography [6]. In refineries equipped with a deasphalting unit, asphaltenes are recovered as asphalt and not upgraded to transportation fuel.

1.1.2 Metal containing compounds

Metals found in crude oil include copper, lead, iron, magnesium, sodium, molybdenum, zinc, vanadium, cadmium, nickel, titanium, manganese, chromium, cobalt, antimony, uranium, gold, aluminium, tin, barium, gallium and silver. The metals exist in combination with naphthenic acid as soaps and in the form of complex organometallic compounds such as metalloporphyrins (Figure 1.1.2) [7,8].

Vanadium and nickel are the most abundant and undesirable of the metals [8]. Depending on the origin of the crude oil, the concentrations of vanadium and nickel vary from a few mg/L to more than 1000 mg/L. However, it should be noted that metal and metalloid constituents could be naturally found in crude oil or they could be added during production, transportation or storage [9,10]. There are other metal impurities too, which can be present at low concentrations, like arsenic and mercury.
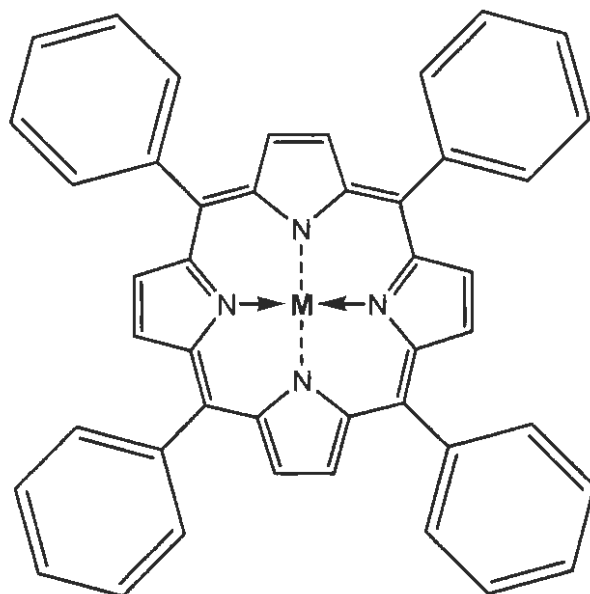
Figure 1.1.2: Porphyrine structure for chelating metal ions (M) like nickel and vanadium.

1.1.3 Toxicities of metals in crude oils

Metals are among the most harmful heteroatoms toxicants in crude oil. Metallic compounds exist in all crude oil types in trace amounts (ranging from 0.1 to 1200 mgL^{-1}). Their concentration must be reduced to avoid operational challenges and to prevent metals from contaminating the products. The presence of metals could be deleterious to refining processes, as they cause poisoning to the catalysts used for hydroprocessing and cracking [11,12]. Even minute quantities of metals in the feedstock to the catalytic cracker affect the activity of the catalyst and result in increased gas and coke formation and reduced gasoline yields [9].

For high-temperature power generators, the presence of metallic constituents, such as vanadium may lead to ash deposits on the turbine rotors, reducing the efficiency of heat

transfer and causing severe corrosion [9]. Also, ash deposits in engines may result in abrasion of the moving parts, and the ash is injurious to the walls of the boilers and furnaces.

Besides, when metals enter the environment through combustion products of the refined oil, they pose potential hazard to the health of animals and humans. Metals pose a toxicity concern if emitted directly to the environment from a stack- could be responsible for emission of mutagenic and carcinogenic compounds [13-15]. In view of metals having detrimental impacts on the refining processes and high toxicities to the environment, effort ought to be made to reduce their concentrations in crude oil to lowest possible levels or remove them completely.

1.2   Methods for removing heavy metals from crude oils

Since the most common metal contaminants are nickel and vanadium, which are generally present in the form of porphyrins and are concentrated in residues, many methods have been explored for the treatment of crude oil residues as well as for their removal. Each of the methods has its own advantages and limitations.

1.2.1 Chemical treatments

The basic chemical concept of demetallization is to selectively remove the metal from the organic moiety with minimal conversion of the remaining crude oil [16]. The demetallization of metalloporphyrin by acids is a reversible reaction and can be represented by the following equation:

6
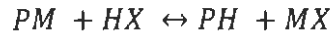
$$PM + HX \leftrightarrow PH + MX \qquad\qquad eqn\ 1$$

Treatment of crude oil products with acids is, like caustic treatment, a procedure that has been in use for a considerable time in the crude oil industry. Various acids, such as hydrofluoric acid, hydrochloric acid, nitric acid, phosphoric acid, and phosphorus acid, have been used in addition to the more commonly used sulphuric acid [17].

The objective of the treatment is to remove sulphur, nitrogen, metals, and various hydrocarbon types so as to improve the quality of products. The method was first employed for refining animal and vegetable oils, and since the beginning of the crude oil industry, about one hundred and fifty years ago, sulphuric acid was successfully employed in various purification steps of crude products. A number of patents for the use of sulphuric acid were issued at the very beginning of the crude oil industry [18,19].

Kukes and Battise [20] of Phillips Petroleum also used phosphorus acid to remove nickel and vanadium from heavy oils. It is believed that phosphorus acid reacts with the metals contained in the hydrocarbons to form oil insoluble compounds that can be removed either by filtration, centrifugation, or decantation.

However, the fact that sulphuric acid reacts with and promotes reactions of hydrocarbons is a drawback to its use as an agent for removing metals, sulphur and nitrogen from crude oil. Large excesses of acid are required for efficient removal, which may cause marked changes in the remainder of the hydrocarbon mixture and decrease the yield of fuel products. Generally, acids have a number of disadvantages, including extensive side reactions and product contamination [21].

1.2.2 Electrochemical treatments

The electrochemical treatment is an alternative route that eliminates heteroatoms from crude oils [22]. Electrochemical demetallization of crude oils was found to be dependent on some electrochemical variables such as the composition of the electrolytic medium, electrode material and reduction potential.

Branthaven et al. [23] reported 85% and 92% of vanadium removal and sulphur removal, respectively, for Boscan crude oil porphyrin using a graphite cathode, platinum anode, ethylenediamine as solvent, lithium chloride as electrolyte at 36 V and 2 A for 18 h. Incorporation of protonating agents was confirmed to improve the demetallization process [22].

Conversely, electrochemical removal technologies have not been widely applied because they involve relatively large capital investment and electricity supply [24].

1.2.3 Precipitation

The precipitation of asphaltenes for metal removal is a complex phenomenon that involves asphaltenes and resins. It is of great importance to know under which conditions that the asphaltenes precipitate and to what extent precipitated asphaltenes can be redissolved [25]. In other words, to what extent the process of asphaltene precipitation is reversible with respect to the change in thermodynamic conditions.

Anderson and Stenby [26] studied the effect of the temperature on asphaltene precipitation/dissolution in crude oil. They used a mixture of toluene and n-heptane and performed solvent reversibility runs at 24, 50, and 80 $^{\circ}$C. The results showed that asphaltenes partially redissolved with an increase in the temperature.

Buckley et al. [27] showed that asphaltene precipitation occurs by not only adding alkanes as a solvent but also increasing the temperature. According to the study, the size of precipitated particles as a result of the increasing temperature was less than 10 μm. The observed size was much smaller than the precipitated particles as a result of adding solvent.

Mousavi-Dehghani et al. [28] showed that asphaltenes precipitation in crude oil increases with an increase of the temperature and asphaltene precipitation is an irreversible process. *Ashoori et al.* [29] reported that asphaltene precipitation is reversible with respect to the temperature and composition.

However, asphaltene precipitation makes oil production more arduous and costly because of the partial plugging in the oil well, pipeline, and equipment.

1.2.4 Solvent deasphalting

Solvent deasphalting process (SDA) which is based on liquid-liquid extraction is one of the efficient approaches to reduce metal and asphaltene contents of heavy oil cuts before sending them to hydro-desulphurization and hydrocracking units [30]. SDA is a unique separation process in which residue is separated by molecular weight (density) instead of by boiling point.

The SDA process produces low contaminant deasphalted oil (DAO) that is rich in paraffin type of molecules. Solvent deasphalting has the advantage of being a relatively low cost process that has the flexibility to meet a wide range of DAO qualities [31,32].

During the SDA process, the feed is mixed with a light paraffinic solvent ($C_4 - C_7$), where the oil is solubilised in the solvent. The insoluble pitch precipitates out of the mixed feedstock as

asphaltene in which most of the metals remain insoluble and are removed from the product stream. The separation of the DAO phase and the pitch phase occurs in the extractor. The extractor is designed to efficiently separate the two phases and minimize contaminant entrainment in the DAO phase [33].

Yamada et al. [34] described a method of extraction by heating the oils to 177 − 238 °C, refluxing the oils with an organic solvent, and centrifuging the mixture. Thus, a residual oil containing 159 mgL^{-1} vanadium was heated [3°/min to 182 − 216 °C for 1 h], refluxed with hexane, and then centrifuged to give a hexanesoluble portion containing 0 mgL^{-1} V. However, the disadvantages of the method are that it performs no conversion, produces a very high-viscosity by-product pitch, and where high quality DAO is required, SDA is limited in the quality of feedstock that can be economically processed.

1.2.5 Adsorption

Adsorption is a mass transfer driven process wherein molecules in a free phase become bound to a surface by intermolecular forces [35]. Adsorption is the most effective and economic demetallization method currently used to achieve ultra clean fuels [36]. In addition, it allows for the regeneration and reuse of the sorbents after they have been desorbed. The effectiveness of the adsorption process depends on the characteristics of the sorbent used. The adsorption process could therefore be explored for removal of heavy metals in organic media. So far, to the best of our knowledge, two kinds of adsorbents, including silica hydrogel and manganese dioxide have been used.

Silica hydrogel sorbents: These have been used in removing heavy metals from crude oil. A US patent [37] described a method for extraction of metal ions by weighing hydrogel silica in 20 g of crude oil (a Saudi Heavy grade). The crude oil contained 58 mgL^{-1} vanadium, and 18

10

mgL^{-1} nickel. 80 g of petroleum ether was added as diluent, in order to reduce the viscosity of the oil. The results showed the residual vanadium to be less than 0.1 mgL^{-1}; and the residual nickel to be less than about 0.1 mgL^{-1}. However, silica hydrogel sorbents are still subject to attrition and are not selective.

Manganese dioxide sorbents: Adeyi et al. [38] reported the extraction of impurities from crude oil by contacting 2 g of the adsorbent-activated manganese dioxide (MnO$_2$) with 20 ml of crude oil in a 250 ml flask and stirred with a magnetic stirrer for a period of 60 min at 120 rpm and at a temperature of 30 °C. However, its adsorption capacity was low and not selective or reusable and the adsorbent thus limited in its application. Therefore, developing sorbent materials that would address those limitations will be a better alternative.

Imprinted sorbents: These include imprinted polymers and imprinted electropun nanofibers that have attracted extensive widespread attention in adsorption applications because they have the ability to overcome the limitations (non-selectivity, reusability, low adsorption capacity, attrition) of the other kinds of sorbents [39]. Other advantages of imprinted sorbents include high mechanical strength, durability with respect to heat and pressure, long shelf life, and applicability in harsh chemical media [40].

The imprinting process offers the flexibility of combining imprinted polymers (MIPs) with electrospun fibers as it enables their utilization as a sorbent in separation and accumulation processes associated with complex sample treatment [41]. The selective recognition capabilities of the imprinted polymers are enhanced when they are fabricated into nanofibers due to a larger surface area. These remarkable features of imprinted sorbents make them the preferred materials for the development of a platform for removing of heavy metals from fuel oil.

1.3 Scope of the thesis

The studies conducted in this thesis were developed with the view to increasing knowledge about useful strategies that could enhance the recognition abilities in imprinted sorbent materials. The primary aim was to develop imprinted sorbents that have tunable characteristics for the selective clean-up of metalloporphyrins from organic media. The specific objectives were as follows:

- To investigate for suitable functional monomer via molecular dynamic simulation method. The activity was focused on pre-screening of all possible interactions between the functional monomers and the template molecule in the prepolymerization complexes.

- To develop both imprinted polymers and nanofibers, and to characterise them in terms of their reusability and loading capacities.

- To characterize the imprinted sorbents in terms of their morphologies, porosities and thermal stabilities.

- To investigate the parameters affecting adsorption such as the quantity of template, type of spinnable polymer and extraction solvent.

- To investigate the effects of solvents and their properties on electro-spinnability of the polymer solutions and the morphological appearance of the nanofibers.

- To validate the accuracy and the capacities of the sorbents by employing a residual fuel oil certified reference material.

2

Imprinted polymers and nanofiber sorbents

2.1 Overview

This chapter discusses the various methods for producing imprinted polymers and nanofibers. These methods include bulk, suspension, precipitation, two-step swelling and emulsion core-shell polymerizations, as well as template synthesis, melt blowing, self-assembly, drawing and phase separation. Molecular imprinting and electrospinning are considered in detail in Chapter Three.

2.2 Methods for producing molecularly imprinted polymers (MIPs)

To date, imprinted polymers in the form of particles are made by various polymerization designs, each of them developed to suit specific targets and application. Several methods for producing imprinted polymers have been outlined in the literature (Fig. 2.2)[42,43]. Each of these methods involves the control of different parameters during the synthesis with production of polymers with different properties and characteristics.

2.2.1 Bulk polymerization

Traditionally, molecular imprinting has mostly been performed by the bulk polymerization method. It is the most widely used owing to its simplicity and universality. Most investigations still rely on it for the purpose of demonstrating the imprinting effect and potential applications [44].

Typically, the reaction mixture of template, functional monomers, initiator, cross-linker, and solvent are added to a glass tube, the mixture is purged with nitrogen to remove oxygen, and polymerizing them. The result is a polymeric block that needs to be crushed and ground to obtain particles of irregular shape and size between 20 and 50 μm [43]. In this method, the apparatus required for synthesis is relatively simple, and the reaction conditions can be easily controlled [42]. Despite the ease of preparation by this polymerization method, it has

the disadvantage that most of the polymer produced (an estimated 70%) is wasted in the process of grinding [43]. Furthermore, the irregular shape and size of the polymers that result from this polymerization method can be avoided by employing other methods.
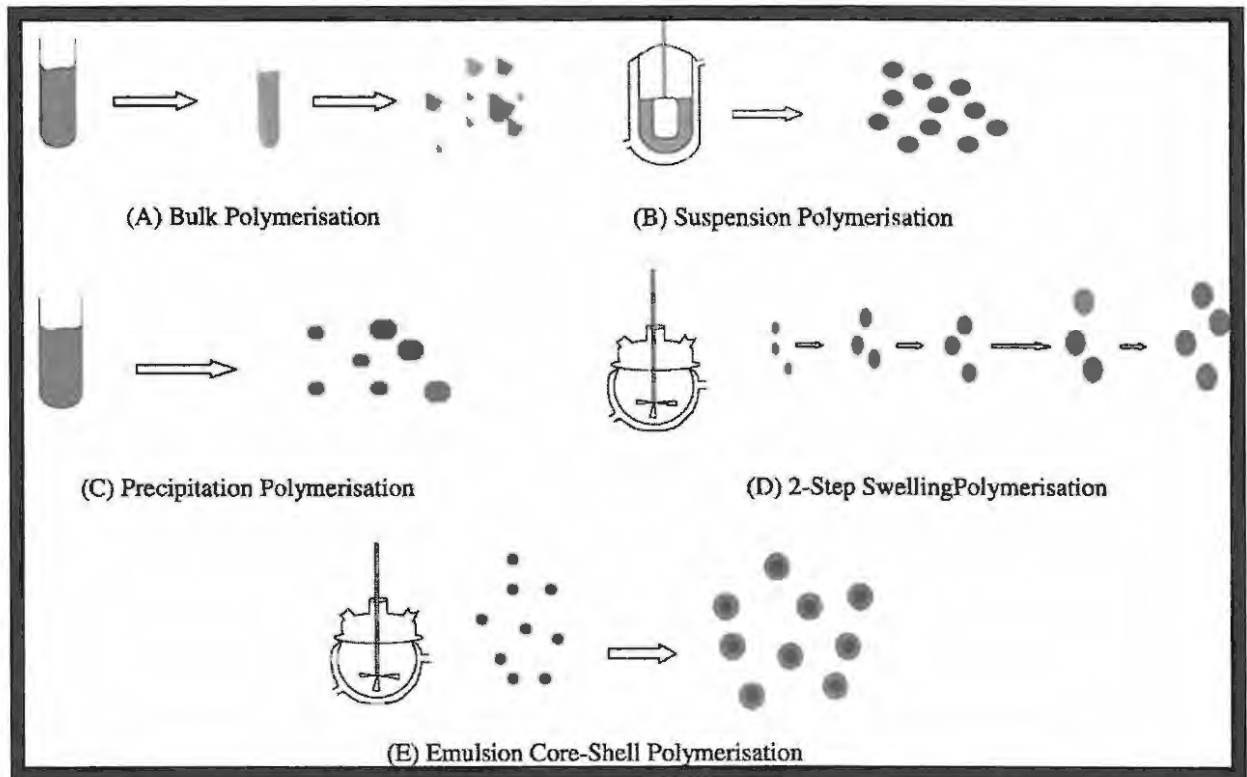
Figure 2.2: Schematic representation of the synthetic steps in the different polymerization procedures (Adapted from: [43]).

2.2.2 Suspension polymerization

Strategies for generating imprinted beads were developed to improve the characteristics of the bulk monolith formations. Suspension polymerization is one of the simplest and most common approaches for the production of imprinted beads. The technique was first reported by Mayes and Mosbach [45]. It is a fast and reliable methodology that synthesises particles by UV irradiation in less than 2 h (or as little as 10-15 min for easily-polymerising monomers) [45].

In the case of suspension polymerization, all the components involved in the polymerization process are dissolved in an appropriate organic solvent and this solution is further added to a larger volume of an immiscible solvent. Afterwards, the system is vigorously stirred in order to form droplets and then the polymerization reaction is induced [46]. Each droplet acts like a mini bulk reactor producing beads of a broad size range, 10–100 μm size. The beads have improved adsorption capacities as well as high selectivity coefficients [47].

2.2.3 Precipitation polymerization

Amongst the methods developed to overcome the drawbacks of bulk polymerization, precipitation polymerization is the most widely used for obtaining spherical particles. The precipitation polymerization method was first reported by Ye *et al.* [48,49]. The method is carried out in experimental conditions that are similar to those of bulk polymerization mixture, with the exception that, comparatively, 2 to 10 times the amount of porogen is used.

The basic principle of this approach is that, when the polymeric chains growing in solution reach a certain critical mass, they precipitate from the solution. The particles thus obtained do not typically exceed 10 μm [50].

2.2.4 Two-step swelling polymerization

Two-step or multistep swelling polymerization is another common approach for preparing imprinted beads and was first reported by Hosoya *et al.* in 1994 [51]. In this method, preformed uniformly-sized seed particles are suspended in water and, after several additions of suitable organic solvents, the initial particles swell to a final size. Once the particles have swollen to the desired size, all the components involved in the production of the imprinted sorbent are added to the solution and incorporated into the particles in the swelling state and afterwards polymerization is induced [46].

The method is time consuming and sophisticated but produces monodisperse particles in the micro size range (2–50 μm) with good control of the size and number of the particles. The spherical particles obtained have separating abilities comparable with other methods, and the approach is more robust when imprinting any given molecule because none of the compounds involved in the polymerization process influences the process of obtaining spherical particles.

2.2.5 Emulsion core-shell polymerization

Emulsion core-shell polymerization is a heterogeneous type polymerization since it requires two non-miscible phases, one of them being the continuous phase and the other the dispersed phase. In this technique, droplets of monomers are emulsified with surfactants in a continuous phase containing the initiator.

The process has been used by Ashraf *et al.* to prepare hydrophobic imprinted resins using methylmethacrylate and phenyl methacrylate as monomers, a mercury(II)dithizonate complex and a non-ionic alkyl-oligo(ethylene glycol) surfactant [52]. Particles obtained by this method are monodisperse and can be produced in a colloidal size range of 0.05–2 µm. They can also be used for surface imprinting. However, the implementation of emulsion core-shell polymerization remains unusual probably because of the difficulty experienced in separation of the particles and possible contamination by the surfactant.

2.3 Methods for producing nanofibers

Nanofibers belong to the area of nanomaterials, and their production centers around organic polymers and inorganic materials. Synthetic methods for obtaining nanofibers are numerous and have been reviewed by various authors recently [53,54]. They can be categorized into 5 major groups including– template synthesis, phase separation, drawing, self-assembly, and electrospinning.

2.3.1 Template synthesis

Template synthesis is probably one of the most versatile methods for the synthesis of nanofibers. In template synthesis, the polymer solution is extruded through a metal oxide membrane having pore diameters in the nano range [55,56]. Upon coming into contact with a solidifying solution, the extruded solution forms nanofibers whose diameters are determined by the pores in the template [57].

Fibers of specified diameter can easily be made using an appropriate template. Park *et al* [58] used a set-up similar to the one illustrated in Fig 2.3.1 to synthesize polypyrrole (PPY)

nanofibers. Nanofibers having diameters ranging from 50 to 200 nm were obtained from PPY solution using dichloromethane (DCM) as the solvent.

A general feature of the conventional template method is that the membrane should be soluble so that it can be removed after synthesis in order to obtain single nanofibers. The insolubility of the membrane restricts the practical application of the method and gives rise to a need for other methods.
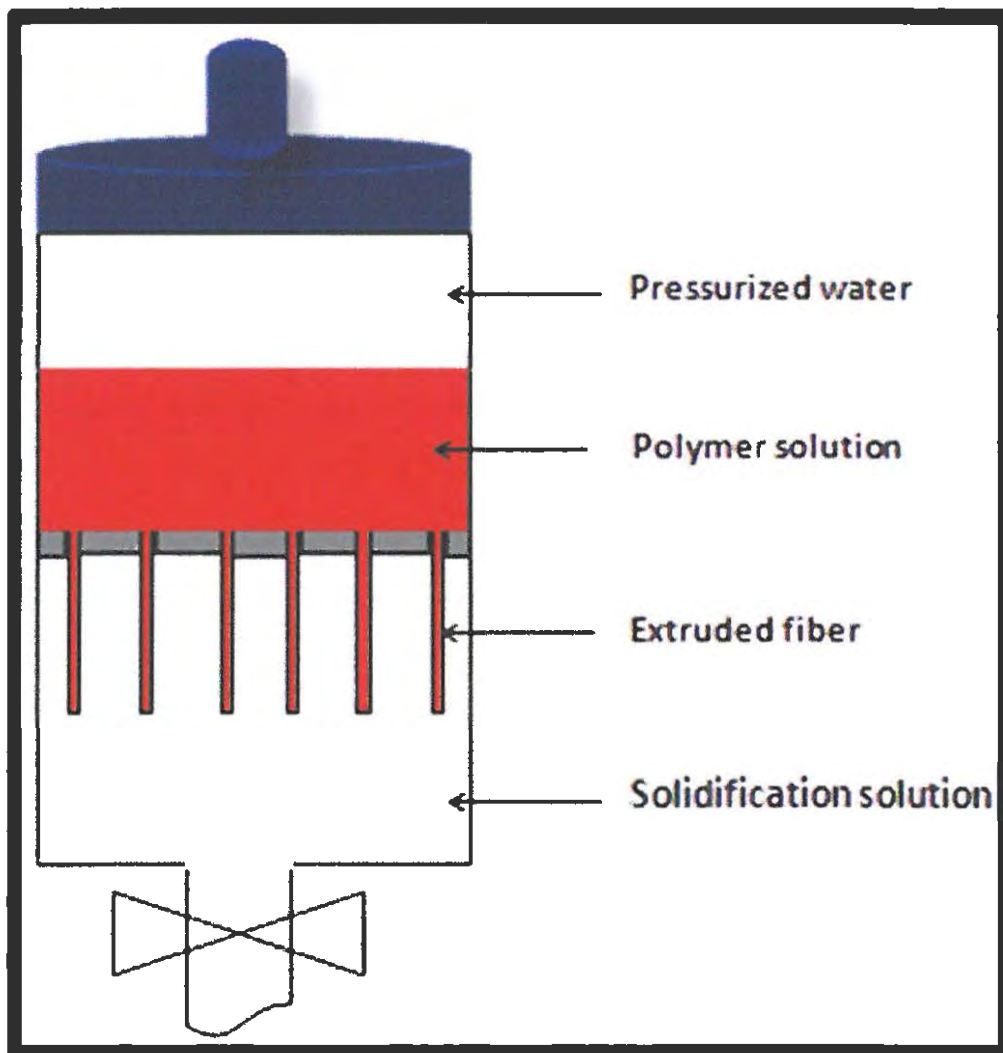
Figure 2.3.1: A Schematic setup for producing fibers through template synthesis.

2.3.2 Melt blowing

Melt blowing is another method for making non-woven webs that has proven to be scalable for commercial production [59-61]. The technology of melt blowing was first developed in the 1950s at the Naval Research Laboratory of United States [62]. In the melt blowing process, a molten polymer is extruded through small orifice into a stream of high velocity hot air. The fibres are formed by the elongation of the polymer streams coming out of the orifice by air-drag and are collected on the surface of a suitable collector in the form of a web [63,64]. Figure 2.3.2 is a schematic representation of the melt blowing equipment.

The process can be controlled to produce fibers ranging in diameters from 1 to 50 μm [59]. Although traditional melt blowing is an efficient and economical process for commercial production of non-woven fiber products, it cannot produce fibers with diameters in the same size range as electrospun fibers and it is limited to thermoplastic polymers [65].
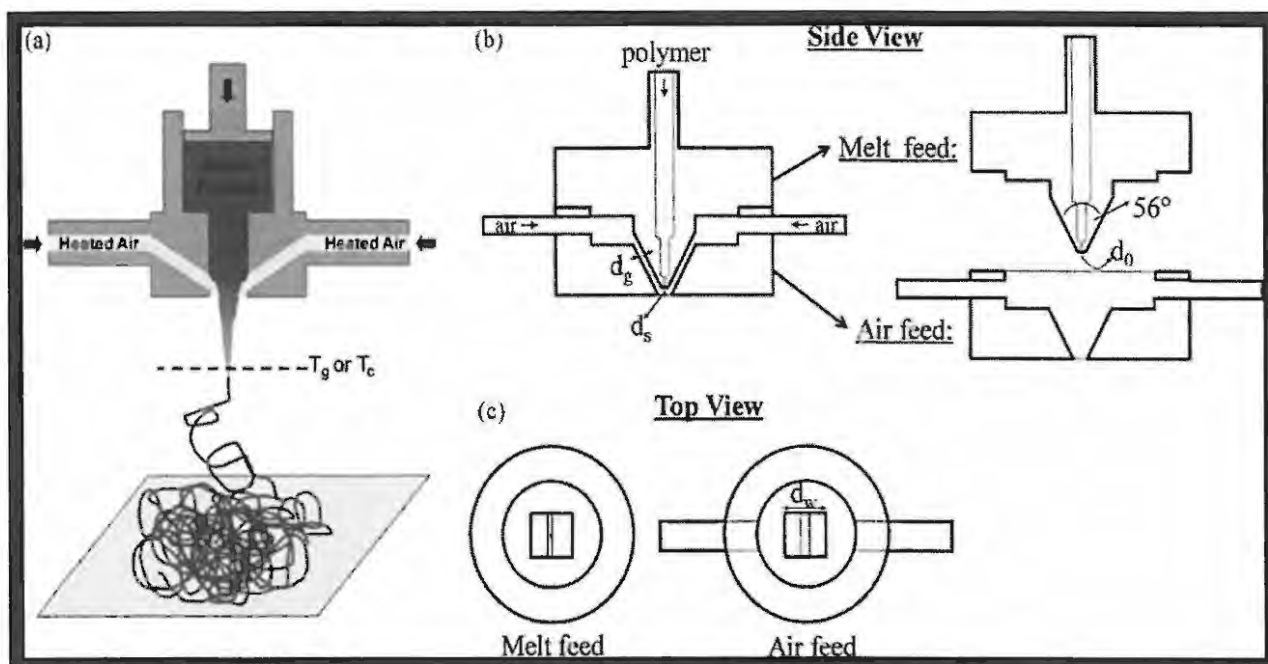
Figure 2.3.2: Schematics representation of the melt blowing equipment: (a) the entire melt blowing equipment, (b) side, and (c) top view of the homebuilt melt blowing die (Adapted from: [64]).

2.3.3 Self-assembly

Self-assembly is a bottom-up approach employed to create nanofibers from small building blocks, including small molecules, peptides, and nucleic acids [66]. The small molecules are arranged in a concentric manner and upon extension in a normal plane produce the longitudinal axes of the nanofibers. In self-assembly, the shape and properties of nanofibers depend on the molecules and the intermolecular forces that bring the molecules together. Nanofibers of various polymeric configurations such as diblock and triblock copolymers of peptide amphiphile and dendrimers have been successfully generated using the self-assembly approach [67,68].

2.3.4 Drawing

An iron/silica rod or micropipette is dipped into the droplet of a viscous polymer solution near the contact line [69]. The method was used by Xing *et al* to fabricate poly (trimethylene terephthalate) nanofibers with diameters as low as 60 nm, and lengths up to 500 mm [70]. In this technique, nanofibers are drawn directly when a rod is placed in a polymer melt and moved up forming a thin filament that is cooled to form a nanofiber (Fig 2.3.4).
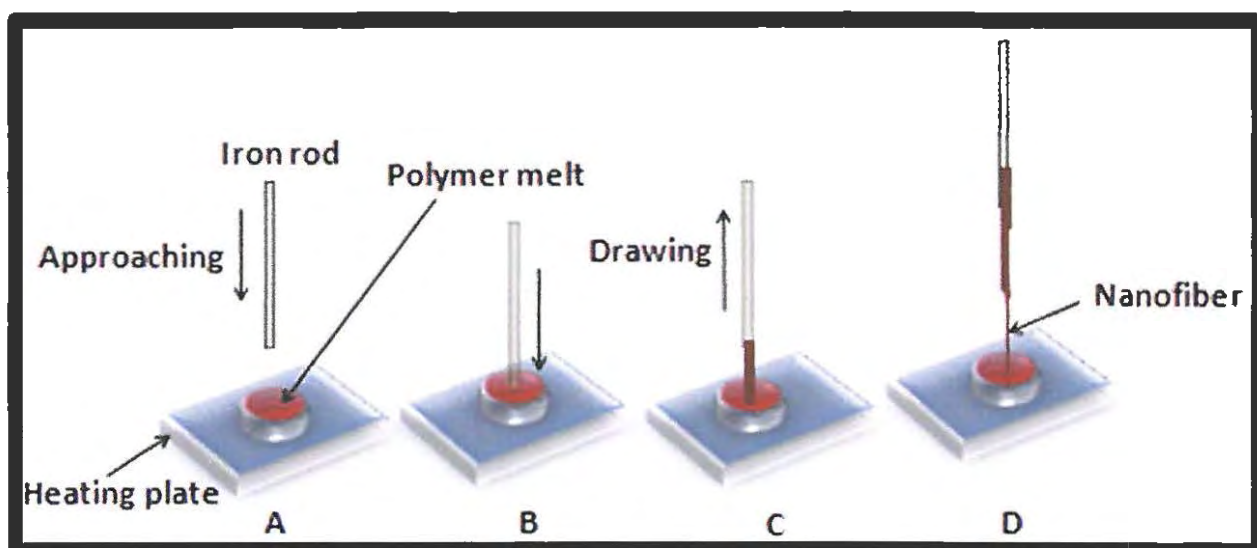
Figure 2.3.4: Schematic of nanofiber fabrication by the drawing technique.

The drawing technique is suitable for viscoelastic materials which can undergo strong deformations. Although the process is simple it is limited to laboratory scale as nanofibers are individually formed.

2.3.5 Phase separation

The phase separation method is a thermodynamic separation of polymer solution into polymer-rich and polymer-poor layers. The technique involves dissolving a polymer in a solvent at a high temperature followed by a liquid-liquid or solid-liquid phase separation induced by lowering the solution temperature [71].

The fiber network formation depends on the solvent of the polymer solution and the gelation temperature. The fibers formed in this manner have diameters ranging from 50 to 500 nm, and have porosity in excess of 98% [72]. The advantage of the method is that it is relatively simple, and the requirements are minimal in terms of equipment compared with self-assembly and melt blowing. However, it is limited to a few polymer types and takes a long period of time to transfer the solid polymer into the nano-porous foam.

In order to address all the drawbacks and to further make the MIP binding sites more accessible to the target analyte in solution, new, facile strategies for effective and versatile fabrication of high surface area to volume ratio selective nanomaterials are needed. Recently, the combined technique of molecular imprinting and electrospinning has been identified as a plausible technique to produce such materials, and will be discussed in detail in the following chapter.

3

Molecular imprinting and Electrospinning

3.1 Overview

This chapter consists of two sections. The first section presents background information covering the theory of molecular imprinting, imprinting process and the characterization techniques that are commonly employed to elucidate the structural features of MIPs. The section concludes with a discussion of the rational design of MIPs using the computational approach. The second section discusses the electrospinning process, as well as the combined technique of imprinting and electrospinning.

3.2 Polymers as artificial receptors

Molecular recognition is the underlying principle of many biological processes. Specialized structures fit perfectly with their natural targets, antibodies with their antigens, enzymes with their substrates, or hormones receptors with their hormones [73].

The biomacromolecules are therefore used as recognition systems in affinity technology with applications for example in analytical chemistry and biomedical fields. However, they are unstable out of their native environment, and therefore are difficult to integrate in standard industrial fabrication processes. So, it has been a long-term idea of researchers to be able to build such structures by artificially creating tailor-made receptors that are capable of recognizing and binding the desired molecular target with a high affinity and selectivity [74-80]. One remarkably simple way of generating artificial macromolecular receptors is through the molecular imprinting of synthetic polymers.

Molecular imprinting is a technique that is used to create artificial receptors by the formation of a polymer network around a template molecule. This is achieved by forming a

highly cross-linked polymeric matrix between functional monomers and a target compound (template) [81].

3.3 Molecular imprinting process

The process of molecular imprinting starts with the selection of an appropriate imprinting approach. The imprinting process involves complexation in solution of the template molecules with functional monomer(s), through either non-covalent or covalent interactions, followed by a polymerization reaction with an excess of cross linking monomer.

There are three approaches to molecular imprinting: covalent, non-covalent, and hybridization of covalent and non-covalent, which is also called semi covalent imprinting. The most widely used approach for preparing MIPs is non-covalent imprinting [82]. First, the preparation of a non-covalent MIPs is relatively straightforward and requires few steps. In this approach, the complex of template and functional monomer is formed *in situ* by non-covalent interactions, such as electrostatic forces, hydrogen bonding, van der Waals forces, or hydrophobic interactions.

There are several advantages of this approach including easy preparation of the template/monomer complex, easy removal of the template from the polymers, fast binding of templates to MIPs, and its potential application to a wide range of target molecules [83]. However, the binding constants in non-covalent imprinting are essentially weak compared to those of a covalent bond due to the nature of the interaction involved. However, when weak interactions are present as multiple docking points, they lead to strong binding. In order to compensate for the effect of the weak interactions, an excess proportion of functional monomer is added.

A major contributor to the molecular recognition afforded by MIPs is the binding affinity [84]. Binding affinity refers to the strength of the binding interaction, often given as a binding constant (K, mol^{-1}) or as free energy (ΔG, kcal/mol). Table 3.3 gives the ranges of binding energies for several major types of non-covalent interactions.

Table 3.3: Range of binding energies for non-covalent interactions [85].

	Types of binding interaction	Range of binding energies (+) (kcal/mol)
1.	Electrostation	
	a. ion-ion	20–80
	b. ion-dipole	12–50
	c. dipole-dipole	1–10
2.	Coordination bond	20–50
3.	Hydrogen bond	1–30
4.	π-π stacking	0–12
5.	van der Waals	0–1.5

Covalent approach differs from non-covalent imprinting only in the formation of the template-polymer complex and the subsequent removal of the template. The covalent procedure of imprinting was first developed by Wulff *et al* [86,87]. In the approach, the

complex is formed by covalent-linkage of a functional monomer and template prior to polymerization.

The main advantages of the approach are that the monomer/template complexes are stable and stoichiometric [88]. However, the template-monomer bond is not easily broken for the removal of the template, and as a result, the study of covalent imprinting is not as widespread as its non-covalent counterpart.

In the intermediate approach, the polymers are prepared like those in covalent imprinting, while the guest binding employs non-covalent interactions [89-90]. The studies conducted in this thesis relied more on non-covalent imprinting.

The representation of the general scheme of non-covalent imprinting used for the preparation of MIPs is highlighted in Figure 3.3. MIPs are prepared by copolymerizing a monomer with a cross-linker in the presence of a template molecule. The template molecule is allowed to form reversible interactions via the non-convalent approach with one or more functional monomers. The monomers form spontaneous complexes around the template. Upon complex formation, crosslinking monomers are then added to a suitable porogen (solvent that aids pore formation) to drive polymerization. An extensive wash procedure is used to remove the template from the polymer, leaving imprintings or binding sites that are sterically and chemically complementary to the template.
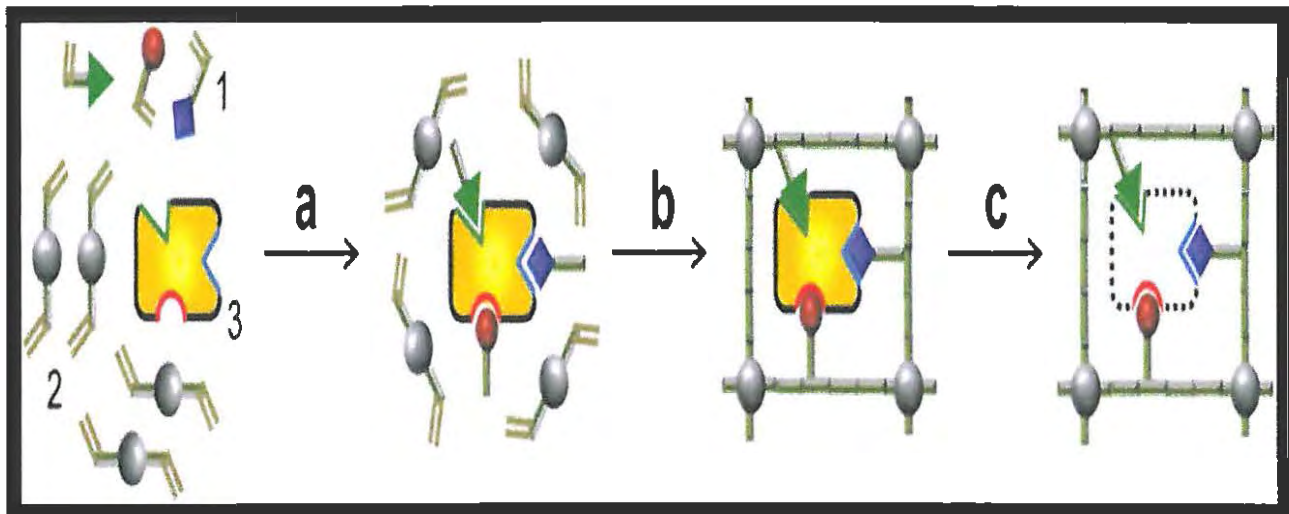
Figure 3.3: Schematic representation of the imprinting process (1-functional monomers, 2-crosslinker monomer, 3-template molecule; a-self assembly, b-polymerization, c-removal of template molecule) [73].

3.4 Factors affecting the imprinting process

The molecular imprinting process is quite straightforward. However, there are several factors that influence the imprinting process, and hence the subsequent performance of the imprinted polymers. For example the template, the nature of the functional monomer(s), ratio of functional monomer(s) to template, solvent(s), crosslinker(s), initiator, temperature, pressure, polymerization time, and the dielectric constant of the components of monomer mixture employed.

Binding site orientation, stability, and accessibility are governed by the structural characteristics of the polymeric matrix and are essential to recognition of the polymers formed. For this reason, investigating and optimising various parameters is essential in order to make progress in maximising recognition effects [91].

29

3.4.1 Template (Print molecule)

In all imprinting processes the template is fundamental in that it directs the organization of the functional groups pendent to the functional monomers. For practical applications, the analyte of interest is generally used as the print molecule for preparing the MIPs. The template should have the highest number of polymerizable sites that will interact well with the monomer as much as possible but should be chemically inert during the polymerization reaction [92].

The template with a high number of binding sites yields imprinted polymers of higher specificity and affinity for the analyte. The removal of the template provides a cavity, which matches the physical and chemical characteristics of the template species.

Although the choice of the template is almost, always the target analyte, where the molecule is very expensive to buy, not readily available, a structural analogue termed a "surrogate" or "dummy template" can be employed to deal with these challenges [93]. The dummy approach may also be required if the species demonstrates sensitivity to the conditions of polymerization.

In addition to the type of template, the stoichiometric ratio of template to functional monomer is very significant to the ultimate performance of the MIPs, in particular where interactions are noncovalent. The optimum ratio has to be determined for each individual template [94].

3.4.2 Functional monomers

The nature and type of monomer are some of the parameters that determine the quality and performance of the polymer product. The choice of appropriate functional monomer(s) is critical for achieving good imprints, because the self-assembly process is governed by attractive interactions between the monomer(s) and template [95].

It is very important to match the functionality of the template with that of the monomer(s) in a complementary fashion, (e.g H-bond donor with H-bond acceptor) in order to maximise complex formation and thus the imprinting effect. When two or more functional monomers are used simultaneously in "cocktail" polymerization [95], it is important to always remember the reactivity ratios of the monomers to ensure that copolymerization is feasible. Figure 3.4.2 illustrates some frequently used non-covalent functional monomers, which are divided into groups corresponding to their acidic, basic or neutral character.

Acidic

| Methacrylic acid (MAA) | 4-Vinylbenzoic acid (4-VBA) | Trifluoromethacrylic acid (TFMAA) | Acrylic acid (AA) |

Basic

| Allylamine (AA) | 4-Vinylpyridine (4-VPY) | N-Vinylpyrrolidone (NVP) | 1-Vinylimidazole (1-VID) |

Neutral

| Styrene (S) | Acrylonitrile (AN) | Acrylamide (ACM) | 2-Hydroxyethyl methacrylate (2-HEMA) |
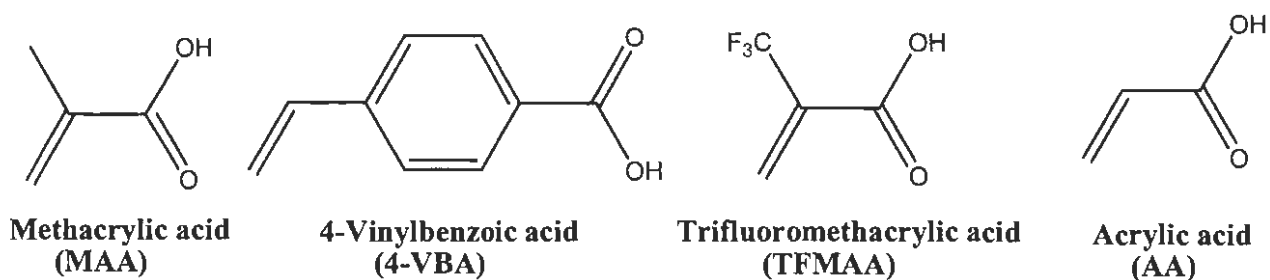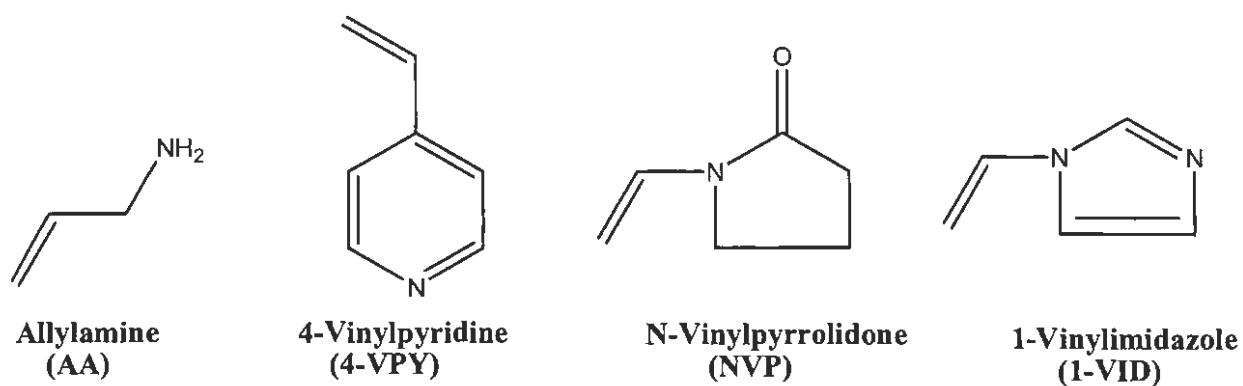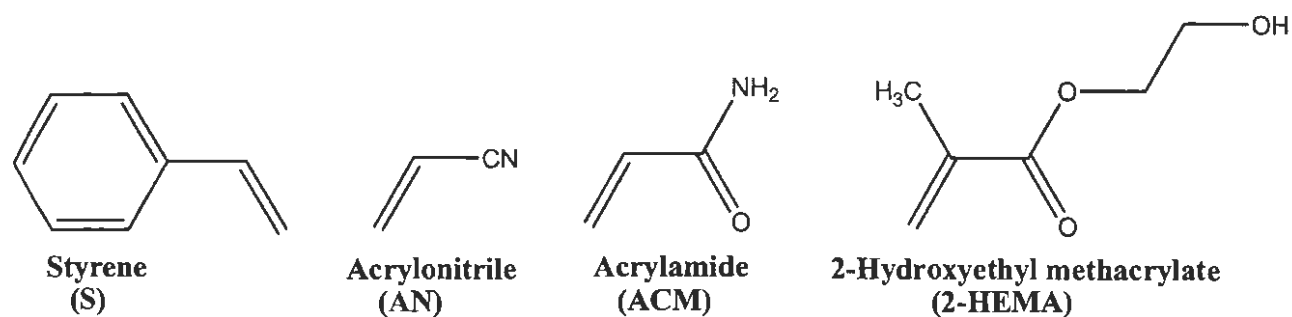
Figure 3.4.2: A range of functional monomers used in the noncovalent approach.

32

Finally, when choosing the functional monomer one should consider the chemical environment and application for the MIP.

3.4.3 Cross-linking monomer (Cross-linker)

Any discussion of the chemistry of MIPs should not overlook the cross-linker, since the cross-linker typically can make up anything between 70% and 98% of the final MIPs. In MIPs the cross-linker fulfils three major functions;

(1) It imparts mechanical stability to the polymer matrix.

(2) It serves to stabilize the imprinted site.

(3) The cross-linker is important in controlling the morphology of the polymer matrix, whether it is gel-type, macroporous or a microgel powder.

A number of cross-linkers reported in the literature are illustrated in Figure 3.4.3. A few systematic investigations of the effect of cross-linkers on the recognition properties of MIPs have been carried out, notably by the groups of Wulff [96] and Spivak [97].

The degree of cross-linking is important in preserving the binding specificity of MIPs. When functional groups are not satisfactorily attached by cross-linking, i.e. levels of cross-linking are too low, the binding specificity by the MIPs decreases. On the other hand, when the levels are too high, the loading capacity of the MIPs is reduced, and the diffusion of substrates into the imprinted cavities during rebinding may also be obstructed.

Of all the cross-linking monomers, the most commonly used is ethylene glycol dimethacrylate (EGDMA) [98], because of its availability and ability to easily cross link with a wide range of functional monomers.
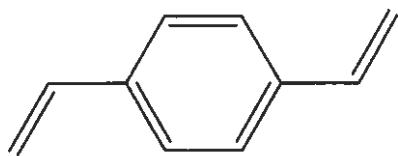
Divinylbenzene
(DVD)
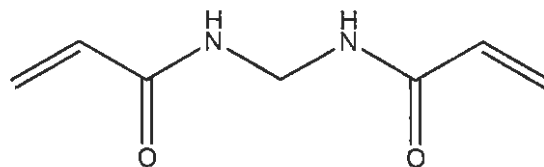
N,N'-Methylene-bisacrylamide
(NNMB)
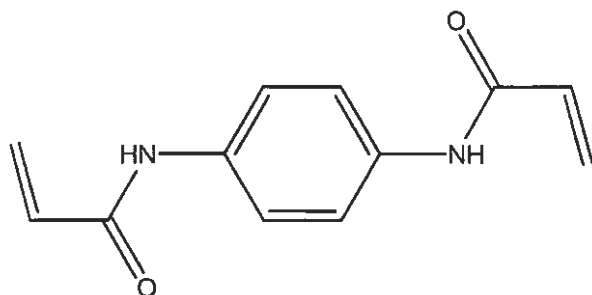
Phenylene-diacrylamide
(PD)
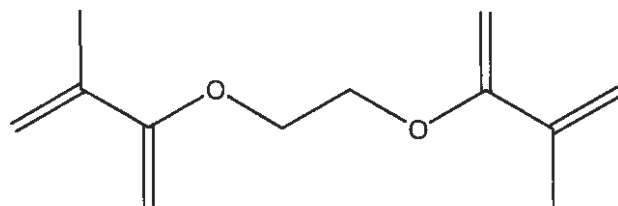
Ethyleneglycol dimethacrylate
(EGDMA)
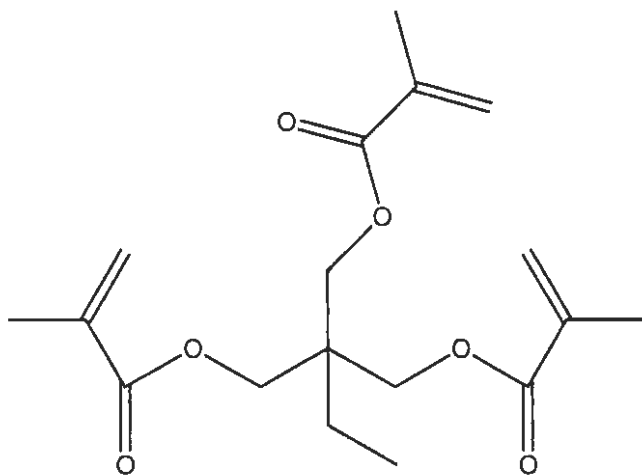
Trimethylolpropane trimethacrylate
(TRIM)
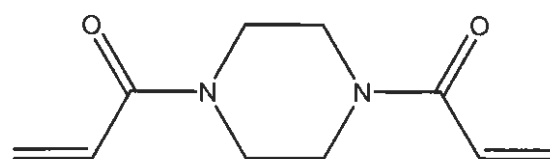
Bisacryloyl piperazine
(BP)

Figure 3.4.3: Selection of cross-linkers used in molecular imprinting protocols.

3.4.4 Solvents

The solvent is one of the most important factors determining effective molecular recognition because the accuracy of the assembly between the template and the monomer is related to the physical and chemical characteristics of the solvent. One must use a solvent that dissolves all the components of the pre-polymerization mixture, allows for optimal template-monomer interaction, and contributes to good porosity characteristics in the final MIPs.

The morphological properties of porosity and surface area are determined by the type of solvent used in the polymerization. Porosity arises from phase separation of the solvent and the growing polymer during polymerization. Solvents with low solubility phase separate early and tend to form larger pores and materials with lower surface areas. Conversely, solvents with higher solubility phase separate later in the polymerization providing materials with smaller pore size distributions and greater surface area.

However, the polymers made using chloroform are solvated to a high degree, and MIPs made without any solvent do not exhibit any selectivity as the substrate cannot access the polymer. Thus, diffusion of substrates through the MIP appears to be fast enough through the chloroform solvated polymers without requiring porosity [99].

Some typical solvents commonly used in the noncovalent approach, together with their dielectric constants and hydrogen bond type are listed in Table 3.4.4.

Table 3.4.4: Physical properties of some solvents commonly used in the non-covalent approach [85].

Solvent	Dielectric constant	Hydrogen bond type	General effect as imprinting solvent
Toluene	2.40	P	+
Methylene chloride	8.90	P	+
Chloroform	4.80	P	+
Acetonitrile	37.50	P	+
Acetic acid	6.20	S	−
Methanol	32.70	S	−
Dimethylformamide	37.00	M	−
Water	80.00	S	−

P = Poor hydrogen bonding solvent, **M** = Moderate hydrogen bonding solvent and **S** = Strong hydrogen bonding solvent.

3.4.5 Initiators

The role of the initiator in radical polymerization is well-known as it is responsible for the creation of monomer radicals in order to propagate the polymer formation. The initiator is homolytically cleaved by thermal decomposition, photolysis or ionizing radiation. These two latter techniques are rarely used for MIP preparation. Mueller *et al.* performed photochemical polymerization with 2,2-azobis(2-methylpropionamidine)dihydrochloride (AAPD) as an initiator [52,100]. Shamsipur *et al.* also made an aminopropyl silica gel react

with 4,4-azobis(4-cyanopentanoic acid chloride) to obtain initiator-modified silica particles

[101]. In most cases, when radicals are produced by thermal decomposition of the initiator,

2,2-azobisisobutyronitrile (AIBN) is used because its temperature of decomposition is

compatible with the polymerization solvents. The chemical structures of selected

polymerization initiation are shown in Figure 3.4.5.

Azobis-(cyclohexanecarbonitrile)
(ACC)

Benzoylperoxide
(BPO)

Azobisisobutyronitrile
(AIBN)
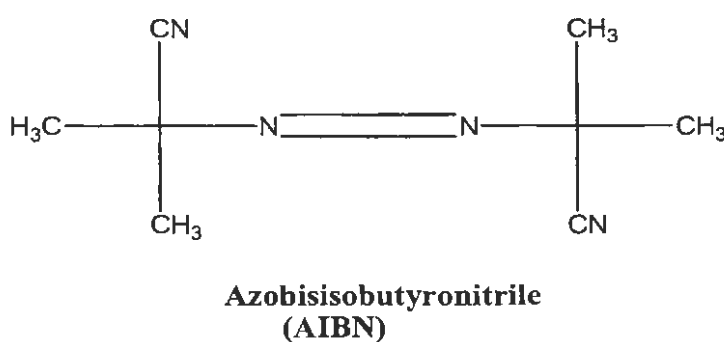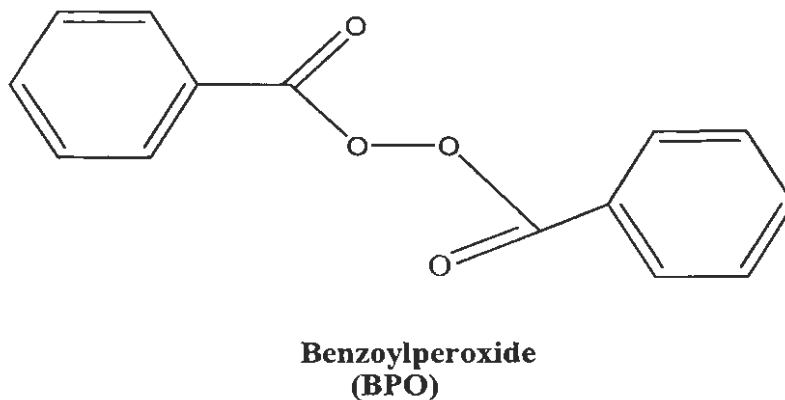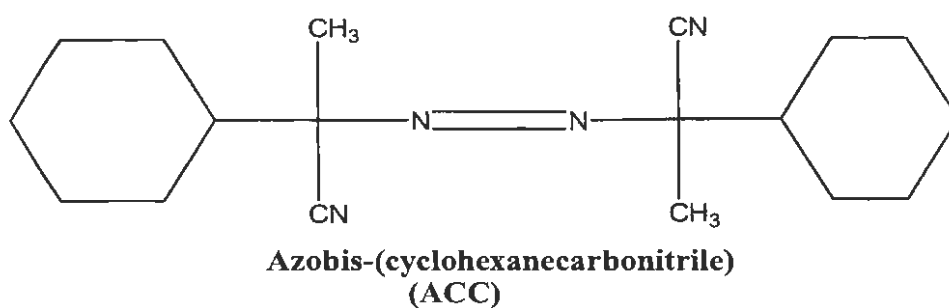
Figure 3.4.5: Chemical structures of selected chemical initiators.

3.4.6 Polymerization temperature

The position of equilibrium between free template-monomer(s) and their corresponding complexes is a product of both temperature and pressure [102]. Several studies have shown that polymerization of MIPs at lower temperatures forms polymers with greater selectivity versus polymers made at elevated temperatures. To polymerize at colder temperatures, it is necessary to use photochemical polymerization.

Mosbach *et al.* [103] presented a study on enantioselectivity of L-phenylalanine anilide imprinted polymers, one polymer being thermally polymerized at 60 ^{o}C, the other photochemically polymerized at 0 ^{o}C. The results of the study showed that better selectivity was obtained at the lower temperatures. The reason for this has been postulated on the basis of Le Chatelier's principle, which predicts that reduced temperatures will drive the pre-polymer complex toward complex formation, therefore increasing the number and possibly, the quality of binding sites formed [104].

3.5 Characterization of molecularly imprinted polymers

This section presents various chemical and morphological characterizations that are commonly employed for MIPs at both pre and post-polymerization stages.

3.5.1 Pre-polymerization characterization of MIPs

In the noncovalent approach the stability of the template-monomer complex formed in the pre-polymerization mixture will govern the resulting binding site distribution and the distribution properties of the imprinted polymer matrix. A close analysis of the pre-

polymerization solution can provide some insights into the various interactions occurring during imprinting.

Furthermore, since the reorganization of functional groups at the binding sites is required during rebinding, the spectral studies before and after rebinding can also shed light on rebinding. Various types of spectrometric techniques such as nuclear magnetic resonance (NMR) [105] and ultraviolet (UV) [106] have been employed to confirm the possible noncovalent monomer-template interactions during MIP synthesis.

3.5.1.1 Ultraviolet (UV)

Template-monomer self assembly has also been studied using UV spectroscopic titrations in order to calculate the dissociation constants for the solution adducts and the relative concentration of fully complexed templates in the polymerization mixture [135]. The main advantage of this technique is its simplicity and the possibility to control template-monomer complex formation in aqueous media [107,108].

Striegler *et al.* characterized by UV spectroscopy and relied on spectrometric data to choose the best ligand for copper capable of providing effective functional monomers for carbohydrate imprinted polymer synthesis [107]. The experimental data firstly estimated the copper-ligand stability in order to select the best ligand, and secondly to evaluate the apparent binding constants between the copper-containing functional monomers and different hexoses in alkaline pH. The complex [(diethylenetriamine) copper(II)] dinitrate appeared to be the most promising monomer for the complexation with sugars, as it was found that the binding involved only hydroxyl groups at C_1 and C_2 of the carbohydrates.

3.5.1.2 Fourier transform infrared (FTIR)

FTIR spectra provide the fundamental analytical basis for rationalizing the mechanisms of recognition during the imprinting process probing the governing interactions for selective binding site formation at the molecular level [109]. FTIR has been used particularly for dissolved samples or in the solid state. The interaction between the functional monomer and template during pre-polymerization complex formation and the template incorporation into the imprinted polymer during rebinding can be confirmed by the characteristic FTIR absorption analysis [96].

Duffy *et al.* characterized by FTIR pre and post-polymerization binding properties of an imprinted membrane for thymine using 2,6-diacyldiaminopyridine as a functional monomer [110]. Liquid spectroscopy clearly showed the three hydrogen bonds linking the monomer and template molecules in the pre-polymerization mixture. The three characteristic bands of the amino groups above 3000 cm^{-1} remained after the polymerization, indicating that the template-monomer complex was still present in the polymer.

However, it should be noted that the presence of a solvent could interfere with the determination of specific characteristics of complexation. Thus, explains why FTIR technique has not been applied extensively to the analysis of pre-polymerization solutions [110,111].

3.5.1.3 Nuclear magnetic resonance (NMR)

The NMR characterization has been applied to the study of the template-monomer interactions [112]. NMR titration experiments are known to facilitate the observation of hydrogen bond formation between bases and carboxylic acid through hydrogen bonding. The studies were introduced in molecular imprinting so as to investigate the extent of

complex formation in pre-polymerization solutions and as a means of identifying the specific sites in interacting structures that engage in complexation [113].

In most of the NMR studies, it has been possible to determine the exact composition of the complex. Nicholls *et al.* investigated in detail the characterization of complexes between nicotine and methacrylic acid [114]. It was shown that template self-association complexes were present in the pre-polymerization mixture and that the extent of template self-association was dependent both upon solvent and the presence of monomer. Thus the dimerization of the template was more stable in chloroform than in acetonitrile due to electrostatic interactions. However, the presence of acetic acid, an analogue of methacrylic acid, resulted in nicotine-nicotine complexes that were stronger in acetonitrile.

3.5.2 Post-polymerization characterization of MIPs

Macroscopic network polymers are notoriously difficult to characterize largely on account of their insoluble and intractable nature. MIPs are no exception. MIPs are solids, and therefore cannot be characterized by more commonly employed polymer characterization methods that would require polymer solutions; e.g gel permeation chromatography, solution NMR techniques and UV measurements directly on the polymers. Furthermore, because MIPs are amorphous, crystallographic or microscopy methods cannot be used to determine the structure of the MIP binding sites, although microscopic techniques like scanning electron microscopy (SEM), transmission electron microscopy (TEM), atomic force microscopy (AFM) have aided the macroscopic understanding of their morphology [115]. Therefore, there are only a limited number of direct physical characterization methods for imprinted polymers. These include nitrogen sorption porosimetry measurements, FTIR spectroscopy, solid state

41

carbon-13 nuclear magnetic resonance cross polarization-magnetic angle spinning (NMR ^{13}C-CPMAS) spectroscopy, swelling and thermogravimetric analysis (TGA).

3.5.2.1 Nitrogen sorption porosimetry

Nitrogen sorption porosimetry involves a fixed mass of dry polymer being exposed to a gas (usually nitrogen) at a series of fixed pressures. By measuring the amount of sorbed as a function of pressure, sorption isotherms can be constructed from which, following application of BET (Brunaure, Emmett and Teller) theory and mathematical models, information on the specific surface area (m^2/g), specific pore volume (ml/g), average pore diameter and pore size distribution can be extracted [92].

The method is particularly useful for analysing in detail medium-sized (meso-) and small (micro-) pores. The IUPAC definitions of size as applied to pores are as follows: micropores <2 nm; mesopores 2-50 nm; macropores >50 nm, and this is well illustrated in Figure 3.5.2.1.
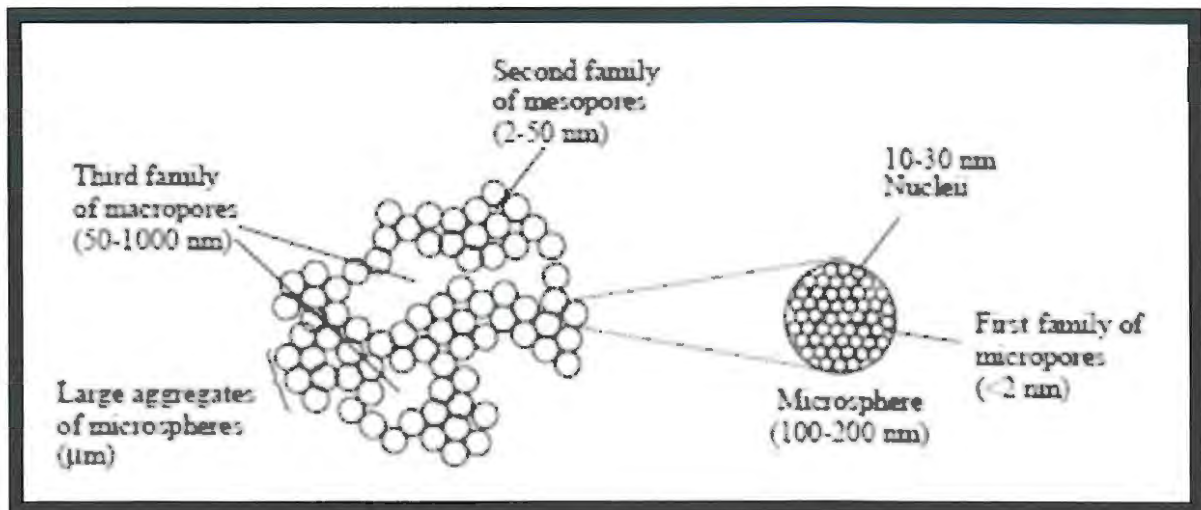
Figure 3.5.2.1: Model of morphology formation that provides the porous network in MIPs [116].

3.5.2.2 Microscopy

Microscopy can be used in a variety of distinct ways to probe imprinted polymers on a variety of length scales. For instance, light microscopy can be used to verify the structural integrity of polymer beads whereas SEM can often be used to image macropores [92].

3.5.2.3 Thermal gravimetric analysis (TGA)

TGA can be used to determine mass changes during a reaction. Typical applications of TGA include the assessment of thermal stability and decomposition temperature, extent of cure in condensation polymers, composition and some information on sequence distribution in copolymers, and composition of filled polymers, among many others [117].

3.5.2.4 Characterization of MIP swelling

The efficiency of a functional polymer is governed by the accessibility of the reactive functional groups anchored on it, which in turn depends upon the extent of swelling and salvation [118]. Swelling in MIPs has most often been measured using volumetric methods published by Sellergren and Shea [115].

There are some difficulties, however, due to buoyancy (i.e. the polymers float) especially for the polymers in chlorinated solvents; and general accuracy of volumetric methods. A more accurate technique that can be used measures changes in volume for a single bead. Its size is then observed under a microscope in the absence and presence of solvent. The particles are then photographed in swollen and unswollen states, and the ratios in surface area calculated to give the percent swelling [119]. In many cases the particles have irregular shape giving wide ranges of different sizes for the particles. Consequently, it is best to follow the same particle from the swollen state to the dry state. Swelling studies are generally carried out in parallel on a non-imprinted polymer (NIP), also referred to as the control or blank polymer. The NIP is obtained by applying the same procedure of polymerization of MIP but in the absence of the template.

3.5.2.5 Solid state NMR

Solid state NMR techniques circumvent the need to work in solution and therefore enable the NMR spectra of insoluble species to be acquired. For network polymers, insight into the different chemical environments present in the sample and information on the degree of chemical cure can be obtained. As far as molecular imprinting work is concerned, solid state NMR has been relatively under-exploited [92].

3.6 Rational design of MIPs (Computational approach)

Computational approach (CA) uses molecular modelling software to design and screen a virtual library of monomers against the desired template. Through CA it is possible to calculate binding energies and predict template-monomer interaction positions, making it easier to select the best functional monomer to be used [120-123]. Following CA approach, polymers with high binding capacity and selectivity have been obtained for different analytes. For example, the study presented recently by Chianella *et al.* [124] where the use of a computational protocol allowed the preparation of a MIP for the drug abacavir with a surprisingly high binding capacity of up to 157 mg of drug per gram of polymer, were remarkable.

In another example, functional ephedrine MIPs were predicted and tested [130]. The best example to date is probably the use of CA to generate MIPs for Microcystin-LR, an algal toxin [125]. This would have been difficult to achieve using conventional imprinting approaches due to the expense and toxicity of the template, but was attempted with some success following virtual imprinting to give likely recipes for successful polymers. A real strength of the approach is its ability to deal with mixtures of functional monomers and predict likely complexes and stoichiometries.

Another consideration of combining molecular imprinting together with electrospinning technique is to enhance the characteristics of the sorbents formed through molecular imprinting technique, and to broaden their usage. By combining both techniques it would be possible to incorporate cavities/binding sites into electrospun fibers.

3.7 Electrospinning

Electrospinning nanotechnology is the most promising of all the methods to fabricate nanofibers. The technique is applicable to virtually every soluble or fusible polymer and is capable of spinning fibers in a variety of shapes and sizes with a wide range of properties to be used in a broad range of biomedical and industrial applications [126,127].

3.7.1 Historical background of electrospinning

In 1600, the first record of the electrostatic attraction of a liquid was observed by William Gilbert [186]. Christian Friedrich Schönbein produced highly nitrated cellulose in 1886. In 1887 Charles Vernon Boys described the process in a paper on nanofiber manufacture. John Francis Cooley filed the first electrospinning patent in 1900. Between 1931 and 1944 Anton Formhals took out at least 22 patents on electrospinning. In 1938, N.D. Rozenblum and I.V.Petryanov-Sokolov generated electrospun fibers, which they developed into filter materials [128].

Between 1964 and 1969 Sir Geoffrey Ingram Taylor pioneered the beginnings of a theoretical underpinning of electrospinning by mathematically modelling the shape of the (Taylor) cone formed by the fluid droplet under the effect of an electric field. In the early 1990s several research groups (notably that of Reneker who popularised the name electrospinning) demonstrated that many organic polymers could be electrospun into nanofibers. Research on electrospinning gained momentum in past decade due to increased knowledge on the application potential of nanofibers in various fields such as high efficiency filter media, protective clothing, catalyst substrates, and adsorbent materials. There are currently over 80 patents filed on various aspects of electrospinning in the United State alone [129].

3.7.2 Description of the electrospinning process

In the electrospinning process, an electric field is generated between the polymer solution contained in a syringe and a metallic collection plate by connecting the spinneret of the syringe to a high voltage power supply as shown in Fig. 3.7.2. Charge is induced on the liquid surface by an electric field. Mutual charge repulsion causes a force directly opposite to the surface tension. As the intensity of the electric field is increased, the hemispherical surface of the solution at the tip of the spinneret elongates to form a conical shape known as the Taylor cone [130].

When the electric field reaches a critical value at which the repulsive electric force overcomes the surface tension force, a charged jet of the solution is ejected from the tip of the Taylor cone. Since this jet is charged, its trajectory can be controlled by an electric field. As the jet travels in air, the solvent evaporates, leaving behind a charged polymer fiber which lays itself randomly on a collector. Thus, continuous fibers are laid to form a non-woven fabric.
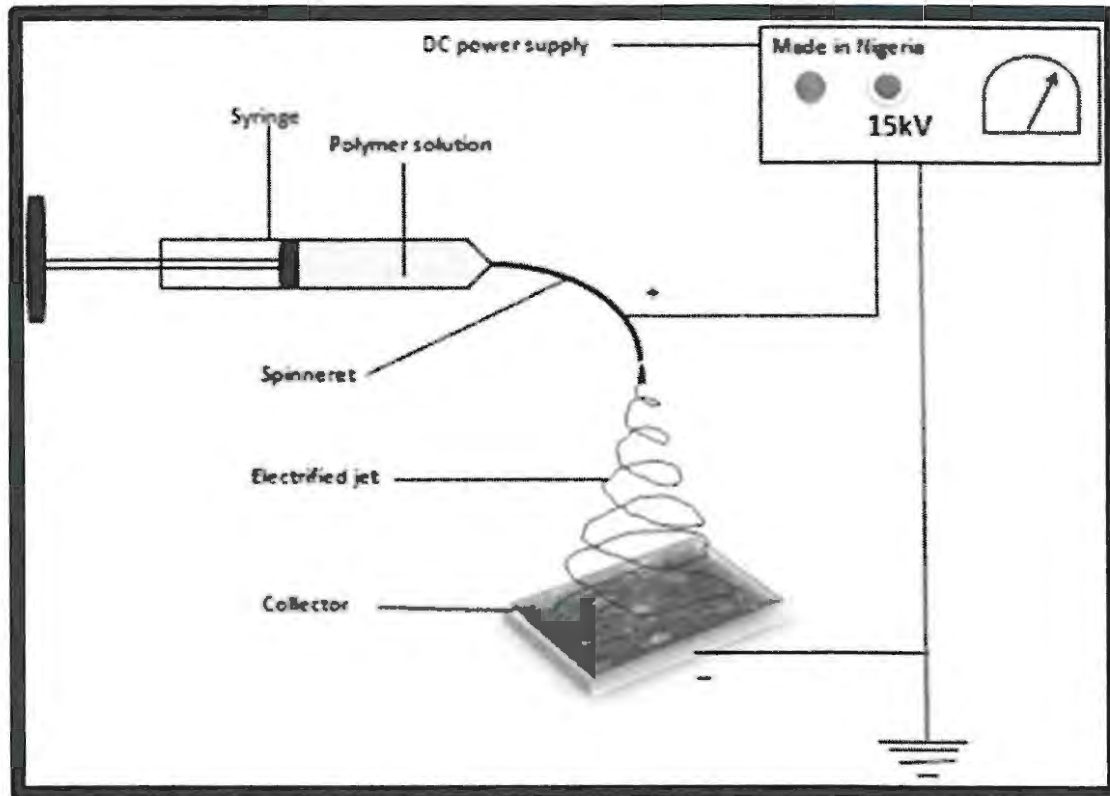
Figure 3.7.2: A schematic diagram of a typical electrospinning setup

3.8 Physical principle of the electrospinning process

Electrospinning is a highly coupled process involving high speed nonlinear electrohydrodynamics, complex rheology, and transport of charge, mass, and heat within the jet. The process consists of three stages: jet initiation, jet elongation with or without branching and/or splitting, followed by solidification of jet into nanofibers. Studies conducted by Rayleigh [131], Zeleny [132], and Taylor [130] provided insight into the behaviour of the liquid jets.

3.8.1 Jet initiation

Taylor showed that a conical surface, referred to as the Taylor cone, is formed with an angle of 49.3° when the droplet is subjected to an external electric field (Fig. 3.8.1). Due to the

48

application of the electric field, a charge is induced on the surface of the drop. This charge offsets the forces of surface tension and the droplet changes shape from spherical to conical [133].
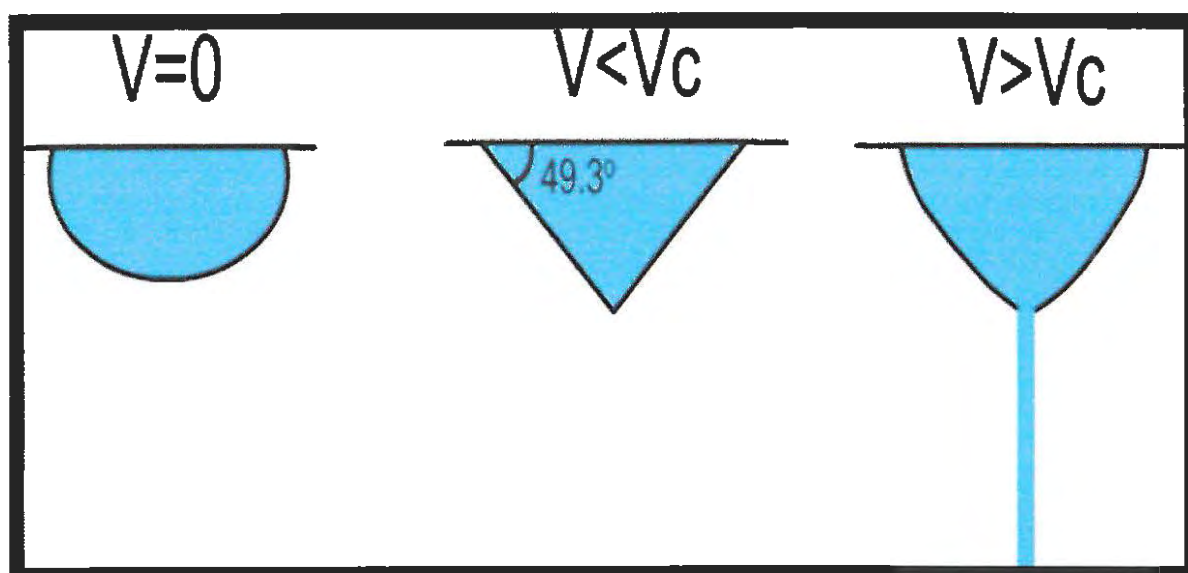
Figure 3.8.1: Changes in the polymer droplet with applied potential [149].

When the intensity of the electric field (V) attains a certain critical value (Vc), the electrostatic forces overcome the surface tension of the polymer solution and force the ejection of the liquid jet from the tip of the Taylor cone. The highest charge density is present at the tip of the cone from where the jet is initiated [134]. Taylor showed that Vc (in kilovolts) is given by

49

$$Vc^2 = 4\left(\frac{H^2}{L^2}\right)\left(\ln\frac{2L}{R} - 1.5\right)(0.117\pi R\gamma)$$ eqn 3.1

where H is the air-gap distance, L is the length of the capillary tube, R is the radius of the tube (units: H, L, and R in centimetres), and γ is the surface tension of the fluid (dyn/cm).

The Taylor cone angle was independently verified by Larrondo and Manley, who experimentally observed that the semivertical cone angle just before jet formation is 50° [135-137]. In another publication, it was reported that the Taylor cone's angle should be 33.5° instead of 49.3° [138].

3.8.2 Jet thinning

Parameters such as solution concentration, field strength, flow rate, jet velocity and shear rate impact the electrospinning process. In the case of low molecular weight fluids, the rate at which the radius of an electrostatically driven jet decays depends on the flow rate of the polymer solution. If the flow rate is slow, the radius of the jet decays very rapidly. On the other hand, if the flow rate is fast, the radius of the jet decreases slowly. Deitzel et al. [139] explained this phenomenon by assuming a simple cylindrical geometry to represent the volume element of the electrospinning jet.

From Eq. 3.2, the ratio of surface area to volume ratio (specific surface area) is inversely proportional to the jet radius. Therefore, an increase in the jet radius results in a corresponding decrease in the specific surface area associated with that specific volume

element. If the density of the polymer solution and the surface charge density are assumed to be constant, then it follows that the charge to mass ratio will decrease with increasing jet radius. From Eq. 3.3, the acceleration is directly proportional to the ratio of charge to mass; hence, an increase in jet radius results in a decrease in the acceleration of the fluid [139].

$$\frac{A}{V} = \frac{2}{R} \, ,$$

<div align="right">eqn   3.2</div>

where A is the surface area of the cylindrical volume element, V is the volume, and R is the radius of the jet,

$$a = E\left(\frac{q}{m}\right),$$

<div align="right">*eqn*   3.3</div>

where a is acceleration, E is the electric field strength, q is the available charge for the given volume element, and m is the mass of a given volume element.

It should be noted that the simplified model of a cylinder was only meant to provide a gross illustration of the interaction between the solution feed rate, electrospinning voltage, and the charge to mass ratio. This idea is consistent with the results reported by Baumgarten [140]. His experiments illustrated that as the viscosity of the polymer solvent decreased, the spinning drop changed from hemispherical to conical. By using equipotential line approximation calculations, he obtained an expression to calculate the radius r_0 of a spherical drop as follows:

$$r_0^3 = \frac{4\varepsilon m_0}{k\pi\sigma\rho} ,$$

<div align="right">*eqn* 3.4</div>

where ε is the permittivity of the fluid (C/V cm), m_0 is the mass flow rate (g/s) at the moment, where r_0 is to be calculated, k is a dimensionless parameter related to the electric currents, σ is the electric conductivity (A/V cm), and ρ is the density (g/cm^3).

3.8.3 Jet instabilities

The travelling liquid jet stream is subject to a variety of forces with opposing effects; as a result, various fluid instabilities also occur in this stage [141]. The jet may undergo splitting into multiple subjects in a process known as splaying or branching [142]. This happens when changes occur in the shape and charge per unit area of the jet due to its elongation and the evaporation of the solvent. This shifts the balance between the surface tension and the electrical forces, and the jet becomes unstable. In order to reduce its local charge per unit surface area, the unstable jet ejects a smaller jet from the surface of the primary jet [142].

Hohman *et al.*[143,144] and Shin *et al.*[145] investigated the stability of electrospinning PEO jet and concluded that the possibility for three types of instabilities exists. The first is the Rayleigh instability, which is axisymmetric with respect to the jet centreline. The second is also an axisymmetric instability and the third is a nonaxisymmetric instability, called "whipping" instability, mainly by the bending force. Rayleigh instability occurs due to opposing forces acting on the surface area of the jet. Electrostatic repulsion of the charges in the jet tends to increase its surface area.

On the other hand, the surface tension tends to reduce the total surface area of the jet. Therefore, instability occurs, which causes the jet to break up into droplets, each with a surface area minimizing spherical shape. This effect is known as Rayleigh instability [131].

3.8.4 Jet solidification

The solidification of the jet results in the deposition of a dry nanofiber on the collector. The solidification rate varies with the polymer concentration, electrostatic field, and gap distance. Yarin *et al.* used a quasi-one-dimensional equation to describe the mass decrease and volume variation of the fluid jet due to evaporation and solidification, by assuming that there is no branching or splitting from the primary jet. They also reported that the cross-sectional radius of the dry fiber was 1.31×10^{-3} times that of the initial fluid jet [146].

Conglutination is the process by which partially solidified jets can produce fibers that are attached at points of contact. Strong attachments at crossing points stiffen the mat. This is an important factor in determining the mechanical properties of the nonwoven structure. After the onset of bending instability, the jet path may follow a very complicated path and successive loops of coil may touch in flight and form permanent connections. The resulting network formed is called a garland (Figure 3.8.4) [147].
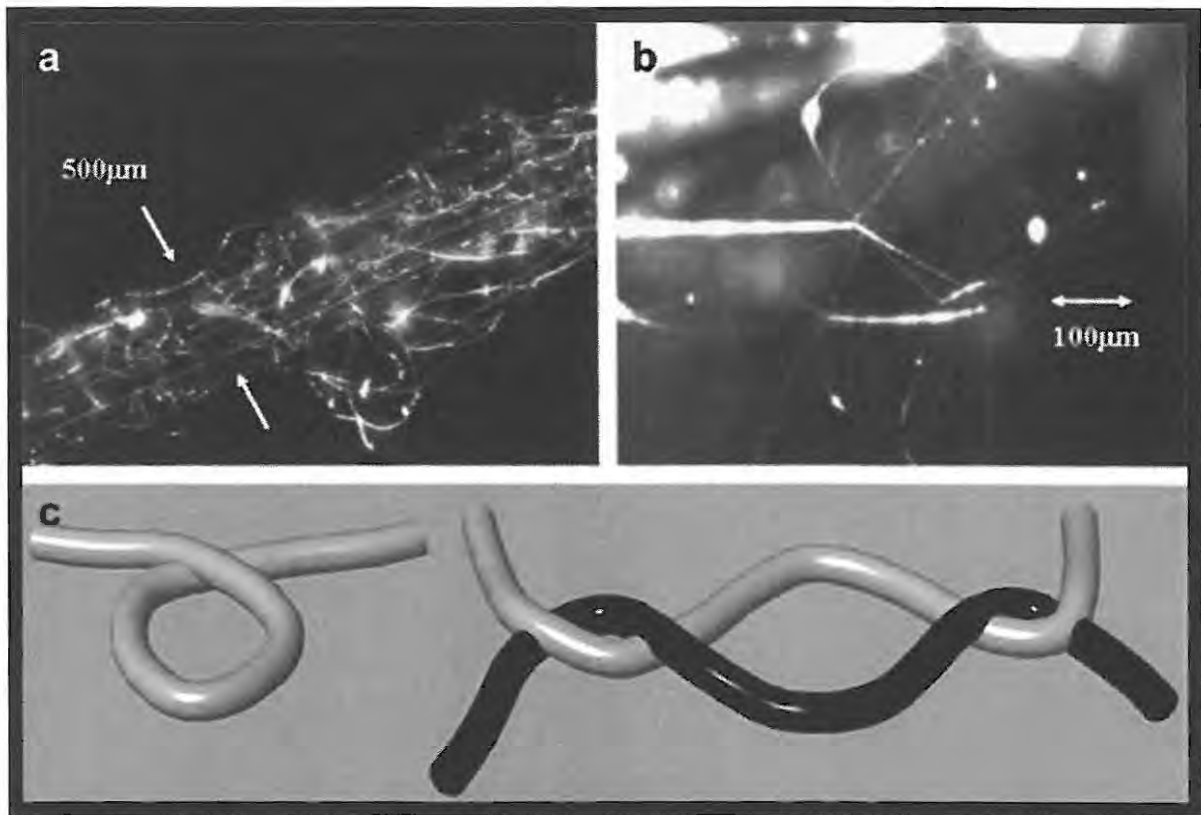
Figure 3.8.4: (a) A short segment of a garland yarn, (b) details of the conglutinated solid fibers, and (c) a diagram of a loop in a segment of one fiber and another loop [147].

3.9 Electrospinning innovations and modifications

Several innovative electrospinning processing techniques to enhance the function and properties of electrospun fibers have been described in this section. Desirable physical and biological properties of electrospun nanofibrous scaffolds can be obtained by using the innovations.

3.9.1 Coaxial electrospinning

In the process of coaxial electrospinning, two polymer solutions can be coelectrospun without direct mixing, using two concentrically aligned spinnerets. The same voltage is applied to both metal spinnerets and it deforms the compound droplet on the top of tip. A

jet is generated on the tip of the deformed droplet, and in an ideal case, a core-shell nanofiber is created [148]. The experimental setup is shown in Figure 3.9.1.

The electrospinning of a concentric jet solution was first reported by Sun *et al.* [149]. They successfully created coaxial fibers made of combinations of different materials, PEO-poly(dodecylthiophene), PLA-palladium, and PEO-polysulfone, or of a composition of identical polymers (PEO-PEO) contrasted by dyeing agents such as bromophenole. The fabrication of a core shelled structure with polycaprolactone (PCL) as the shell and gelatine as the core was fabricated by Zhang *et al.* [150].
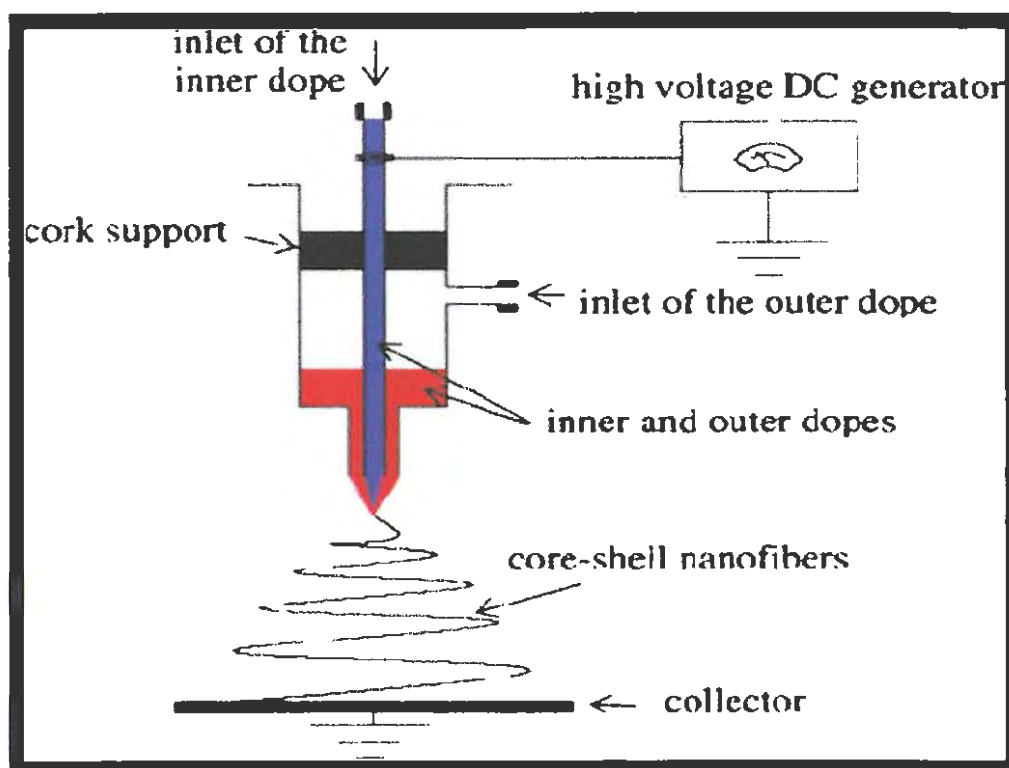
Figure 3.9.1: Experimental setup for coelectrospinning to produce core-shell nanofibers [150].

3.9.2 Multilayer and mixed electrospinning

In mixed electrospinning, two or more different polymers solutions can be electrospun from two or more different polymer syringes under different processing conditions (Figure 3.9.2). Multilayer and mixed electrospinning was first demonstrated by Kidoaki *et al.* to fabricate scaffolds containing three different polymers, segmented PU, styrenated gelatine, and type 1 collagen for use as an artificial blood vessel [151].

The resulting fibrous mesh consisted of layers sequentially deposited on the same target collector. Moreover, multilayer electrospinning has been studied using PCL, PLA, PDO, poly(glycolide-*co*-trimethylene carbonate), gelatine, and elastin. These studies demonstrated different uses of multilayered techniques. Smith *et al.* [152] electrospun PDO-elastin bilayered constructs with a suture wound in the center for reinforcement. Yang *et al.* [153] created a layered structure of polymers and cells by electrospinning PCL and collagen together, seeding human dermal fibroblasts, and then repeating the polymer and cell layers. These cellularized constructs were produced in sheet form and not with tubes. Thomas *et al.* [154] utilized PGA, elastin, and gelatin in a three layered form.

However, the use of PGA and gelatine would not be conducive to an arterial graft as gelatin, *in vivo*, has been shown to display a large cytotoxic response and PGA is a rapidly degrading polymer that would result in arterial graft failure due to loss of mechanical integrity [155]. McClure *et al.* successfully fabricated multilayered electrospun conduit composed of PCL blended with elastin and collagen in the ratio 45:45:10, and 65:25:10, with distinct material properties for each layer. It was demonstrated that these layers changed the overall graft properties with regard to suture retention and compliance, containing values that were within the range of native artery [156].
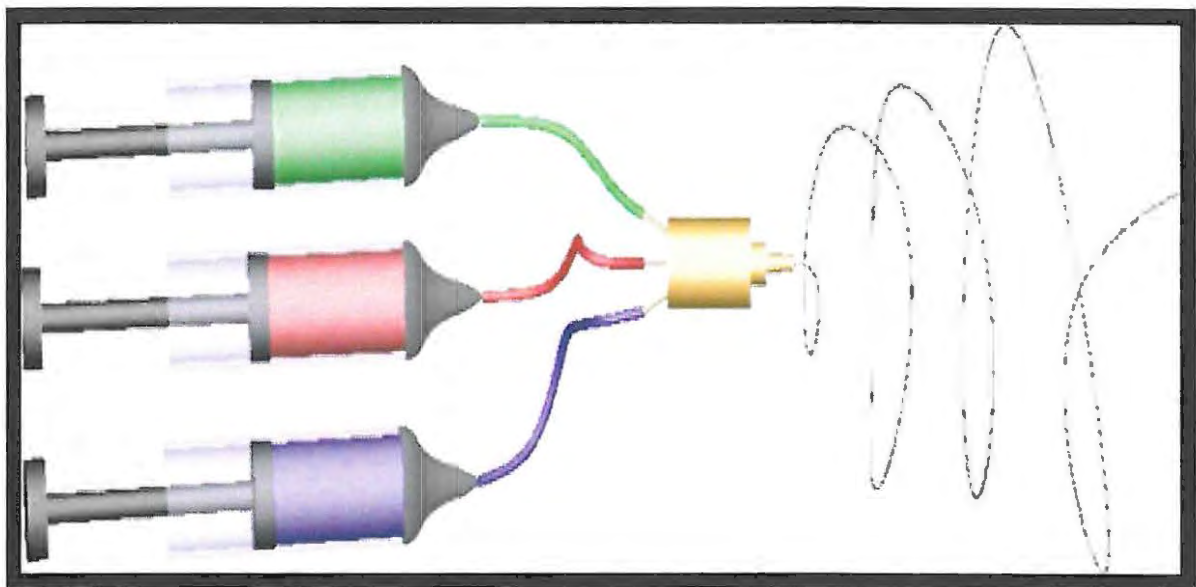
Figure 3.9.2: Multiple syringe electrospinning setup depicting a three syringe input and a single needle output [156].

3.9.3 Force air assisted electrospinning

The method has been used for the electrospinning of aqueous hyaluronic acid (HA) that could not be electrospun using conventional electrospinning due to its very high solution viscosity and high surface tension at fairly low solution concentrations [157]. In this process, air flows parallel to the straight portion of the jet concentrically surrounding the polymer. The experimental setup is shown in Fig. 3.9.3. In the study, the air-blowing system was attached to the regular electrospinning apparatus. This resulted in the modified apparatus having two simultaneously applied forces, an electrical force and an air-blowing shear force, to fabricate the nanofibers. The air blow system consisted of two components, a heater and a blower. The air generated by the blower was heated by passing it through the heating elements.

It was found by Um *et al.* [157] that the combination of air-blowing force and the applied voltage was capable of overcoming the high viscosity as well as the high surface tension of the HA solution. In addition, the elevated temperature of the blowing air could further reduce the solution viscosity of the HA solution. The air could also aid in faster solvent evaporation. Thus, the fiber diameter could be customized by controlling the flow rate and temperature of the blown air.
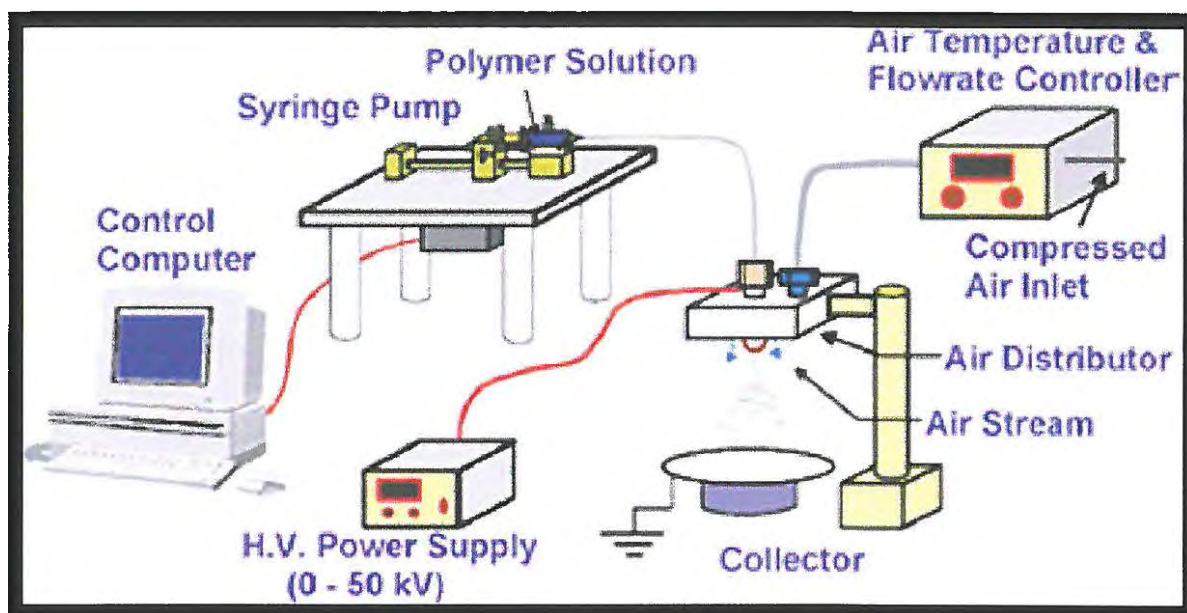
Figure 3.9.3: Experimental setup of forced air assisted electrospinning system [157].

3.9.4 Air-gap electrospinning

Huang *et al.* [158] first developed an approach for fiber alignment by using a rectangular frame structure under the spinning jet. Sell *et al.* [159] described the use of an "air-gap" electrospinner for ligament tissue engineering. Jha *et al.* [160] fabricated nerve guides of PCL using an air-gap electrospinner. The electrospinner (Figure 3.9.4) allowed the creation

of three-dimensional constructs composed of highly aligned nanofibers, as opposed to creating compacted aligned constructs through traditional electrospinning techniques.

Air-gap electrospinning requires the charged spinneret of the polymer solution to be placed equidistant from a pair of conductive parallel targets. Due to the electric field, the electrospinning jet stretches itself across the air gap and deposits aligned fibers between the charged targets. The charge of the individual fibers creates a mutual repulsion, which enhances their ability to align and be distributed evenly. Using this method, the electrospun scaffold obtained is similar in both overall size and shape as the parallel collecting electrodes. Thus, the shape of the scaffold can be altered by changing the profile of the electrodes. In the air-gap electrospinning system, two stepper motors are mounted on the individual towers to provide rotation of two stainless steel targets (one target per motor). The rotation of the steel targets in the same direction allows for constructs to be created evenly through 360° of rotation or for the stepper motors to be run in opposing directions for a winding action of the constructs to take place during electrospinning.

The towers have the ability to translate as well as rotate in order to create structures of different shape and size. Simply by changing the direction and speed of electrode rotation, it is possible to create a number of unique wound and multilayered electrospun constructs with macrostructures significantly different from those created through traditional electrospinning, while maintaining the same microstructure that makes traditional electrospinning so beneficial for tissue engineering.
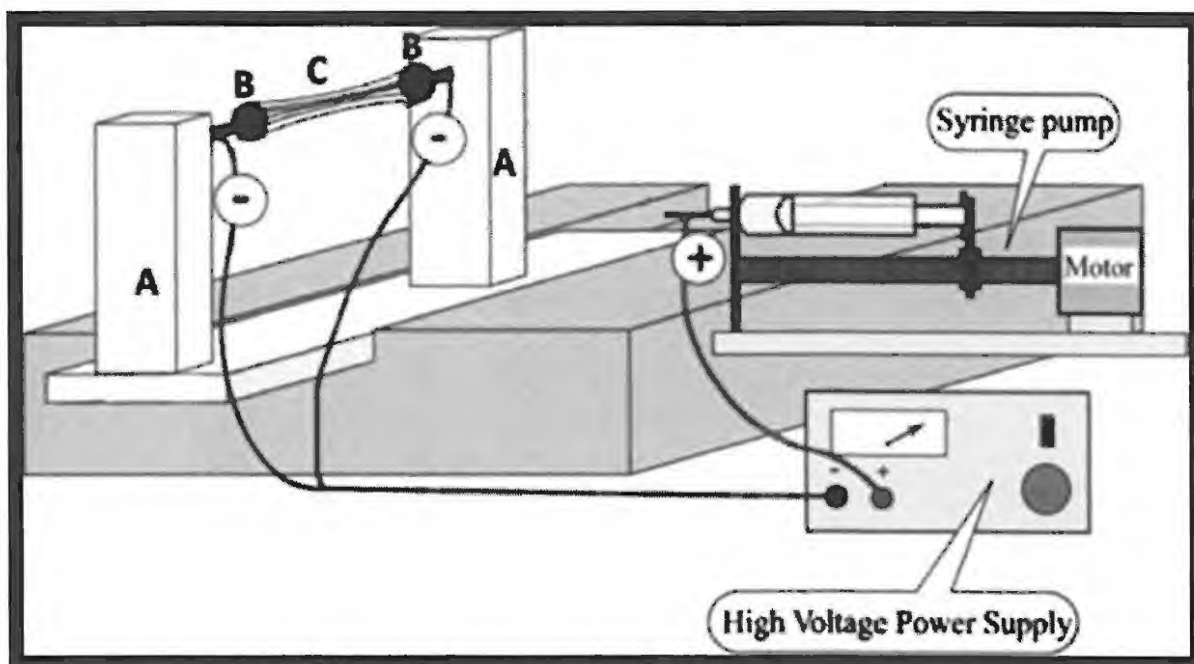
Figure 3.9.4: Air-gap electrospinner setup [160].

3.10 Combined technique of imprinting and electrospinning

There is currently research interest in nanomaterials as their small physical size often offers improved and even new functions that cannot be achieved with bulk materials. In this respect, nanomaterials bearing tailor-made molecular binding properties are very attractive because they can potentially be used to substitute biological receptor molecules to afford high specific target recognition in different applications, e.g. affinity separations, substrate and enantioselective catalysis, assays, and development of biomimetic sensors [161]. Among the different synthetic strategies that are presently studied, molecular imprinting and electrospinning are probably the most straightforward for the purpose of producing nanostructured materials that have predesigned molecular recognition capabilities. Yoshimatsu *et al.* [162] reported that molecularly imprinted nanoparticles were encapsulated inside polymer nanofibers using an electrospinning method. Silvia *et al.* [163]

described polymer nanofibers with entrapped molecularly imprinted polymer nanoparticles and studied their possible use in a fluorescence-based biosensor application.

Most recently the electrospinning technique was applied to the imprinting field by Chronakis et al. [164]. Here electrospun nanofibers were prepared from a mixed solution of poly(ethylene terephthalate) (PET, as a supporting matrix for fiber formation) and polyallylamine (providing functional groups) in the presence of a template molecule, 2,4-dichlorophenoxyacetic acid.

Compared with imprinted microparticles, the imprinted electrospun nanofibers have tunable flexibility of shapes and sizes. The imprinted nanomaterials have also better dispersibility in analyte solutions and thus greatly reduce the resistance of mass transfer [165,166]. Consequently, imprinted electrospun nanofibers are excellent candidates for application in different fields such as biomedical, analytical chemistry, separation sciences and purification.

Chang et al. [167] reported the development of molecularly imprinted polyimide nanofibers prepared by electrospinning using naturally occurring estrogen, called estrone as template molecule and investigated the effects of polyimide structures on binding affinity. Actually, this approach provided new application possibilities for imprinted electrospun nanomaterials.

Thus, to further enhance the selectivity, reusability, and mechanical stability of the imprinted nanomaterials, our research group has successfully fabricated crosslinked electrospun imprinted nanomaterials through strategic imprinting process designs for the

clean-up of metalloporphyrins from organic media as shall be demonstrated in the next

chapter.

4

Experimental

4.1 Overview

This chapter introduces the specific analytes of interest in this thesis together with the materials and methods used in the research. It also describes the experimental procedures that were employed.

4.2 Specific analytes of interest

4.2.1 Vanadyl and Nickel Tetraphenylporphyrins (VTPP and NTPP)

Metalloporphyrins have been observed in various branches of science and industry. Their removal from crude oil is important not only from the scientific point of view but also from both economic and environmental standpoints. Crude oil contains a large variety of metallic compounds with vanadium and nickel being the major metals [168]. Some 6–34 % of total vanadium and nickel content is made up out of metalloporphyrins (see Fig. 4.2.1 for structure) [169].

Five main types of metalloporphyrins have been reported in the literature to be present in crude oil. These are etioporphyrins (Etio), octaethylporphyrins (OEP), deoxophyllocrythroetioporphyrins (DPEP), benzoetioporphyrins (Benzo), and tetraphenylporphyrins (TPPs), with TPPs as the predominant species [170]. Among this group of TPPs, vanadyl and nickel TPPs were found to be the most abundant and undesirable [9]. While the presence of vanadyl and nickel TPPs in crude oil can cause environmental pollution, they also negatively affect catalyst selectivity during the refining process. In addition, TPPs compounds can adversely affect fuel stability [171].

In order to address the detrimental effect associated with vanadyl and nickel TPPs, a sample preparation step employing cheap, rapid and selective materials is needed. Molecularly imprinted sorbents have been identified as examples of such materials. They have been

shown to be suitable candidates for sorbent material hence providing a selective clean-up and pre-concentration step for samples normally associated with complex matrices.

This thesis presents experimental procedures for the preparation and evaluation of the effectiveness of a simple and cheaply prepared imprinted sorbents that are suitable for analytical applications.

NTPP   **VTPP**
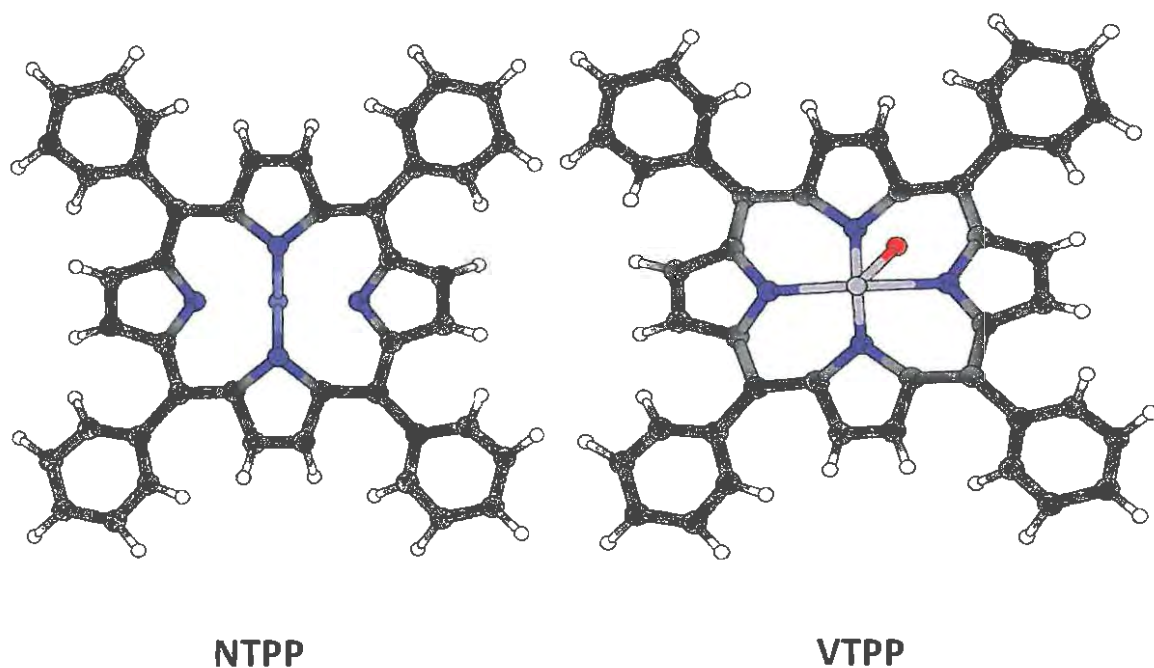
Figure 4.2.1: Molecular structures or geometries of Vanadyl and nickel tetraphenylporphyrins.

4.3 Materials

4.3.1 Chemicals and reagents

All the chemicals were of analytical grade and were used without any further purification. Styrene (99%), divinyl benzene (DVB) (80%), 1,1'azobis(cyclohexanecarbo-nitrile) (ACC) (98%), vanadyl tetraphenylporphyrin (VTPP: M_w 679.67, CAS 14705-63-6), nickel

tetraphenylporphyrin (NTPP: M_w 671.41, CAS 14172-92-0), chloroform (99%), methanol (MeOH) (99.8%), acetic acid (AA) (99.7%), trifluoroacetic acid (TFA) (99%), dichloromethane (DCM) (99.8%), dimethyl sulphoxide (DMSO) (99.7%), and pentane (PEN) (99%) were supplied by Sigma–Aldrich (Johannesburg, South Africa).

Standard solutions were freshly prepared using ultrapure water generated from MilliQ systems (Massachusetts, USA). All glassware was soaked overnight in 4 M HNO_3 solution prior to use. Working standards of metal solutions were freshly prepared from stock solutions.

4.3.2 Polymers

Poly(ethylene terephthalate) (PET: 50,000, CAS 25038-59-9) and linear-polyethylenimine (L-PEI: 2,500, CAS 9002-98-6) were supplied by Sigma-Aldrich (Johannesburg, South Africa). All the polymers were used as received. Polymer solutions were prepared by dissolving known masses of the polymer (pellets or powder) in appropriate volumes of solvents by slowly agitating the solution using Stuart SB-162 magnetic stirrer (Staffordshire, UK).

4.4 Instrumentation

4.4.1 Electrospinning setup

Single nozzle set-ups (Fig. 4.4.1) consisting of an infusion pump KD Scientific Syringe Pump Series 100 or New Era Multi-phaser NE-1000, Farmingdale, (NY, USA) and high voltage source (Glassman High Voltage Inc. Series EL). The collector system was a flat aluminium sheet placed on a support. Electrospinning was carried out at room temperature (293 ± 2 K).

Figure 4.4.1: Electrospinning setup.

4.4.2 Fourier Transform Infrared (FTIR) spectroscopy

FTIR spectra (4000–400 cm-1) of the MIP/NIP particles and nanofibers were recorded by a

Perkin-Elmer 100 FTIR spectrophotometer Waltham, (MA, USA) with an AutoIMAGE system

to confirm the formation/disappearance of bonds.

4.4.3 ^{13}C-NMR spectroscopy

^{13}C-NMR spectra of the preblending mixtures of both the MIP and NIP were recorded on a Bruker (Rheinstetten, Germany) AVANCE 400 MHz spectrometer to confirm the exact assignment of the carbons.

4.4.4 Scanning electron microscopy

Morphology of the MIP/NIP particles and nanofibers was studied using a VEGA TESCAN TS5136ML (Brno, Czech Republic) SEM instrument. Prior to the SEM analyses, the samples were sputter-coated with a gold layer using Balzers Union FL-9496 (Liechtenstein, Germany). Energy dispersive X-ray spectroscopy (EDX) (INCAPentaFET×3 Oxford ISIS EDS) was used to observe the chemical composition of products.

4.4.5 Elemental analysis

Elemental analysis was performed directly with a Vario Elementar Microtube ELIII Series (Hanau, Germany) after carefully drying the samples. The calibration of the instrument was carried out employing sulphanilamide and acetanilide standards.

4.4.6 Pore size analysis and BET surface area

Surface areas and pore characteristics of the MIP/NIP particles and nanofibers were determined using the Brunauer-Emmet-Teller (BET) isotherms obtained from nitrogen adsorption on an Accelerated Surface Area and Porosimetry System (ASAP 2020), Micromeritics (Norcross, GA, USA). Prior to analysis, about 0.3 g portions of samples were

degassed overnight at 180 °C, and specific surface areas were derived from N_2 gas adsorption–desorption isotherms (p/p_o = 0.05–0.20).

4.4.7 Thermal gravimetric analysis (TGA)

TGA of the MIP/NIP particles and nanofibers was carried out using a Diamond TG/DTA (Perkin-Elmer) analyzer at a heating rate of 10 °C min^{-1} in a high-purity nitrogen and air atmosphere.

4.4.8 Differential Scanning Calorimetry analysis (DSC)

DSC analysis of the MIP/NIP particles was carried out using a DSC–60 scanning calorimeter (Shimadzu) at a heating rate of 10 °C min^{-1} in a high-purity nitrogen and air atmosphere.

4.4.9 Inductively Coupled Plasma-Optical Emission Spectrometry (ICP-OES)

ICP-OES analyses were carried out using an iCAP 6000 series Inductively Coupled Plasma-Optical Emission Spectrometer from Thermo Electron Corporation (Cheshire, United Kingdom). The ICP-OES was equipped with a cross flow "high solid" pneumatic nebulizer fitted to a Scott-type double pass chilled spray chamber. For chloroform introduction, an ultrasonic nebulizer U-5000 AT+ (*CETAC*, Omaha, USA) was used. Table 4.4.8 shows the detailed operational conditions of the ICP-OES.

Table 4.4.8: Detailed operational conditions of the ICP-OES

Analysis preferences				
Sample options	Number of repeats:	3		
	Sample flush time:	30s		
Source	Light source:	ICAP		
	Plasma view:	Axial		
Analysis maximum	Low WL Range	Axial 15	Radial	15
Integration times (s)	High WL Range	Axial 5	Radial	5
Calibration mode	Concentration			
Trailing full flame	Intelli-Flame:	Yes		
Options	Max integration time (s):	30		
	WL Range:	Low		
	View:	Axial		
	Source settings			
Nebulizer pump	Flush pump rate (rpm:)	100		
	Analysis pump rate (rpm):	50		
	Pump relaxation time (s):	5		
	Pump tubing type:	Tygon Orange/white		
RF Power:	1150 W			
Auxiliary gas:	0.5 L/min			

4.5 Conductivity, surface tension and viscosity

Conductivity of the solutions was measured using a Mettler Toledo FE 30/EL 30 conductivity meter (Polaris, Columbus). The solutions' shear viscosity and surface tension were measured using a Brookfield Digital viscometer Model DV–1+(at 5.0 rpm) and a KRÜSS School Tensiometer K6, respectively.

4.6 Computer simulation

All computations were carried out on computers with 2GB RAM memory and 150 GB hard disk. Three-dimensional structures were drawn using InsightII visual interface Accelerys. Geometries of all compounds were optimized using the density functional theory (DFT) with B3LYP/6-31G(d) hybrid functional implemented in the Gaussian 03 program.

4.6.1 Design of the pre-polymerization complexes

In order to understand the properties of MIPs at the molecular level, a model of the template-monomers pre-polymerization complexes was set up. In the complexes one template molecule is surrounded by five monomer molecules, taking into account the molar ratio used in the synthetic procedure. Simultaneously, the proposed relationship should allow the formation of as many π-π interactions as possible between the monomers and the template functional groups.

The complexation energies ΔE_C were calculated using Eq. (4.1) as follows:

$$\Delta E_C = E_{Complex} - E_{template} - n.E_{monomer} \qquad\qquad eqn\ 4.1$$

where $E_{complex}$ = energy of the template-monomers complex, $E_{template}$ = energy of free template, $E_{monomer}$ = energy of free functional monomer, n = number of functional monomers in the complex (n=5).

71

4.7 Preparation of MIP particles and molecularly imprinted nanofibers

4.7.1 Preparation of VTPP MIP particles

For the synthesis of the MIP, a thermal bulk polymerization method was employed with styrene and divinyl benzene as the functional and cross linking monomers in the optimal ratio, 1:5 respectively, ACC as initiator, VTPP as the template molecule, and chloroform as the porogenic solvent. The mixture was stirred and ultrasonicated until all the solids were dissolved, and subsequently cooled in an ice water bath (to prevent evaporation). Afterwards, the mixture was purged with nitrogen for 5 min and the tube was sealed and transferred into a heating/stirring module, heated at 70 $^{\circ}$C for 18 h. After the polymerization process, the resultant polymer monolith was ground to powder with particle sizes of ≤ 45 μm in diameter, and then exhaustively washed by refluxing for 14 h with a mixture of MeOH and acetic acid for template removal. Thereafter the particle was left to dry in open air overnight ready to be used for the batch rebinding experiments. As control, NIP was also prepared following the same procedure excluding the use of a template during the polymerization process.

4.7.2 Preparation of NTPP molecularly imprinted electrospun nanofiber (MIN)

For the fabrication of the MIN, poly(ethylene terephthalate)/linear-polyethylenimine solution was prepared by adding 1.5 g of PET and 1.5 g of L-PEI to a 2:8 mixture of DCM and TFA (v/v) with continuous agitation in a closed vial for 5 h at room temperature. The

solution of the MIP containing the cross-linker, monomer, initiator and NTPP as the template molecule (for the different NTPP and styrene molar ratio) in chloroform was blended into the PET/L-PEI solution and stirred overnight (Table 4.7.2). The resulting homogeneous solution was electrospun into nanofiber. The applied voltages used for the electrospinning were 12 kV and 15 kV at the needle tip, and the tip-to-collector distance was 13 cm. The electrospun fiber mat was dried under vacuum at room temperature to remove traces of solvent and kept in a desiccator until analysis. As a control, non-imprinted nanofibers (denoted "NINs") were prepared according to the same procedure but without using NTPP as a template.

Table 4.7.2: Fiber compositions with different NTPP and styrene molar ratios

Fiber	Template:monomer	NTPP (mmol)	Styrene (mmol)	PET (g)	L-PEI (g)
MIN1	1:1	0.48	0.48	1.5	1.5
MIN2	2:1	0.96	0.48	1.5	1.5
MIN3	3:1	1.44	0.48	1.5	1.5
NIN	-	-	0.48	1.5	1.5

4.7.3 Preparation of multiply templated molecularly imprinted electrospun nanofiber (NVMIN)

For the fabrication of the NVMIN, two different template molecules were employed, namely, VTPP and NTPP. The PET/L-PEI solutions were prepared in TFA and some mixed solvent systems of TFA and another solvent or liquid (i.e., DMSO, DCM, and PEN) in various compositional ratios. The solution of the MIP as mentioned in section 5.7.2 and the

73

templates in chloroform was blended into PET/L-PEI solutions and stirred overnight. Non-imprinted nanofibers were prepared following the same procedure without VTPP and NTPP as templates.

4.8 Template removal

Different methods were employed for the removal of templates from the MIP particles and molecularly imprinted electrospun nanofibers.

4.8.1 Template removal method for VTPP MIP particles

To remove the template molecule, the MIP particles were exhaustively washed by refluxing for 14 h with a mixture of MeOH and acetic acid (90:10, v/v). The cooled reaction mixture was centrifuged and the supernatant liquids were tested until no VTPP template was observed to leach from the polymer using a UV-vis spectrophotometer. Then, the polymer was washed several times with pure MeOH to remove the acetic acid and facilitate drying.

4.8.2 Template removal method for molecularly imprinted nanofibers

The molecularly imprinted nanofibers were immersed into a solvent mixture of MeOH and acetic acid for 18 h on a micro-processor controlled orbital platform shaker. Then, the nanofibers were removed and the solutions were tested until no templates were observed to leach from the fiber using ICP-OES. Then, the nanofibers were washed several times with pure MeOH to remove the acetic acid and facilitate drying.

4.9 Swelling analysis of the MIP particles

The solvent swell ratio were evaluated for chloroform, methanol, and acetonitrile based on a method by Mashelkar *et al.* [172]. Polymer particles (300 mg) with a mesh size of 38–67 µm were packed in 1 mL solid-phase extraction cartridges Agilent (Santa Clara, CA, USA). The cartridges were each then filled with 1 mL of chloroform, methanol and acetonitrile respectively. After 6 h equilibration at 20 °C the excess solvent was removed from the polymer by applying reduced pressure for 1 min and the weight of the swollen polymer was measured. The swelling ratio (Sr) of the polymers was calculated using Eq. 4.2 [173] based on the volume of the dry polymer and the volume of the wet polymer:

$$Swelling\ ratio\ (Sr) = \frac{volume\ of\ swollen\ polymer}{volume\ of\ dry\ polymer} \qquad eqn\ \ 4.2$$

4.10 Adsorption studies

Adsorption of VTPP and NTPP by the imprinted sorbents was investigated in chloroform solutions. To the vials containing 20 mL of analyte solutions of known concentrations were added optimized sorbent mass of 30 mg and stirred for 6 h. The imprinted sorbents were filtered off through 0.45 µm sintered filter using suction. The concentration of the analytes left in chloroform solution was then determined using the ICP-OES. Three replicate extractions and measurements were performed for each solution. The concentration of

75

analyte adsorbed was taken as the difference between the initial and the equilibrium concentrations of the solution. The extraction percentage of the analytes was calculated from Eq. 4.3:

$$Extraction\ (\%) = \frac{C_{i-}C_f}{C_i} \times 100 \qquad\qquad eqn\ \ 4.3$$

where C_i was the initial concentration (mg/L) and C_f was the concentration at adsorption equilibrium (mg/L).

4.11 Desorption and reusability

Desorption experiments were carried out on the spent sorbents to confirm the adsorbed concentrations. To evaluate the reusability of the fibers, 30 mg mass of the adsorbent was used repeatedly to adsorb NTPP in 20 mL chloroform solution containing 50 mg/L of NTPP at room temperature. After each adsorption, the saturated sorbent was desorbed by placing it into the mixture of MeOH and acetic acid (90:10, v/v) for 5 min. The fiber was thoroughly washed in de-ionized water, filtered through 0.45 μm filter using suction. The regenerated sorbent was then dried and subsequently reused for the next adsorption experiment.

4.12 Evaluation of fiber selectivity

The evaluation of selectivity of the nanofibers was conducted by immersing the 30 mg of the fiber into 20 ml chloroform solutions containing 50 mg/L of both NTPP and VTPP at room temperature, respectively. The concentration of the NTPP and VTPP left in chloroform

solution was then determined using the ICP-OES. The recognition coefficient (α) was used to evaluate the selectivity [174] and could be calculated using Eq. 4.4:

$$\propto = \frac{[S](imprinted)}{[S](non-imprinted)} \qquad eqn \quad 4.4$$

Where $[S]_{imprinted}$ was the analyte binding amount to the imprinted nanofiber (mgg^{-1}), and $[S]_{non-imprinted}$ was the binding amount to the non-imprinted nanofiber (mgg^{-1}).

4.13 Analytical quality control procedure

Certified reference material (CRM) NIST SRM 1634c (Trace Metals in Residual Fuel Oil) purchased from National Institute of Standards and Technology (Maryland, USA) was used to validate the analytical procedure. Adsorption experiment was carried out using by adding an optimal quantity of the imprinted adsorbent (30 mg) in 0.5 mL portions of the certified reference fuel oil for 6 h. 10 mL of petroleum ether was added as a diluent, in order to reduce the viscosity of the certified fuel oil. The concentration of the metals left in the solution was then determined using the ICP-OES.

5

Results and discussion

5.1 Theoretical study of template-monomer interactions

5.1.1 Selection of the functional monomers

Selection of most suitable functional monomers for a template is critical, in so far as MIP preparation is concerned. The MIP development could, however, be better facilitated through molecular modelling and a computational approach. In the first step, a virtual library of two functional monomers was created and screened for all possible interactions between the monomers and the template molecule in the pre-polymerization complexes. The chemical structures and optimized conformations of the functional monomers and the VTPP template molecule are presented in Figures. 5.1.1a and 5.1.1b, respectively.

Methyl styrene

Styrene
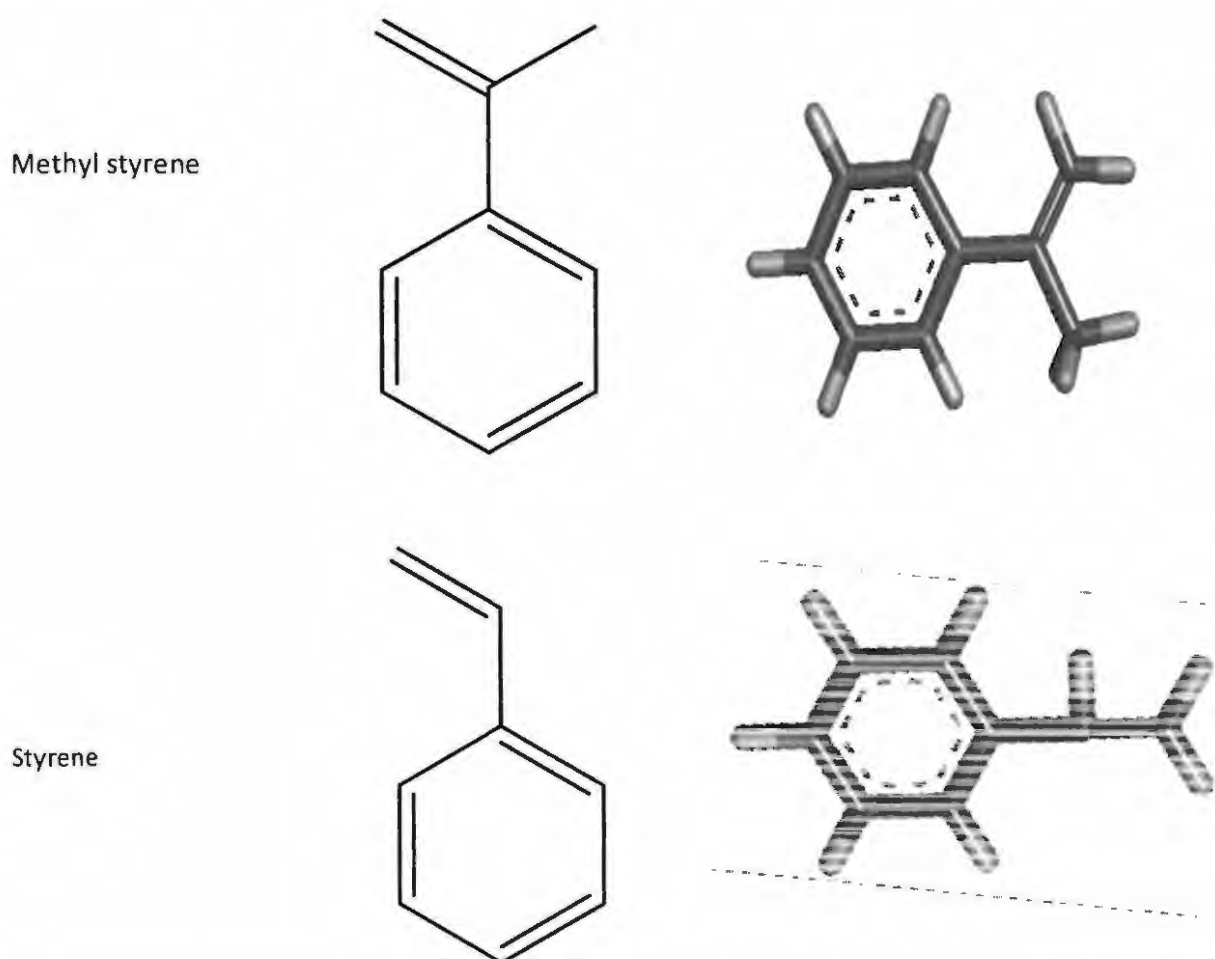
Figure 5.1.1a: Chemical structures and optimized conformations of the functional monomers.

Structure   Conformation
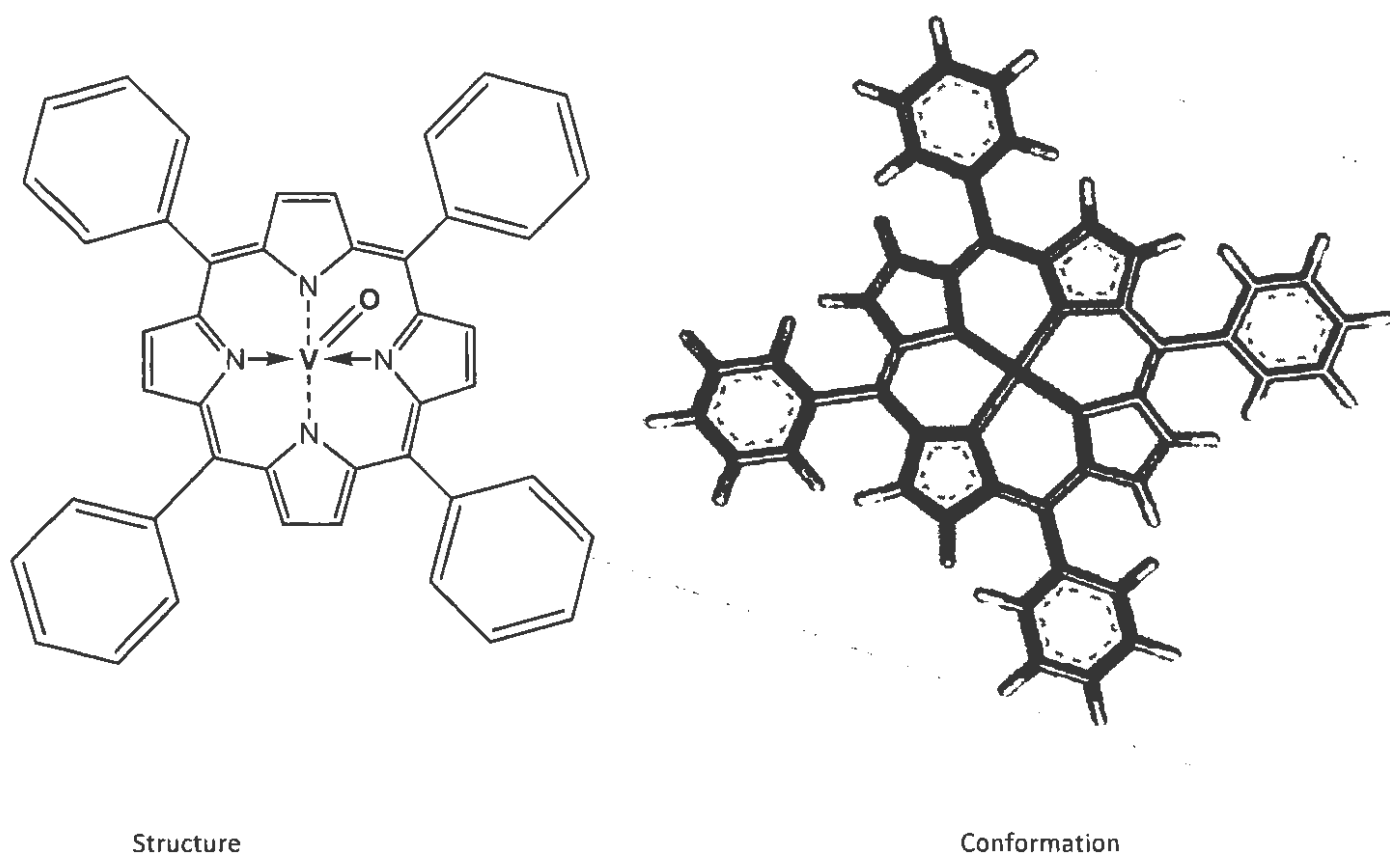
Figure 5.1.1b: Chemical structure and optimized conformation of the VTPP template.

5.1.2 Optimized geometry of complexes

The structures of the optimized prepolymerization complexes (PPC): VTPP-methylstyrene (PPC1), and VTPP-styrene (PPC2) are presented in Figure 5.1.2, and energies of complexation are given in Table 5.1.2.

It can be assumed that the monomer forming the most stable complex with a given template would be most suitable for being used to produce MIP with good recognition properties [175,176]. From the energies analysis (Table 5.1.2), it could be seen that the complex of VTPP with styrene monomer (PPC2) was the most stable, and styrene seems to be the most suitable monomer to produce the imprinted sorbent. Hence, styrene was selected as the best functional monomer for studies conducted in this thesis.
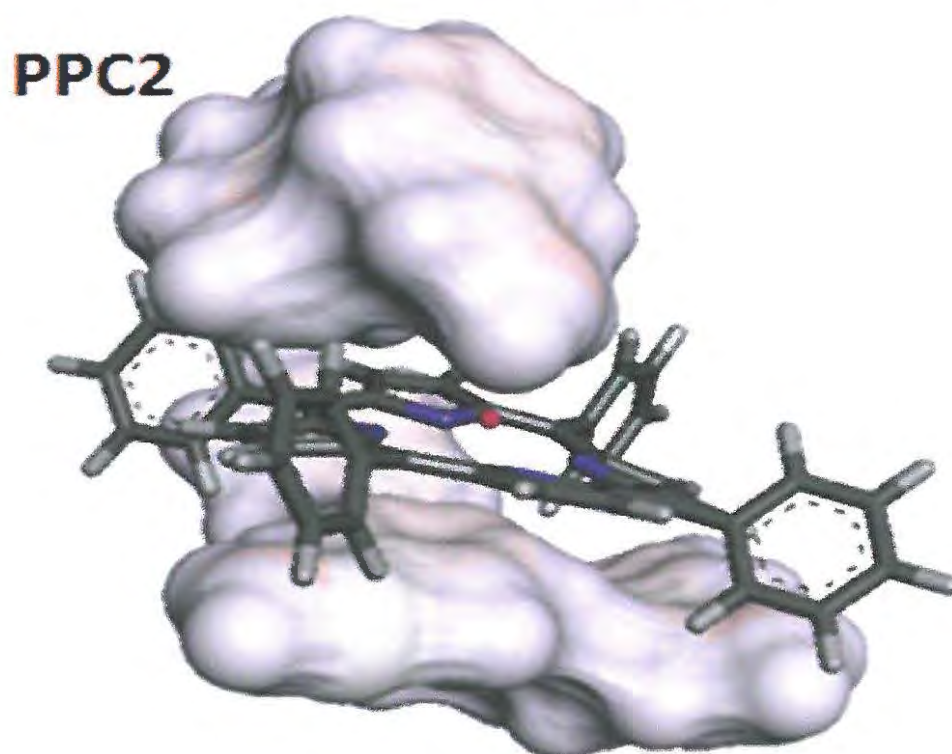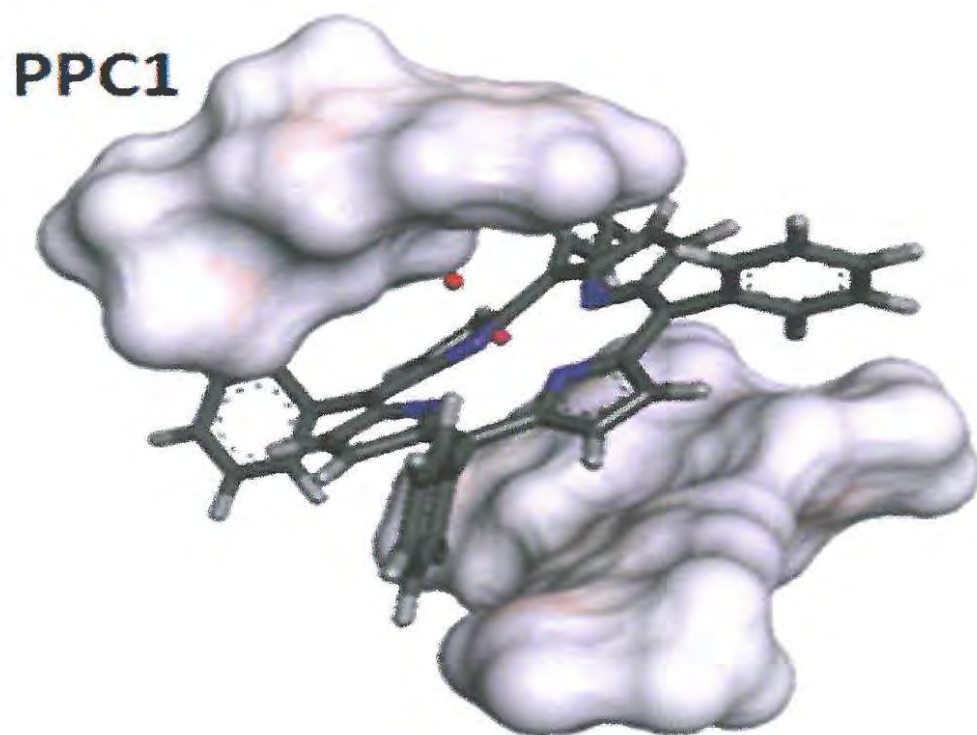
Figure 5.1.2: The most stable complexes between VTPP and methylstyrene (PPC1), styrene (PPC2).

Table 5.1.2: Theoretical optimized complexation energies (ΔEc) of VTPP with: methylstyrene (PPC1), and styrene (PPC2).

Complexes	ΔEc (kcal mol^{-1})
PPC1	−66.077
PPC2	−66.234

5.1.3 Conclusion

A computational model based on the combination of molecular dynamics (MD) simulations and quantum mechanics was successfully applied in the evaluation of the intermolecular interactions between VTPP and selected functional monomers. The process was essential in selecting the monomer that yielded the optimal interaction with VTPP.

Based on the conformational analysis outcome as well as the calculated values of complexation energy, it was concluded that the interactions between VTPP and the styrene monomer were strongest and thus provided more active sites as compared to the interactions with methylstyrene functional monomer.

5.2 Physical characterization and performance evaluation of the VTPP prepared MIP particles

5.2.1 Characterization studies

Scanning electron microscopy (SEM) was employed to observe the morphological features of the particles (Fig 5.2.1.1). From the SEM micrographs, it is obvious that the use of chloroform as porogen lead to the formation of nanosponge aggregates that probably could be attributed to the fact that the chlorinated porogens resulted in the slight swelling of the polymer product. The resulting polymer particles were observed to have irregular and rough morphology. Furthermore, the presence of VTPP in prepolymerization mixture had no effect on morphology of obtained imprinted particles.
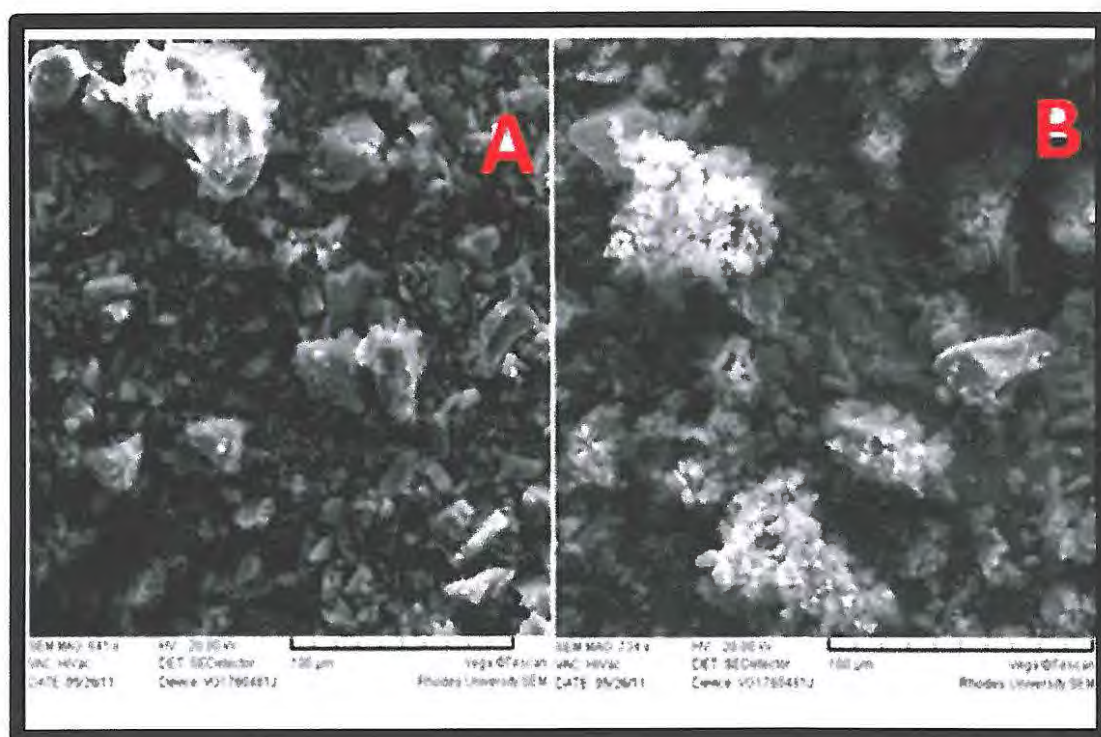
Figure 5.2.1.1: SEM micrographs of the polymers: (A) MIP and (B) NIP.
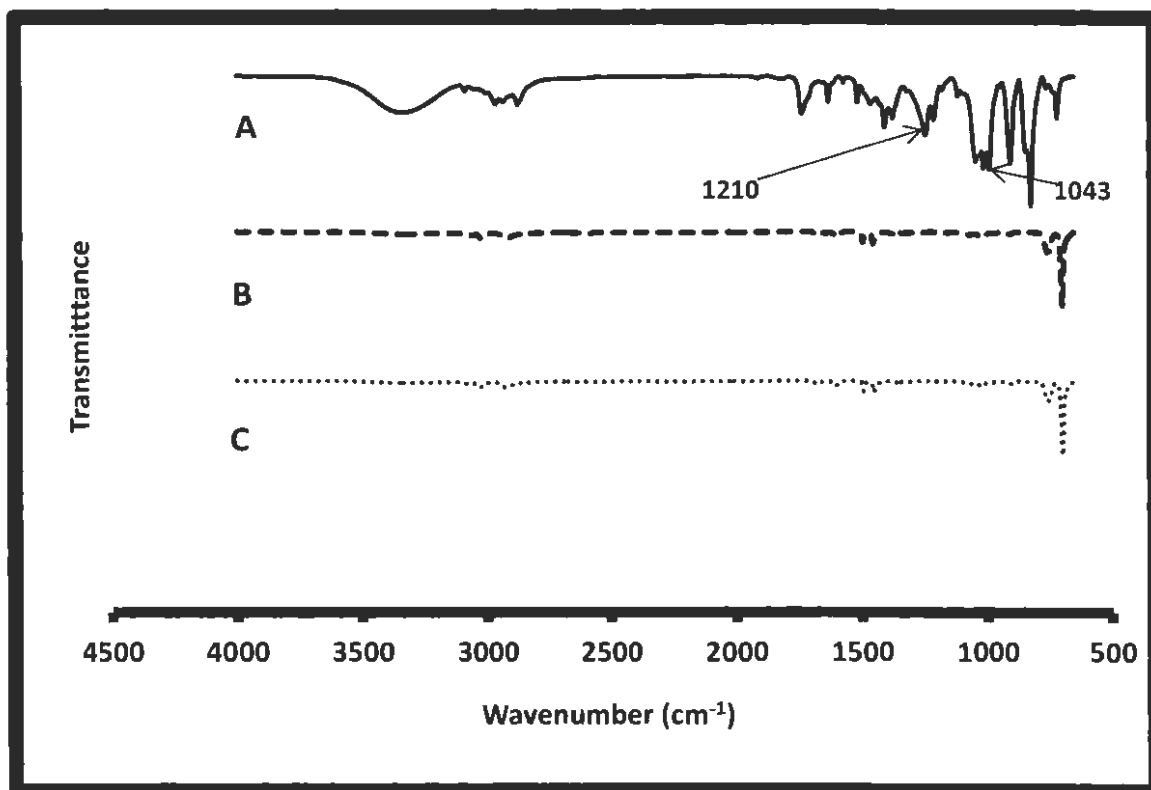
Figure 5.2.1.2: FT-IR spectra for (A) MIP (before leaching), (B) VTPP-removed imprinted polymer (after leaching), and (C) NIP.

In the imprinting synthesis, the FT-IR spectra confirmed VTPP template molecules to have been successfully embedded into the imprinted polymer (see Fig 5.2.1.2). As indicated in Figure 5.2.1.2A, extraction with MeOH/acetic acid could provide efficient removal of the VTPP template. The characteristic peaks of the VTPP molecule at 1043 and 1210 cm^{-1} (spectrum A) disappeared completely after the extraction treatment (spectrum B), and the IR spectrum became identical to that of the NIP (spectrum C), which indicated to the similarity in the backbone structure.

Table 5.2.1: BET surface area of the polymers measured by nitrogen adsorption

Polymer	Surface area (m^2g^{-1})
VTPP-removed imprinted polymer	176.49
MIP	161.22
NIP	35.83

MIP is a class of network materials known as microporous polymers [177]. A comparison of surface areas of the MIP before and after removal of the template could also confirm whether the template was removed from the polymers effectively. However, the determination of polymer BET surface area via gas adsorption analysis revealed significant differences between all polymers (Table 5.2.1).

Two observations were immediately drawn from the data. The first one was that the surface area of MIP (before leaching the template) exceeded that of the NIP, which supported the fact that the MIP had a higher adsorption capacity to VTPP than NIP. The second one was that the associated decrease in surface area between the VTPP-removed imprinted polymer (after leaching the template) and the MIP (before leaching the template) was with about 9% difference, implying that template molecules and the unpolymerized residues were removed efficiently. The observations further suggested that the template was a surface area determinant.

Figure 5.2.1.3 shows the TG plots of unleached and leached VTPP imprinted polymer particles. TG plots with similar characteristics were obtained for unleached (Figure 5.2.1.3A) and leached (Fig 5.2.1.3B) polymer particles. However, the TG plots of both polymer particles showed that the polymers were stable up to 390 °C, after which the polymers degraded until above 480 °C with a weight loss of about 75% for both polymer particles. The result also indicated that decomposition occurs at higher temperature, suggesting a high level of structural cross-linking.
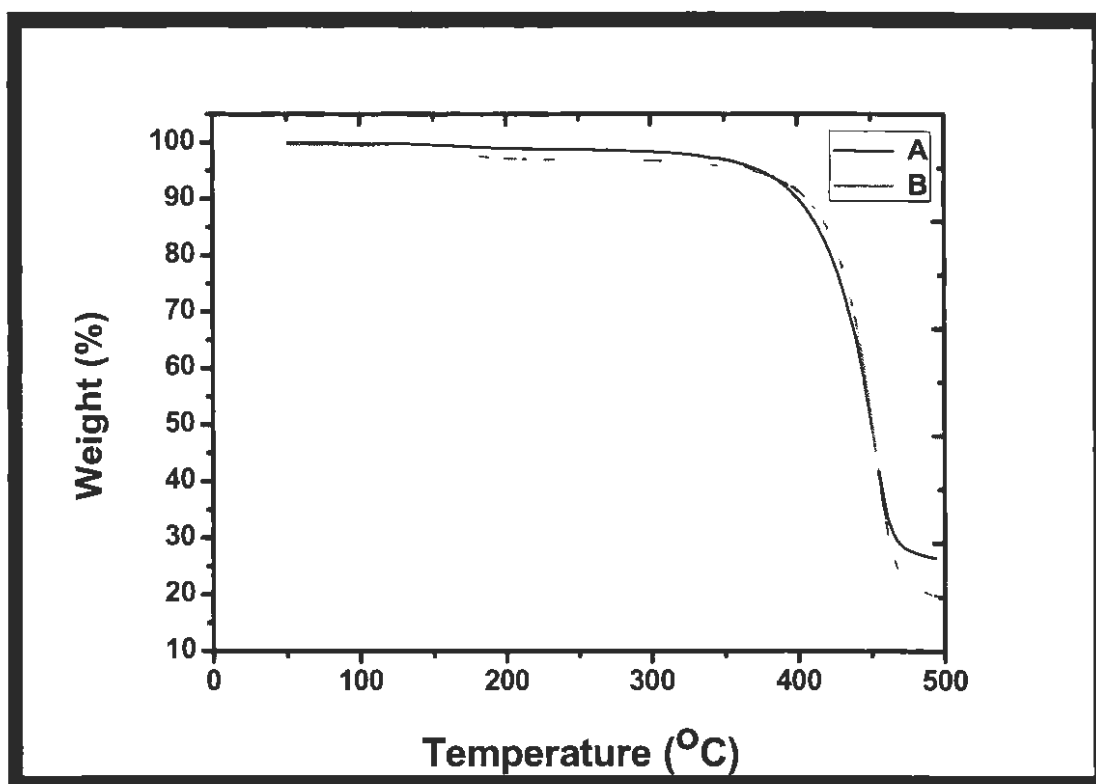
Figure 5.2.1.3: Thermogravimetric analysis of polymers: (A) unleached MIP and (B) leached MIP.

Differential scanning calorimetry (DSC) measurement of the unleached (Fig 5.2.1.4A) and leached (Fig 5.2.1.4B) polymer particles revealed that the profile of the melt in both particles was very broad. For the unleached MIP, a wide and strong endothermic effect was observed in the range of 370-470 °C corresponding to a fusion process of the polymer, and thus suggesting a wide range of molecular weight within the sample. It was also noted that the endothermic transition for the unleached MIP started around 370 °C, which may be related to the melting point shift when a guest molecule is embedded in a polymer cavity [178].
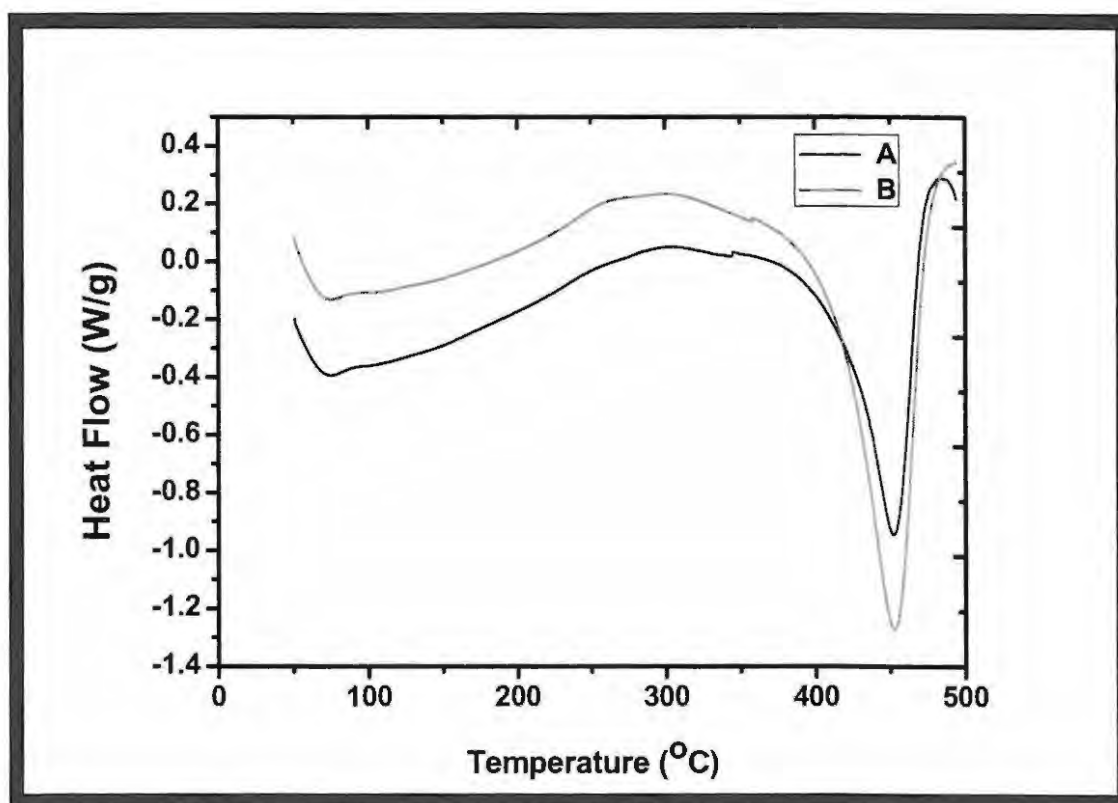
Figure 5.2.1.4: Differential scanning calorimetry thermograms of (A) unleached MIP and (B) leached MIP.

The leached MIP showed an endothermic effect in the range of 380–470 $^{\circ}$C and both polymer particles exhibited a high melting point (450°C), a feature that could also be attributed to higher level of crosslinking.

5.2.2 Swelling studies

The effect of swelling of imprinted polymers on their recognition properties remains unclear. The distance between polymer functional groups and their orientation in the binding cavity is expected to be swelling dependent, thus resulting in specificity loss when immersed in an unsuitable solvent.

To study the swelling, both the leached MIP and the NIP were measured in chloroform, methanol, and acetonitrile respectively. The swell data (Table 5.2.2.) indicated that the non-inclusion of the template molecule in the NIP decreased polymer swelling. Chloroform was found to swell the polymers to a higher degree than methanol and acetonitrile. The outcome also confirmed that chloroform was indeed the porogen as it was expected to fill the pores in accordance with polymerization conditions.

Table 5.2.2: Solvent swell results in CHCL₃, MeOH, and ACN

Polymer	Sr in $CHCl_3$	Sr in MeOH	Sr in ACN
MIP	4.39 (±0.23)	1.88 (±0.17)	1.88 (±0.17)
NIP	4.11 (±0.11)	1.60 (±0.15)	1.70 (±0.26)

Sr = swelling ratio

5.2.3 Adsorption isotherms

The adsorption isotherms of the synthesized particles were evaluated with VTPP-chloroform solution concentrations ranging from 50 to 400 mgL^{-1} at room temperature for 12 h, and the data is shown in Figure 5.2.3.1. It could be seen and was clearly evident that the capability of the MIP to adsorb VTPP was substantially higher than that of the NIP thereby providing evidence for the existence of a selective site for VTPP sequestration on the MIP as compared to that of the NIP. As the concentration of VTPP was 50.0 mgL^{-1}; the adsorbing capacity of MIP particles was 0.259 mgg^{-1} while that of the nonimprinted polymer particles was 0.064 mgg^{-1}. Furthermore, maximum adsorption capacity of MIP (0.600 mgg^{-1}) toward VTPP was higher (about 2.14 times that of the NIP) than that of the NIP (0.281 mgg^{-1}). The VTPP binding by the NIP could be associated with the presence of nonspecific binding due to physical adsorption, and due to random interactions of the VTPP molecules with functional groups in the polymer matrix.
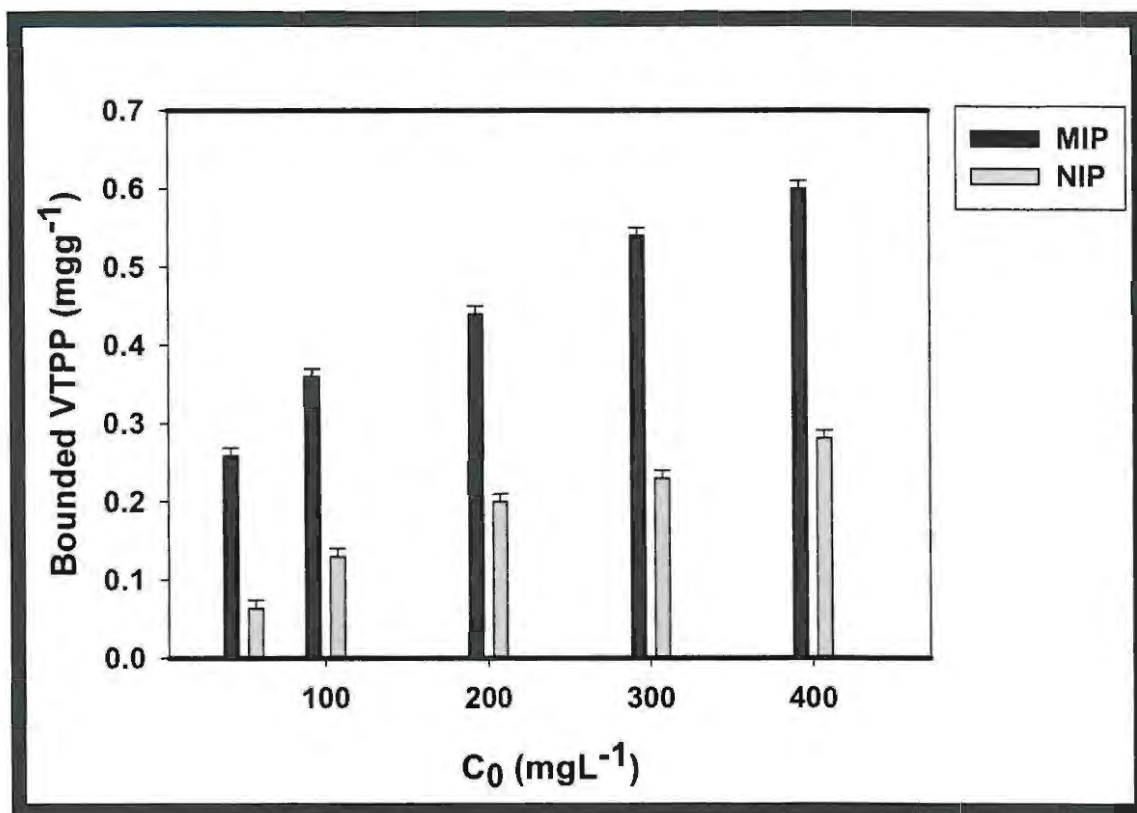
Figure 5.2.3.1: Adsorbing isotherms of VTPP onto MIP and NIP at room temperature for 12 h.

Equilibrium data, commonly known as adsorption isotherm, are basic requirements for designing of adsorption systems [179]. In this study, the equilibrium data for VTPP onto MIP and NIP were evaluated based on the data fit to the Langmuir and Freundlich models (Eq. 5.1 and 5.2, respectively).

The adsorption data were fitted with both the Langmuir and Freundlich isotherm models (see Table 5.2.3, Figures 5.2.3.2 and 5.2.3.3). The Freundlich model has been applied in the adsorption process using noncovalently imprinted polymers [180,181] and Langmuir model has been used in describing a monolayer adsorption without adsorbate-adsorbate interaction [182]. The Freundlich adsorption isotherm is an empirical one for nonideal adsorption on heterogeneous surfaces as well as multilayer adsorption. The calculated

Freundlich isotherm constants and the corresponding correlation coefficients for MIP and

NIP are given in Table 5.2.3.

Table 5.2.3: Parameters of Freundlich isothermal equation and Langmuir adsorption equation for adsorption experimental data

Isotherm	Parameters	Value (MIP)	Value (NIP)
Freundlich	K_F	0.275	0.107
	n	2.747	1.359
	R^2	0.9986	0.9808
Langmuir	Q_m (mgg^{-1})	0.222	0.059
	K_a (mgL^{-1})	19.250	8.620
	R^2	0.8823	0.7110

The values of the correlation coefficients for MIP ($R^2 = 0.9986$) and NIP ($R^2 = 0.9808$) are

higher than those obtained when employing the Langmuir model, showing that the

adsorption in the experiment correlated well with the Freundlich model. The results showed

that the value of n was greater than unity, indicating that the VTPP was favourably adsorbed

onto MIP and NIP [182].

$$\frac{C_e}{Q_e} = \frac{C_e}{Q_m} + \frac{1}{K_a Q_m} \qquad\qquad eqn\ 5.1$$

$$logQ_e = logK_F + \frac{1}{n}logC_e \qquad\qquad eqn\ 5.2$$

where C_e (mg/L) and Q_e(mg/g) are concentration and adsorption amount at equilibrium,

Q_m(mg/g) and K_a (mg/L) are the theoretical maximum adsorption capacity and Langmuir

equilibrium constant related to the theoretical maximum adsorption capacity and energy of adsorption, respectively. K_F and n are the Freundlich constants, which are indicators of adsorption capacity and adsorption intensity.
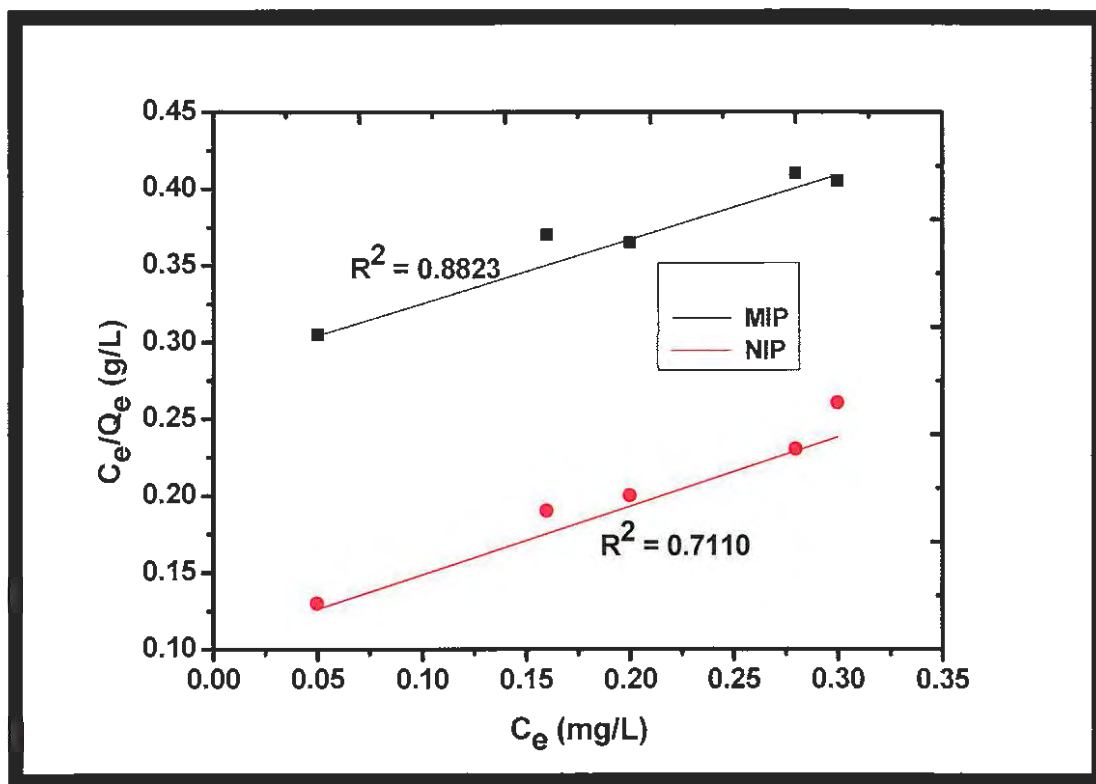
Figure 5.2.3.2: Langmuir isotherm of VTPP adsorbed onto MIP and NIP.
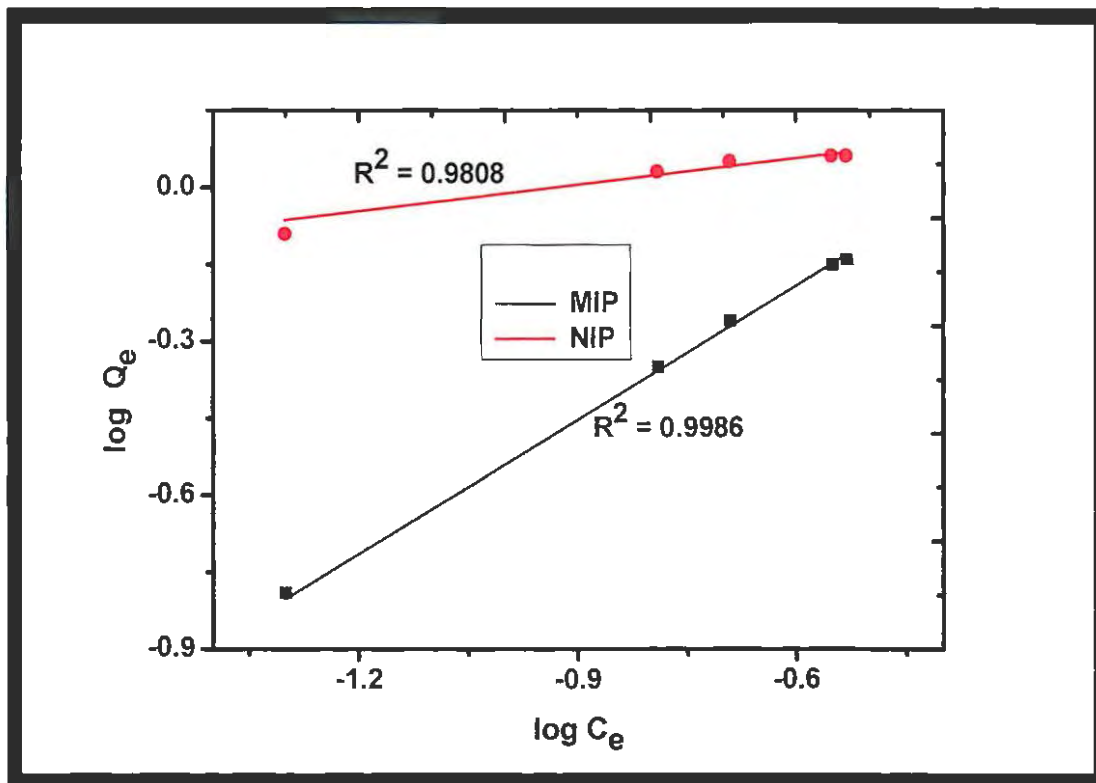
Figure 5.2.3.3: Freundlich isotherm of VTPP adsorbed onto MIP and NIP.

The magnitude of adsorption constant indicates easy uptake of VTPP from the chloroform solution. However, it could be concluded that the Freundlich isotherm model was more suitable for the experimental data than Langmuir isotherm as the high value of the correlation coefficient, suggested that the adsorption of VTPP on MIP to be a multiple layer adsorption.

5.2.4 Regeneration of the MIP sorbent

The regeneration of adsorbent was crucial for improving industrial efficiency at low costs. To test for the reusability of adsorbent, the MIP was reused for its adsorption efficiency seven times in 400 mg/L solution of VTPP, and the results are presented in Figure 5.2.4. After seven adsorption cycles, the results manifested that the MIP could be used repeatedly at least seven times without decreasing its adsorption efficiency.
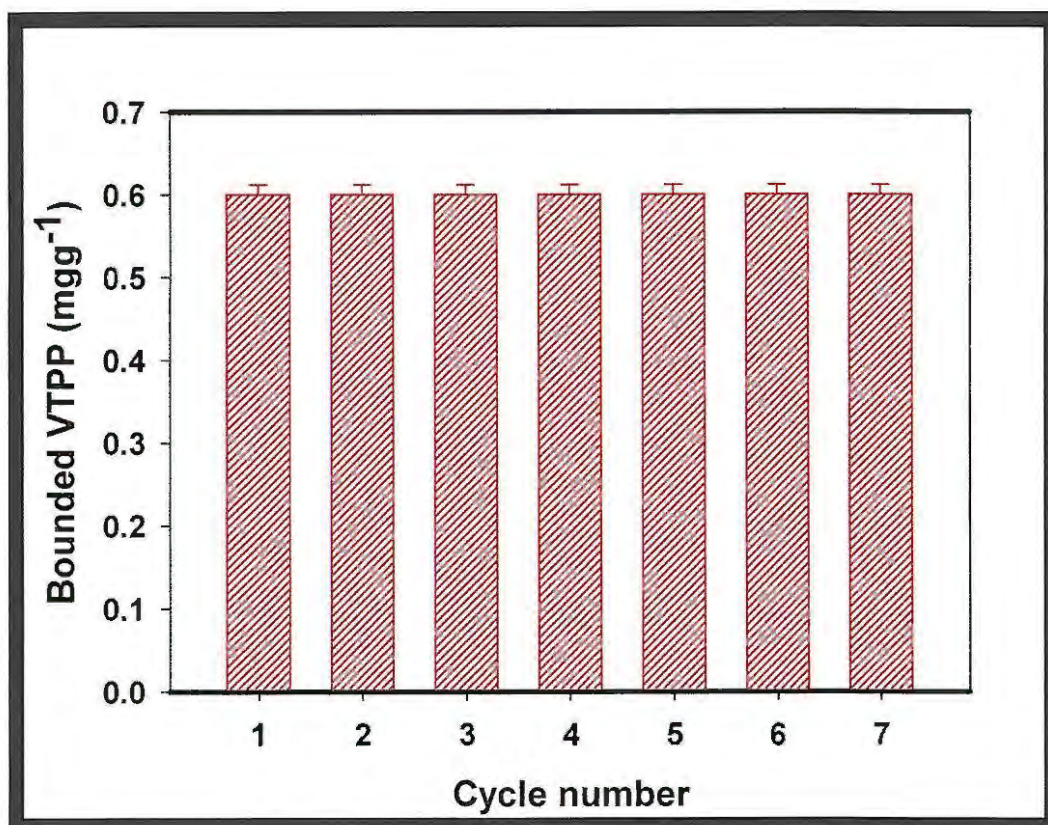
Figure 5.2.4: Bounding amount of the MIP for VTPP in seven consecutive binding-regeneration cycles.

5.2.5 Method validation

The developed method for removal of VTPP from organic media was validated by analysing a custom solution of a certified reference material (CRM) NIST, SRM 1634c, Trace Metals in Residual Fuel Oil, and the concentration of VTPP in the CRM was found to be 28.49 mgkg^{-1}, which was comparable with the certified value of 28.19 mgkg^{-1}.

The results showed that the value obtained from the method is within the error of the standard reference material. It may be concluded from the results that styrene based molecularly imprinted polymer can be effectively used for the specific removal of VTPP from fuel oil.

5.2.6 Conclusion

In this work, a robust molecularly imprinted polymer synthesized by the nonconvalent method using VTPP as template and its molecular recognition properties was studied. The MIP was applied as selective sorbent for the template molecule, which proved that recognition ability can be ascribed to the imprinting process. Moreover, the adsorption isotherm studies indicated that the Freundlich model was better suited to describe the adsorption of VTPP onto MIP than Langmuir model. The suitability was reflected by the higher correlation coefficient, suggesting that the adsorption of VTPP on MIP is a multiple layer process. In addition, MIP exhibited excellent reusability. However, some binding sites in MIPs are embedded in the inner helices of the particles. Thus, imprinted sorbent with much larger surface areas such as nanofibers are urgently needed.

5.3 Molecularly imprinted NTPP electrospun nanofibers

5.3.1 Characterization of nanofibers

The morphologies of the NTPP-imprinted composite nanofibers that were imprinted with various quantities of NTPP (see Table 4.7.2) at two different applied voltages and were obtained by electrospinning at either 12 or 15 kV are shown in Figures 5.3.1.1 and 5.3.1.2. It is evident from the SEM images in Fig. 5.3.1.1 that the composite nanofibers obtained at 12 kV were not tight. It should also be noted that beads were present on the surfaces of the composite nanofibers, particularly those with lower NTPP contents (such as 320 and 645 mg), and a ribbon-like nanofiber was observed when higher NTPP contents were employed. Ribbon-like nanofibers may have formed due to rapid solvent vaporization from the surface of the jet. The poor morphologies of the nanofibers obtained using low NTPP contents were a result of the low solution viscosity. It is well known that the electrospinning solution concentration is one of the most important parameters, as it is strongly related to the overall viscosity [183].

The NTPP-imprinted composite nanofibers electrospun at 15 kV (Fig. 5.3.1.2) had a comparatively smooth surface morphology. However, the results indicated that when the applied voltage was 12 kV, the electric field was not strong enough to provide the electrostatic repulsion required to balance the surface tension, so the jet was not stable and the resulting nanofibers did not have a smooth surface morphology. Thus, increasing the applied voltage (i.e., increasing the electric field strength) increased the electrostatic repulsive force exerted on the fluid jet, favouring the stabilization of the jet and the formation of smooth fibers. Therefore, the most suitable voltage for electrospinning NTPP-

imprinted composite nanofibers was 15 kV, and this voltage was used in subsequent experiments.
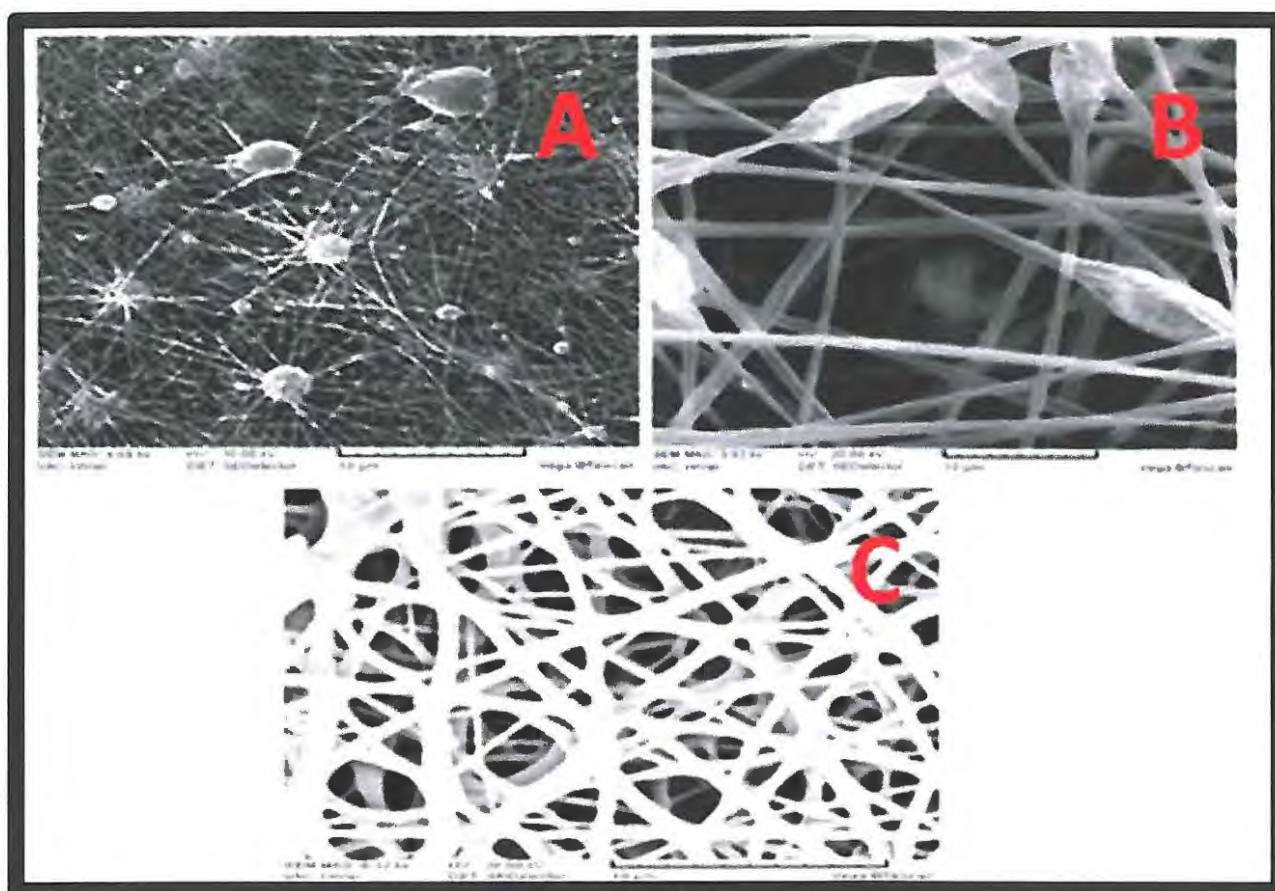
Figure 5.3.1.1: SEM images of NTPP-imprinted composite nanofibers that were imprinted with different NTPP contents: (A) 320 mg (B) 645 mg, and (C) 970 mg. Electrospinning voltage: 12 kV.
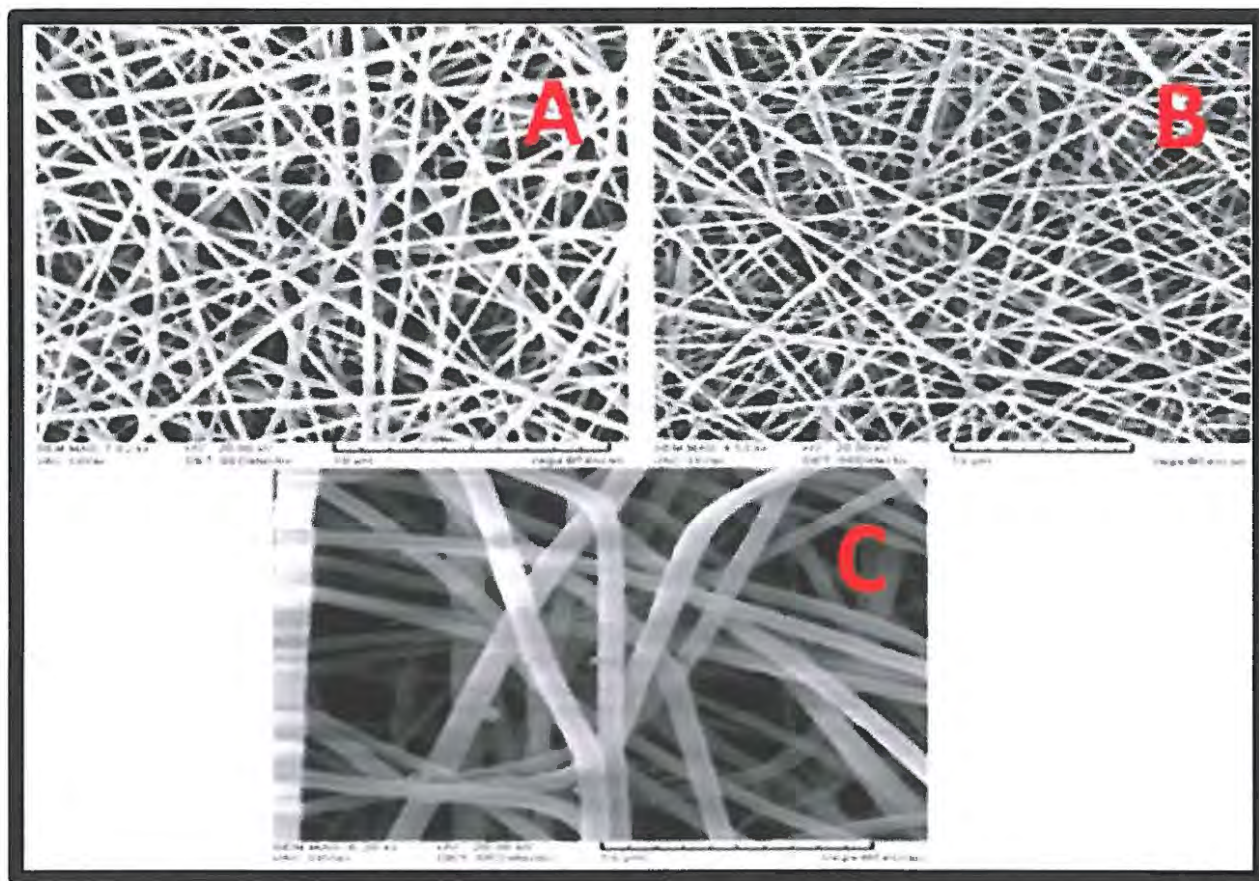
Figure 5.3.1.2: SEM images of NTPP-imprinted composite nanofibers that were imprinted with different NTPP contents: (A) 320 mg (B) 645 mg, and (C) 970 mg. Electrospinning voltage: 15 kV.

FTIR spectra of both leached and unleached nanofibers are shown in Figure 5.3.1.3. NTPP

has a central Ni atom surrounded by four N atoms. The unleached fiber spectrum showed

peaks at 1660, 1200, 530, and 1600 cm^{-1} that were attributed to C=C, C–C, Ni–N, and

conjugated C=N systems, respectively, and these confirmed that the NTPP template

molecule had been successfully embedded into the imprinted fiber. The spectrum for the

leached fiber showed two characteristic peaks. The small peak at 985 cm^{-1} was from C–H

groups in the vinyl monomers. Ester C–O groups in the PET backbone gave rise to a strong

band at 1300 cm^{-1}. On the other hand, the characteristic peaks of the NTPP molecule at

1200 and 530 cm^{-1} disappeared completely after extraction.
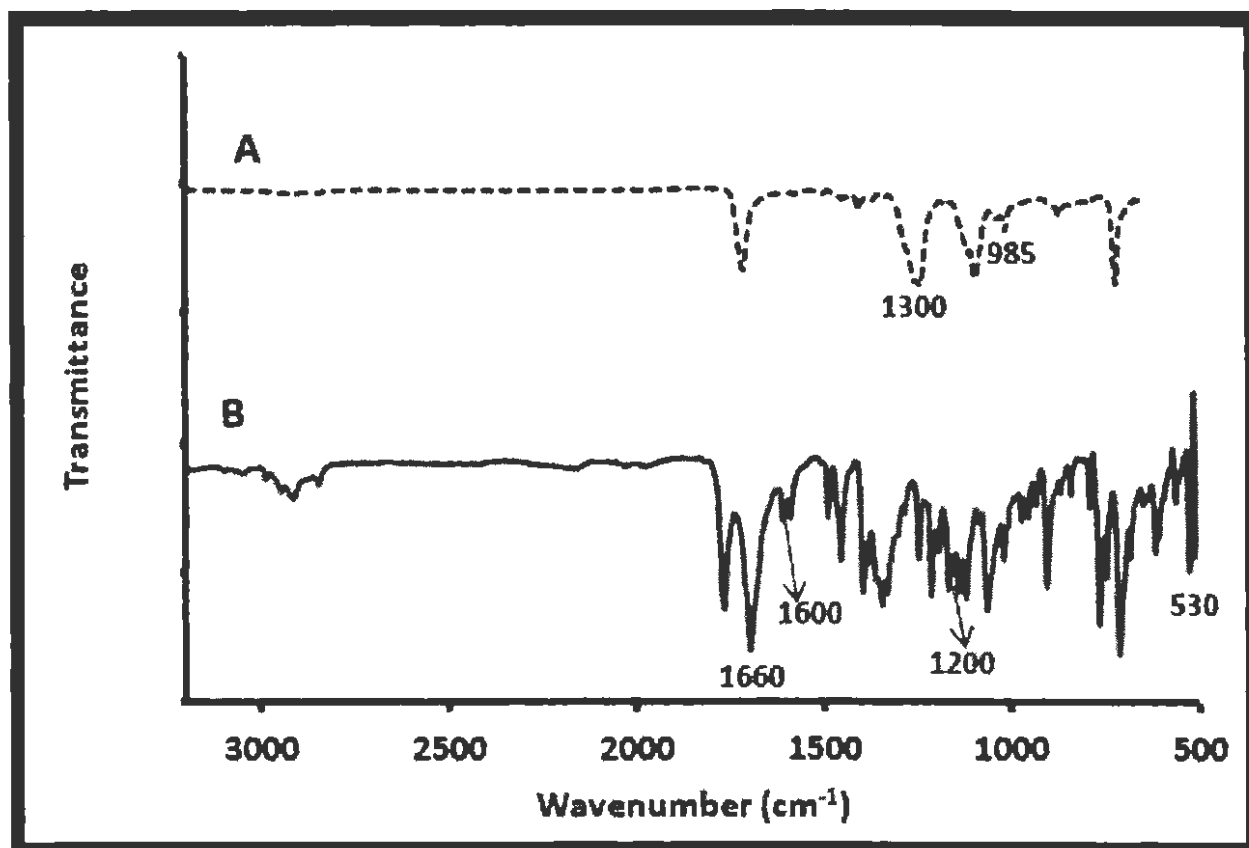
Figure 5.3.1.3: FT-IR spectra for (A) the leached fiber and (B) the unleached fiber.

To further confirm that the template had been removed the fiber, microanalysis of both the unleached and the leached fibers was performed, because a large quantity of nitrogen was introduced during the imprinting process due to the addition of the template. N% = 1.82 for the unleached fiber, whereas N% = 0.033 for the leached fiber, and N% = 0.034 in the control fiber because the initiator was azobis(cyclohexanecarbonitrile).
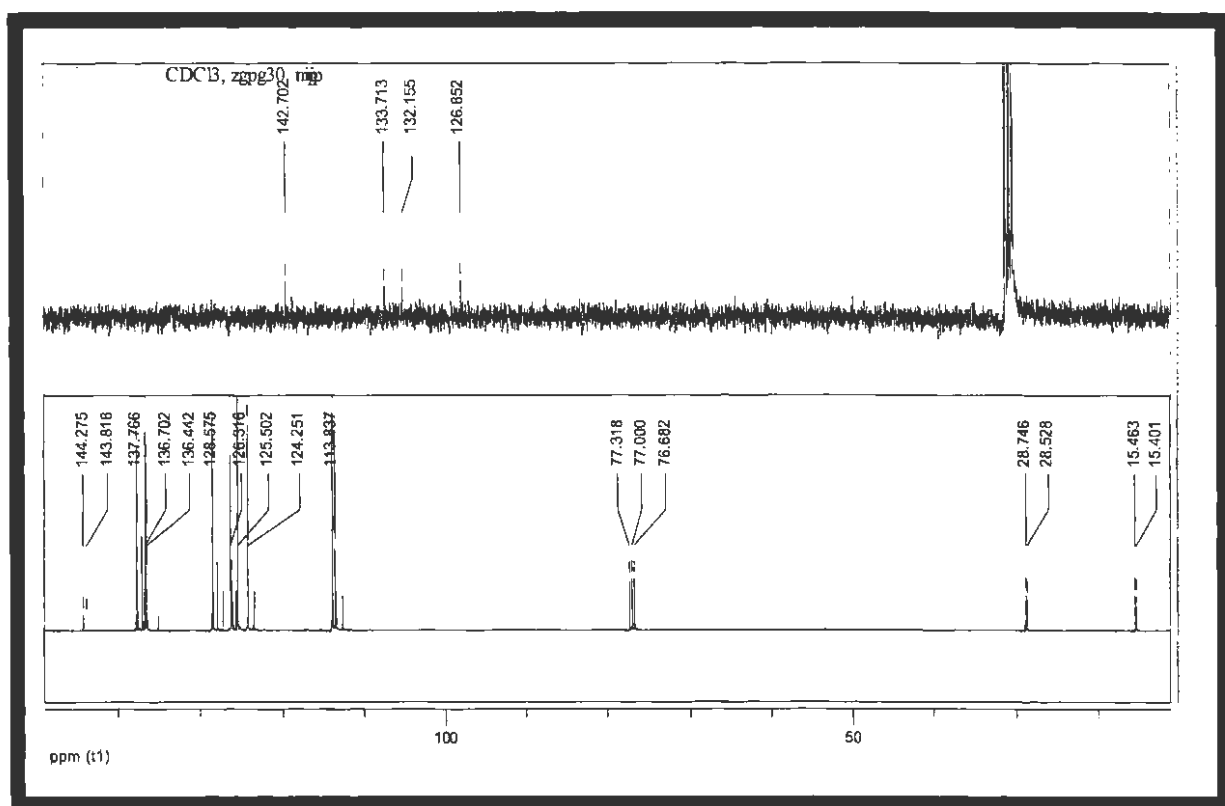
Figure 5.3.1.4: ^{13}C NMR spectra of the imprinted (bottom) and non-imprinted (top) preblending mixtures.

Comparing the ^{13}C NMR spectra of the preblending mixtures of the molecularly imprinted and non-imprinted polymer solutions, differences in the chemical shifts or relative signal

intensities were apparent. The exact assignment of the carbons in NTPP is shown in Figure 5.3.1.4. Two distinct peaks at δ 136.70 and 136.44 ppm were observed, which were assigned to the two –C(C=N)C present in NTPP. Moreover, four peaks at around δ 126.55, 126.34, 125.55, and 124.21 ppm derived from several C=C bonds in NTPP, which in addition confirmed that NTPP molecules were well embedded in the imprinted fiber. These characteristic peaks were not present in the ^{13}C spectrum of the non-imprinted solution.

Table 5.3.1: Pore characteristics of the imprinted and non-imprinted fibers

Porosity parameter	Measurement	
	MIN (leached)	NIN
Specific surface area[‡] (s/g)	71.630	29.095
Average pore size[$] (Å)	22.11	32.42
Micropore volume[$] (cc/g)	0.0792	0.0472

[‡]Specific surface area was calculated using the BET method.

[$]Average pore size and micropore volume was calculated using the BJH method.

The exceptionally porous nature of the unwoven nanofiber produced via electrospinning was an important factor as it could change the surface area of the material and thus increase its capacity to remove NTPP from organic matrices. Table 5.3.1 shows the pore characteristics of the imprinted and non-imprinted fibers. BET analysis showed that the MIN and NIN sorbent materials had average pore diameters of 22.11 and 32.42 Å, respectively. Measurements revealed that the surface area of the imprinted fiber was much higher than that of the non-imprinted fiber (by about 59%), thus confirming the formation of recognition sites on the imprinted fiber. It should also be noted that the micropore volume did not differ between the imprinted and non-imprinted fibers, and thus confirmed that both fibers were prepared in polar solvents.

Thermogravimetric analysis is useful for obtaining additional information on the relative thermal stability of a fiber. TG thermograms of the pure PET/L-PEI and MIN nanofibers are shown in Figure 5.3.1.5. For the pure PET/L-PEI nanofiber, the curve shows that the material loses 5 % of its weight in moisture up to 150 °C, and then loses about 88 wt% by 460 °C and is completely decomposed above 600 °C. For the MIN, the composite fiber degraded in three major steps. The first step involved a more pronounced weight loss (14 wt%) when compared to that of the pure PET/L-PEI (5 wt%) in the range 100–150 °C, which can be ascribed to the loss of physically adsorbed water. The second weight loss was due to ester bond decomposition and the degradation of PET side chains between 260 and 325 °C. The final step occurred above 500 °C due to further decomposition of the PET main chain.
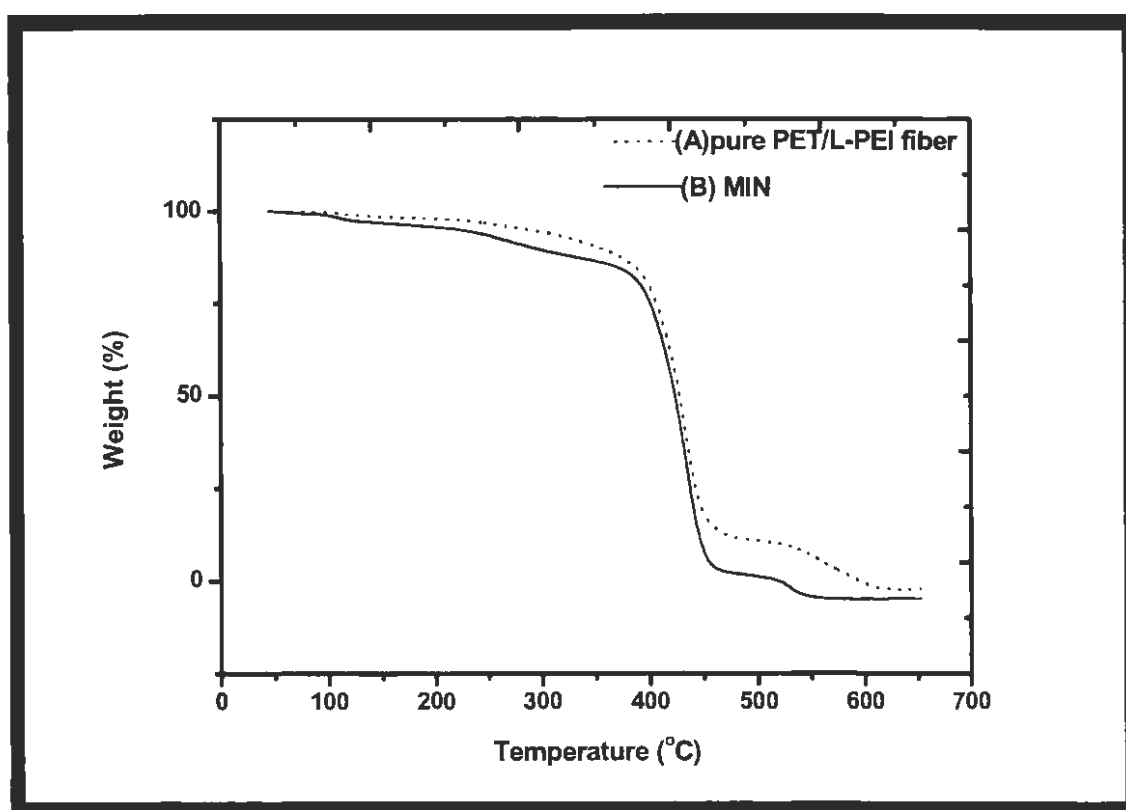
Figure 5.3.1.5: TG curves of (A) the pure PET/L-PEI nanofiber and (B) MIN.

102

5.3.2 Recognition properties of NTPP-imprinted nanofibers

To explore the recognition properties of NTPP-imprinted fibers, was varied the ratio of template to monomer used during MIN creation (see Table 4.7.2). All of the fiber composites (MIN_1, MIN_2, MIN_3) displayed selective recognition towards the template molecule (Figure 5.3.2). All of the imprinted fibers displayed greater binding capacities towards the template molecule with a fiber mass of 30 mg. It is known that to achieve very good imprinting, the template to functional monomer ratio should be 1:6 [184].
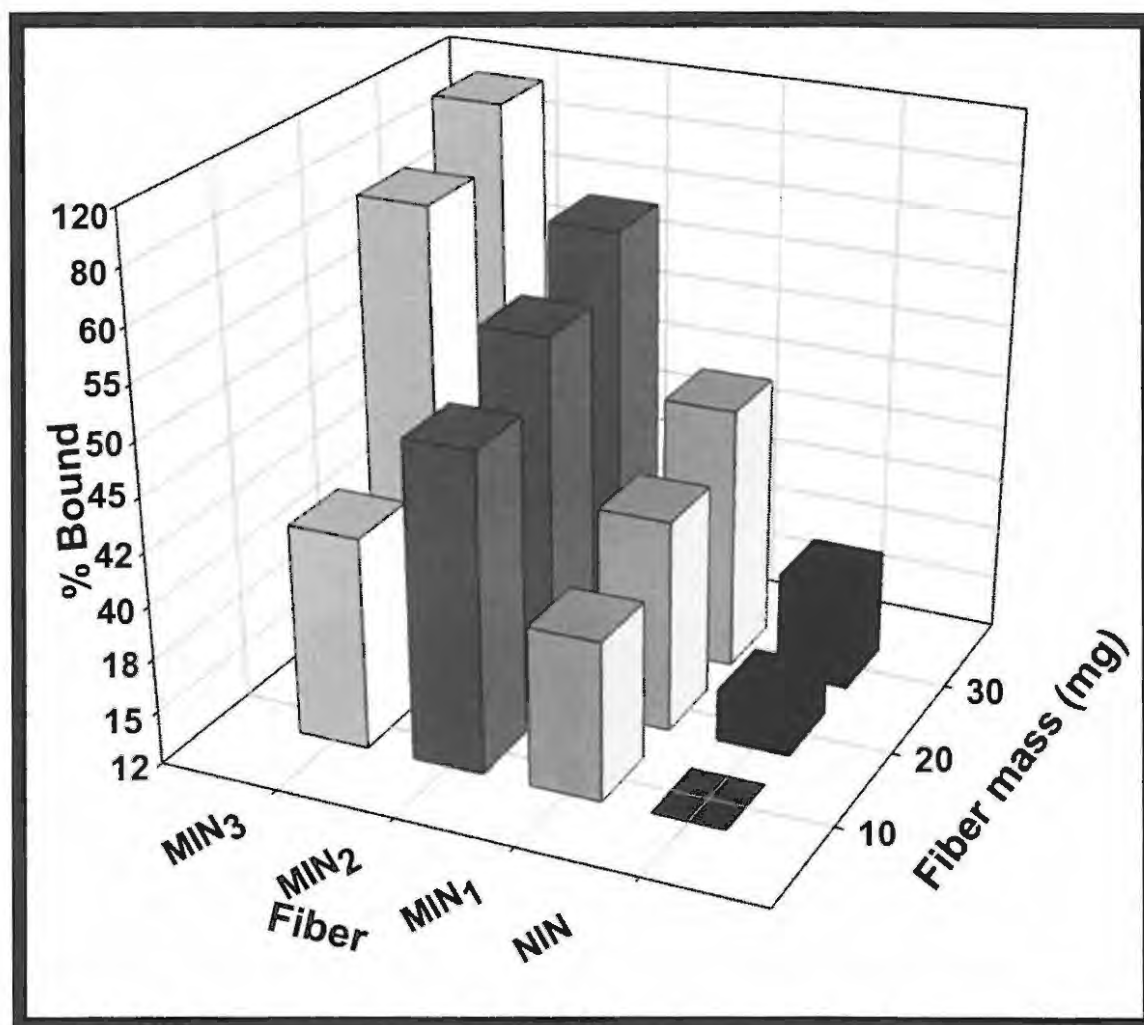
Figure 5.3.2: Analysis of the rebinding of NTPP-imprinted fibers and the non-imprinted fiber with NTPP

It is worth noting that the NTPP adsorption capacity increased as the molar ratio of NTPP to styrene was increased from 1:1 to 3:1. The ratio of template to functional monomer that yielded the best specific affinity and the highest recovery (99.9%) was 3:1.

On the other hand, the observation may be attributed to the fact that an increase in template molar ratio leads to an increase in the number of recognition sites on the imprinted sorbent material. In addition, it could be attributed to the presence of L-PEI (support material), which is known to exhibit a strong affinity for heavy metals, and thus plays a significant role in controlling the adsorption.

To try to gain insight into the performance of the MIN as compared to that of the control fiber, a NIN was also prepared. According to the results obtained, the NTPP adsorption capacity of the MIN was much higher than that of the NIN, which was due to the shape of the cavities in the MIN, which closely matched the structure of NTPP. When the mass of the fiber was 10, 20, or 30 mg, 40.4, 60.2, or 99.9 %, respectively, of the NTPP was bound by the MIN without overloading the active sites. The corresponding values for the NIN, were 12, 15, and 18 %, respectively. Thus, imprinting significantly enhanced the binding of NTPP and the MIN prepared in the presence of NTPP efficiently and promptly adsorbed NTPP in organic media.

5.3.3 Reusability studies

Two important requirements of any sorbent material in addition to selectivity and sensitivity are stability and reusability. Studies were conducted to determine if the NTPP bound to the MIN could be desorbed/released, and whether the MIN could be reused in a new NTPP removal experiment. An MeOH:acetic acid (9:1, v/v) solvent mixture was used as eluent in the measurement of the percentage of the NTPP desorbed from the MIN and to evaluate the reusability of the MIN. The desorption ratio was found to be high: 99.3 %. In order to evaluate the reusability of the MIN, the adsorption–desorption cycle was repeated 11 times using the imprinted material.

Figure 5.3.3 shows that the imprinted fiber was stable for up to nine binding/regeneration cycles without observing any decrease in the removal efficiency for NTPP, and the amount of NTPP bound by the MIN declined in the tenth cycle. These results indicate that the NTPP-MIN could be used repeatedly nine times without incurring any significant loss in removal efficiency.
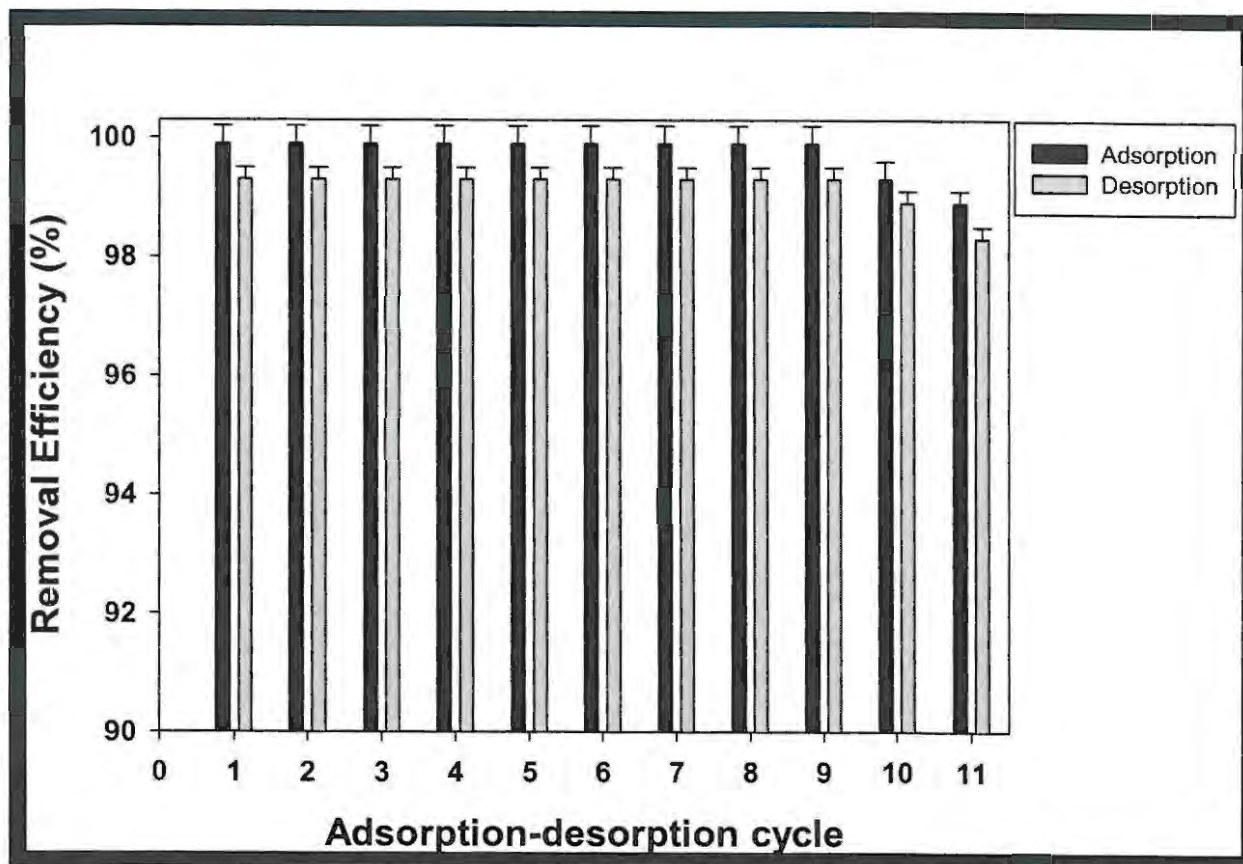
Figure 5.3.3: Amount of NTPP that was adsorbed by the MIN, and the amount subsequently desorbed, in each of eleven consecutive adsorption-desorption cycles

5.3.4 Method validation

The method developed for removing NTPP from organic media was validated by analysing a certified reference material (CRM) NIST, SRM 1634c, Trace Metals in Residual Fuel Oil. The concentration of NTPP in the CRM was found to be 17.53 $mgkg^{-1}$, which was significantly comparable with the certified value of 17.54 $mgkg^{-1}$.

The results showed that the amount of NTPP adsorbed from the CRM using the method developed was within the error of the value assigned to the certified reference material. It

may be concluded from the results presented that the PET/L-PEI-based molecularly imprinted nanofiber is well suited to the specific removal of NTPP from fuel oil.

5.3.5 Conclusion

The fabrication of molecularly imprinted fibers by an electrospinning technique is a very promising approach that could be used in fundamental studies of molecular imprinted sorbent materials, as it excludes the need to grind bulk polymeric materials, which leads to surfaces with nonspecific binding. In the studies conducted in the investigation, a chemical cross-linker was successfully incorporated into a PET/L-PEI solution in order to perform in situ cross-linking of imprinted nanofibers. In the process, three different imprinted fibers were obtained by varying the quantity of template molecule used during imprinting. The results obtained demonstrated that the quantity of template and the type of spinnable polymer used are of considerable importance to the success of the imprinted nanofibers. The results of this study showed that imprinted PET/L-PEI fibers effectively and reliably adsorb NTPP and further showed much more selective adsorption than the corresponding non-imprinted fibers. In addition, the PET/L-PEI nanofibers exhibited excellent reusability. These observations suggest that the developed technique provides a new path for the rational design of imprinted fibers intended for analytical as well as process applications.

Furthermore, in most of the accounts of molecular imprinting strategies, a single template molecule is used to create the specific binding site of the imprinted nanofibers. However, imprinting process does not have to be limited to a single template, thus several compounds can be imprinted simultaneously.

5.4 Multiply templated cross-linked molecularly imprinted electrospun nanofibers

5.4.1 Solution characteristics

The nickel vanadyl PET/L-PEI solutions in pure TFA were prepared at various concentrations ranging from 14 % (w/v) to 30 % (w/v). Prior to electrospinning the shear viscosity, electrical conductivity, and surface tension of the polymer solutions were measured (see Table 5.4.1). The increase in solution concentration could adversely affect the cohesiveness of the liquid/air interface, thus leading to the reduction in the surface tension of the solution. On the other hand, both the viscosity and electrical conductivity of the solutions were found to increase. The increase in the solution viscosity could be explained by the fact that the increased polymer mass fraction in the solution led to the increase of the entangled actions of the polymer molecule chains, which facilitated the formation of the electrospun nanofibers. The increase in the solution electrical conductivity with increasing solution concentration could be due to charged species alternating between conducting polymer chains resulting from the dissolution of PET/L-PEI in the acidic condition of the solutions [185].

**Table 5.4.1: Electrical conductivity, viscosity, surface tension and fiber formation of PET/L-PEI in TFA**

Solution concentration (% w/v)	Electrical conductivity ($\mu S.cm^{-1}$)	Viscosity (cP)	Surface tension ($mN.m^{-1}$)	Fiber formation
14	180.6	385	74.90	Beads
16	191.2	513	74.38	Fused beads
18	230.4	621	73.85	Beads
20	241.3	1207	69.63	Fiber and beads
22	245.2	1475	68.58	Fiber and beads
24	304.2	1699	66.47	Fiber and beads
26	315.4	2800	64.36	Fused smooth fiber
28	332.2	3300	62.94	Fused smooth fiber
30	594.0	4000	61.19	Smooth fiber

5.4.2 Effects of a single and mixed-solvent system on the general spinnability characteristics of nanofibers

PET/L-PEI dissolved easily in TFA and formed a clear homogenous solution at room temperature without any precipitation and air bubbles, while other liquids such as DMSO, DCM and PEN did not.

The SEM images of electrospun nanofibers with pure TFA are shown in Figure 5.4.2.1. For solution concentration less than 18 %, droplet spray occurred with a continuous jet of polymer, i.e., spinning was not formed. The jet from low viscosity solutions breaks up into droplets due to the lower mass of polymer and lower entanglement density than that needed to form a stable jet. With solution concentration between 20 and 24 % w/v, the presence of beads was observed. However, the beads completely disappeared and the formation of finer and more uniform electrospun fibers were observed as the concentration

of the solution was increased to 26, 28 and 30 % w/v. It is believed that the combination of

the relatively high viscosity of the solution and low dielectric constant of the solvent (8.55)
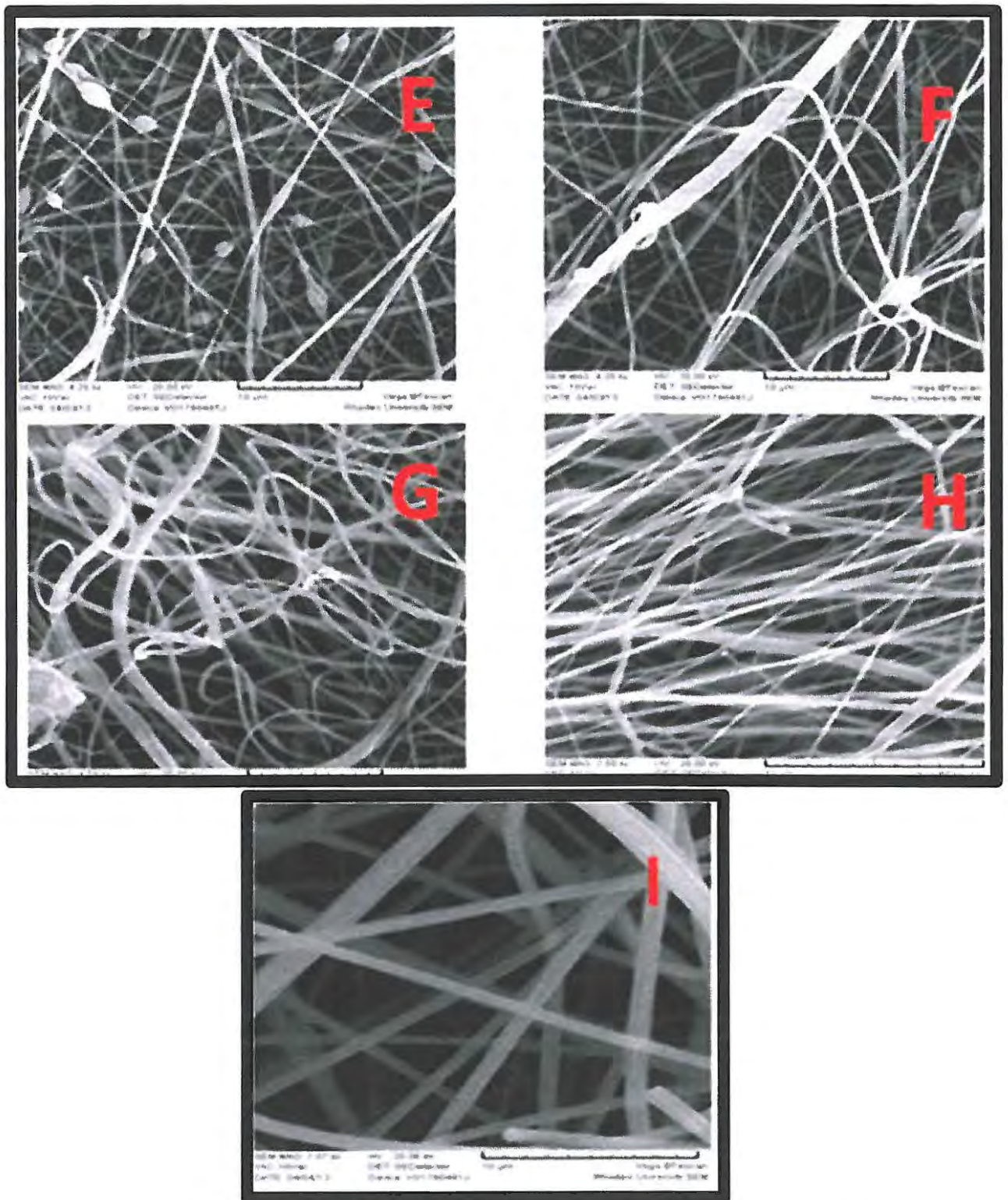
improved the morphology of the fiber.
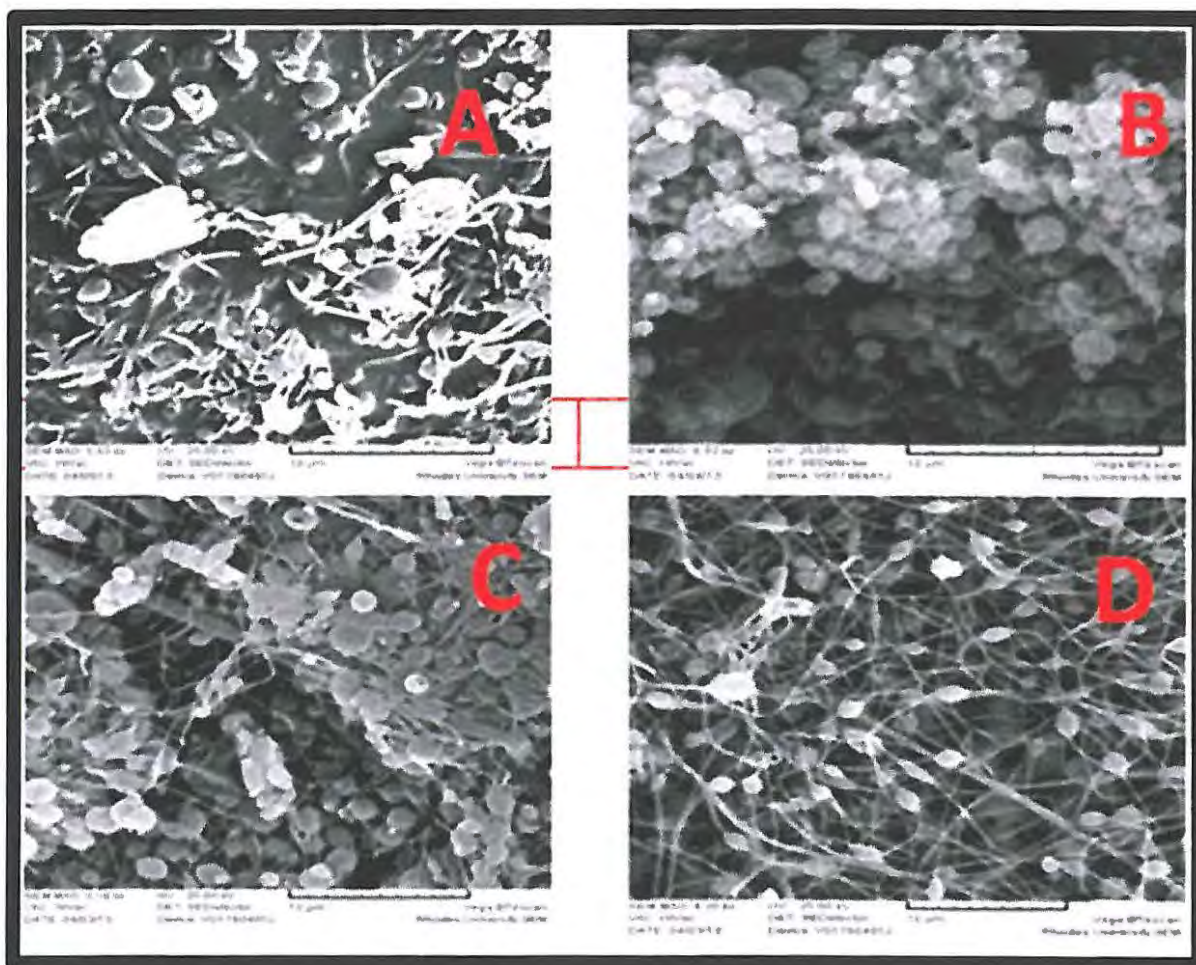
Figure 5.4.2.1: SEM images (scale bar = 10 μm) showing the morphology of fibers electrospun from PET/L-PEI solutions in TFA, at concentration of (A) 14, (B) 16, (C) 18, (D) 20, (E) 22, (F) 24, (G) 26, (H) 28, and (I) 30 % w/v. (voltage of 15 kV and at a constant spinning distance of 13 cm).

111

Mixed-Solvent Systems

Based on the results obtained on the single solvent system, 22 % w/v of the PET/L-PEI solution was chosen to further investigate the effect of the mixed-solvent systems because the viscosity of the solution at the particular concentration in TFA was high enough to allow the formation of fibers with less beads. Another important reason for choosing a 22 % concentration was to evaluate if the addition of the second solvent would be able to totally suppress the formation of beads

Trifluoroacetic acid and Dimethyl sulphoxide

The morphology of the as-prepared fibers from the PET/L-PEI solutions in mixed solvents of TFA and DMSO are shown in Figure 5.4.2.2. The DMSO was mixed with TFA to produce the mixed solvent at the compositional ratios of 95:5, 93:7, 90:10, and 80:20 v/v (TFA/DMSO), respectively. Judging from the high dielectric constant value of the DMSO solvent (46.7), the PET/L-PEI solutions in TFA/DMSO should have been readily spinnable. However, it was not the case, as the solutions were not spinnable in every ratio prepared. It was observed that, upon spinning, the solutions jetted out rather easily, but the ejected streams of the solutions did not form into fibers. The most likely explanation might be due to the extremely high boiling point of DMSO (189 °C) that caused the ejected streams to remain in the liquid form after being deposited on a collective target.

Figure 5.4.2.2: SEM images (scale bar = 10 μm) showing the morphology of fibers electrospun from 22 % PET/L-PEI solutions in a solvent mixture between TFA and DMSO (A) 95:5, (B) 93:7, (C) 90:10, and (D) 80:20. (voltage of 15 kV and at a constant spinning distance of 13 cm).

Trifluoroacetic acid and Dichloromethane

The morphology of the as-prepared fibers from the PET/L-PEI solutions in mixed solvents of TFA and DCM are shown in Figure 5.4.2.3. The DCM was mixed with TFA to produce the mixed solvent at the compositional ratios of 95:5, 93:7, 90:10, and 80:20 v/v (TFA/DCM), respectively. At 95:5 ratio, a large amount of beaded fiber was obtained. Interestingly, the increase in the quantity of DCM in the solvent mixture increased the thinning of the jet and fiber formed appeared to be smaller than those from the solution in pure TFA.
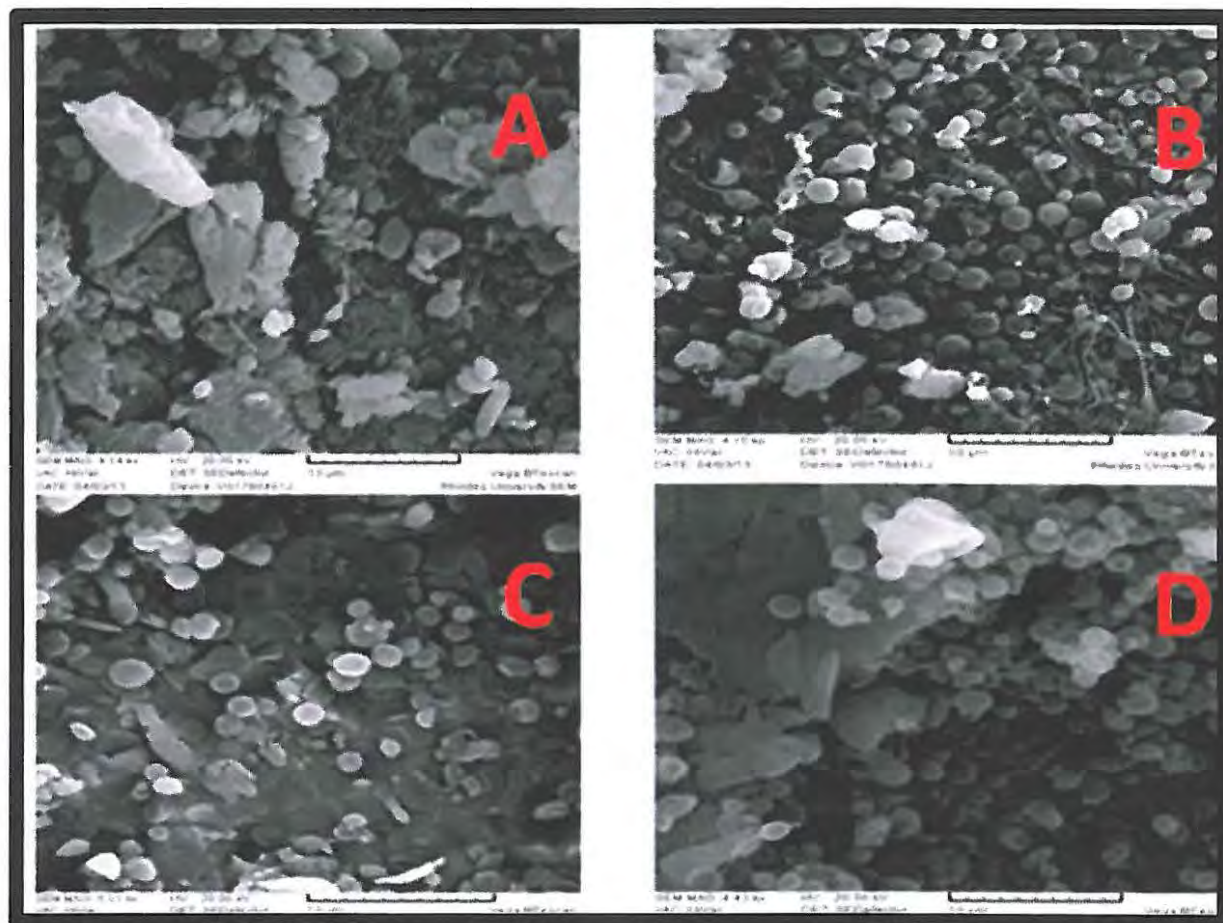

Figure 5.4.2.3: SEM images (scale bar = 10 μm) showing the morphology of fibers electrospun from 22 % PET/L-PEI solutions in a solvent mixture between TFA and DCM (A) 95:5, (B) 93:7, (C) 90:10, and (D) 80:20. (voltage of 15 kV and at a constant spinning distance of 13 cm).

Trifluoroocetic acid and Pentane

The morphology of the as-prepared fibers from the PET/L-PEI solutions in mixed solvents of TFA and PEN are in Figure 5.4.2.4. The PEN was mixed with TFA to produce the mixed solvent at the compositional ratios of 95:5, 93:7, 90:10, and 80:20 v/v (TFA/PEN), respectively. In comparison with PET/L-PEI solutions in TFA, TFA/DMSO, and TFA/DCM, the electrospun PET/L-PEI nanofibers using TFA/PEN as mixed solvent were continuous and smooth without any beads or droplets on the surface, indicating excellent electrospinnability of the PET/L-PEI solutions TFA/PEN mixed solvent. It could be attributed to the low boiling point (36.1) and low surface tension (15.48) of PEN solvent.
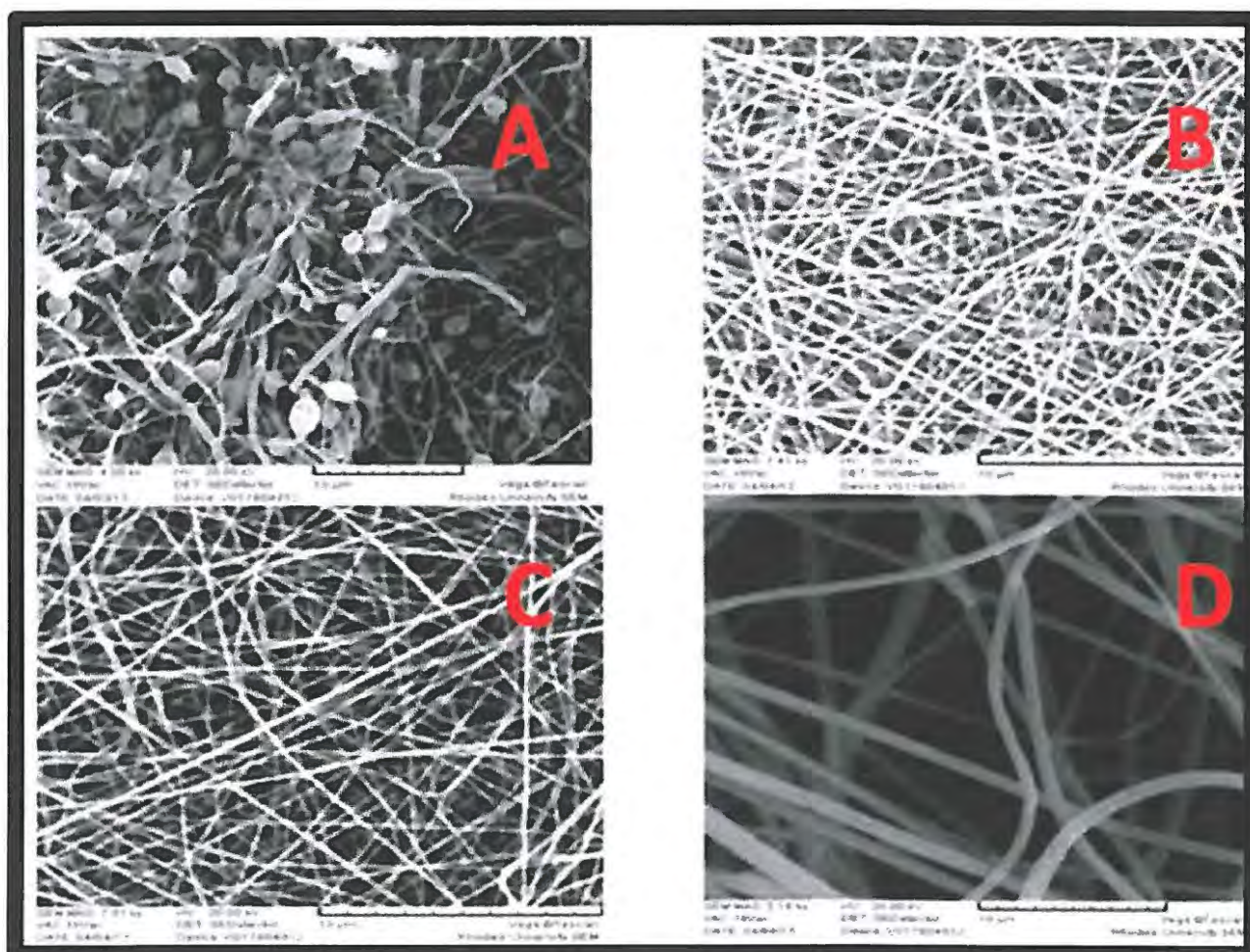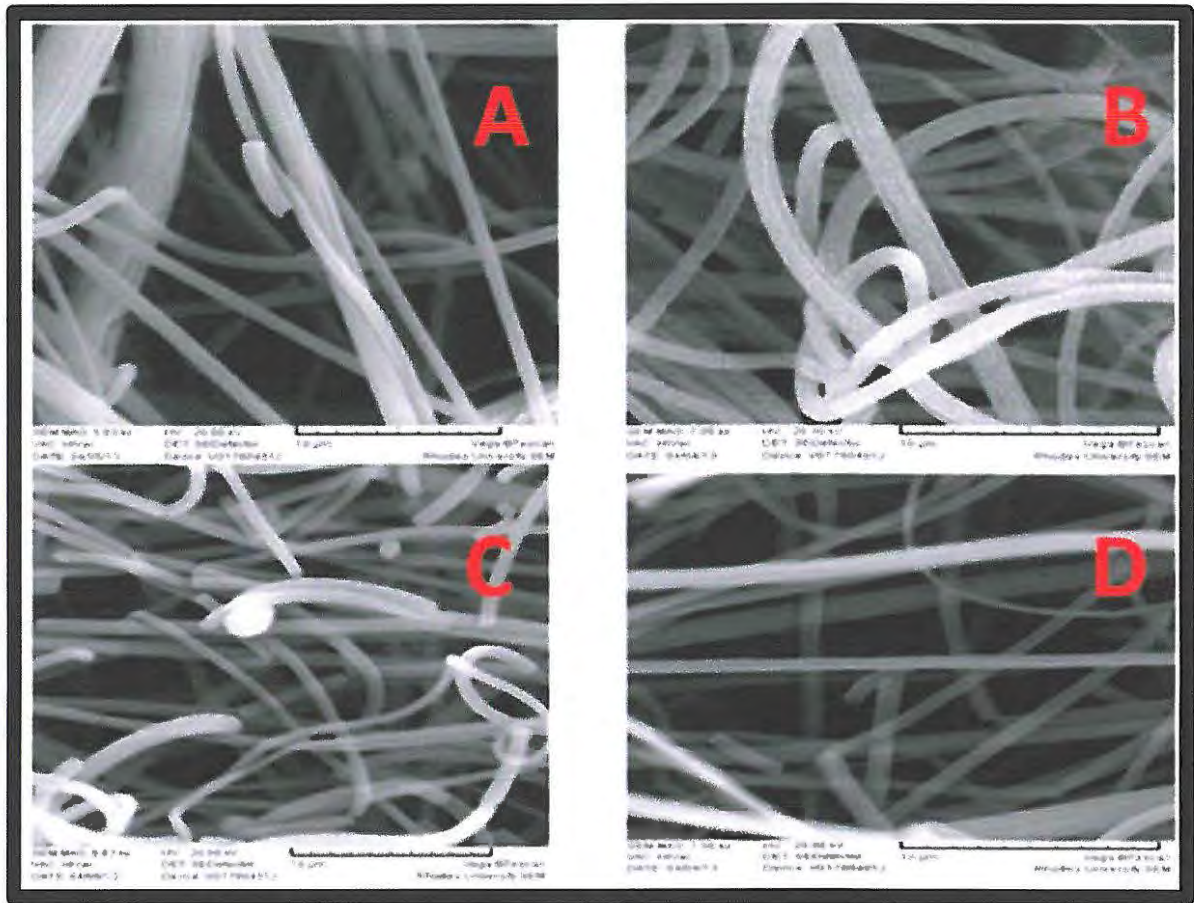
Figure 5.4.2.4: SEM images (scale bar = 10 μm) showing the morphology of fibers electrospun from 22 % PET/L-PEI solutions in a solvent mixture between TFA and PEN (A) 95:5, (B) 93:7, (C) 90:10, and (D) 80:20. (voltage of 15 kV and at a constant spinning distance of 13 cm).

5.4.3 Characterization of nanofibers

In order to obtain more structural information and understand the adsorption mechanism of the NVMIN, an energy dispersive X-ray spectrometer (EDS) was used to investigate the elemental composition of the imprinted fibers as shown in Figure 5.4.3.1. The EDS detects X-rays from the sample excited by the highly focused, high-energy primary electron beam penetrating into the sample.
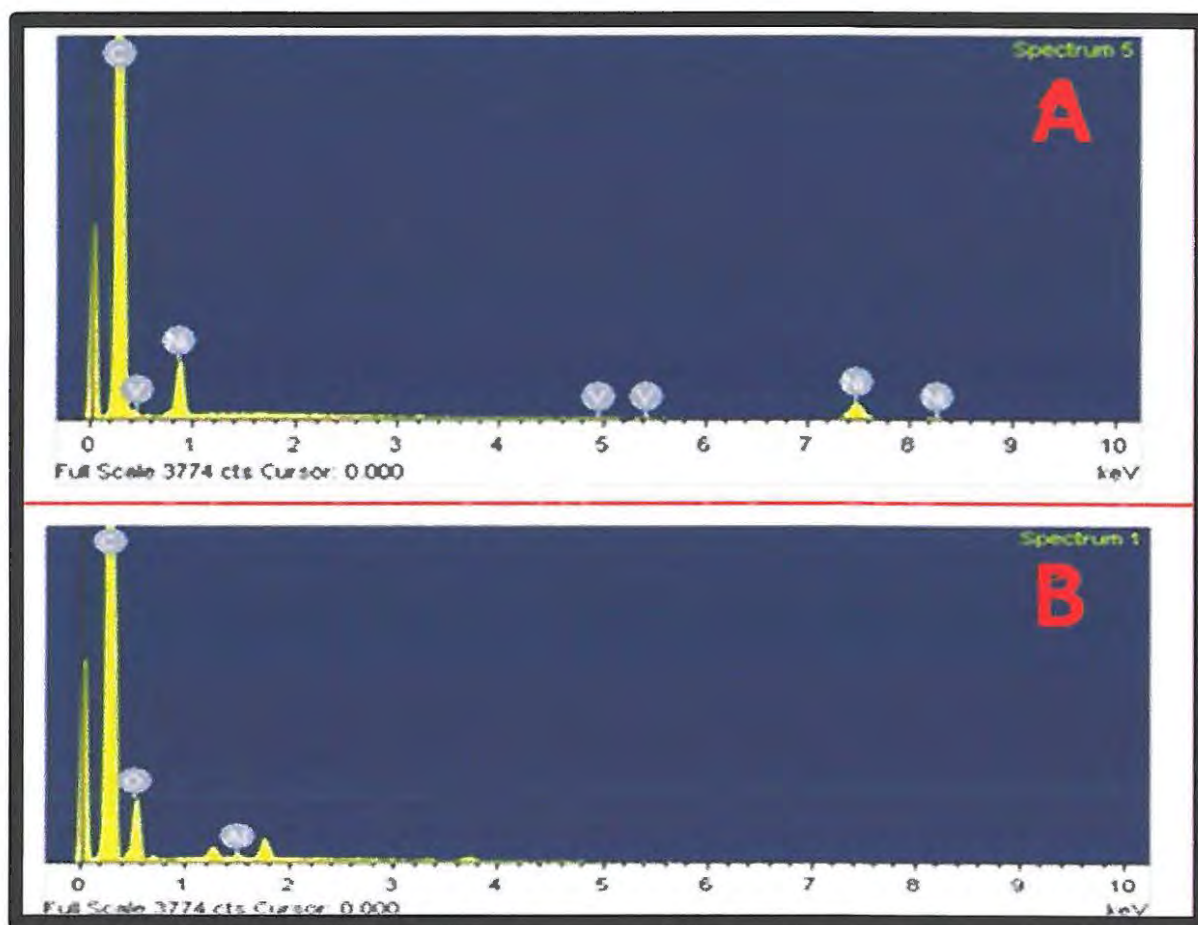
Figure 5.4.3.1: SEM-EDX spectra of imprinted fiber (A) NVMIN (B) NV removed-MIN

Comparing EDS images of NVMIN and nickel vanadyl removed-MIN confirmed that signals caused by the presence of VTPP and NTPP were clearly observed for NVMIN-containing fiber but not for nickel vanadyl removed-MIN which implies complete removal of the templates from the imprinted fiber and this is in corroboration with FT-IR study.
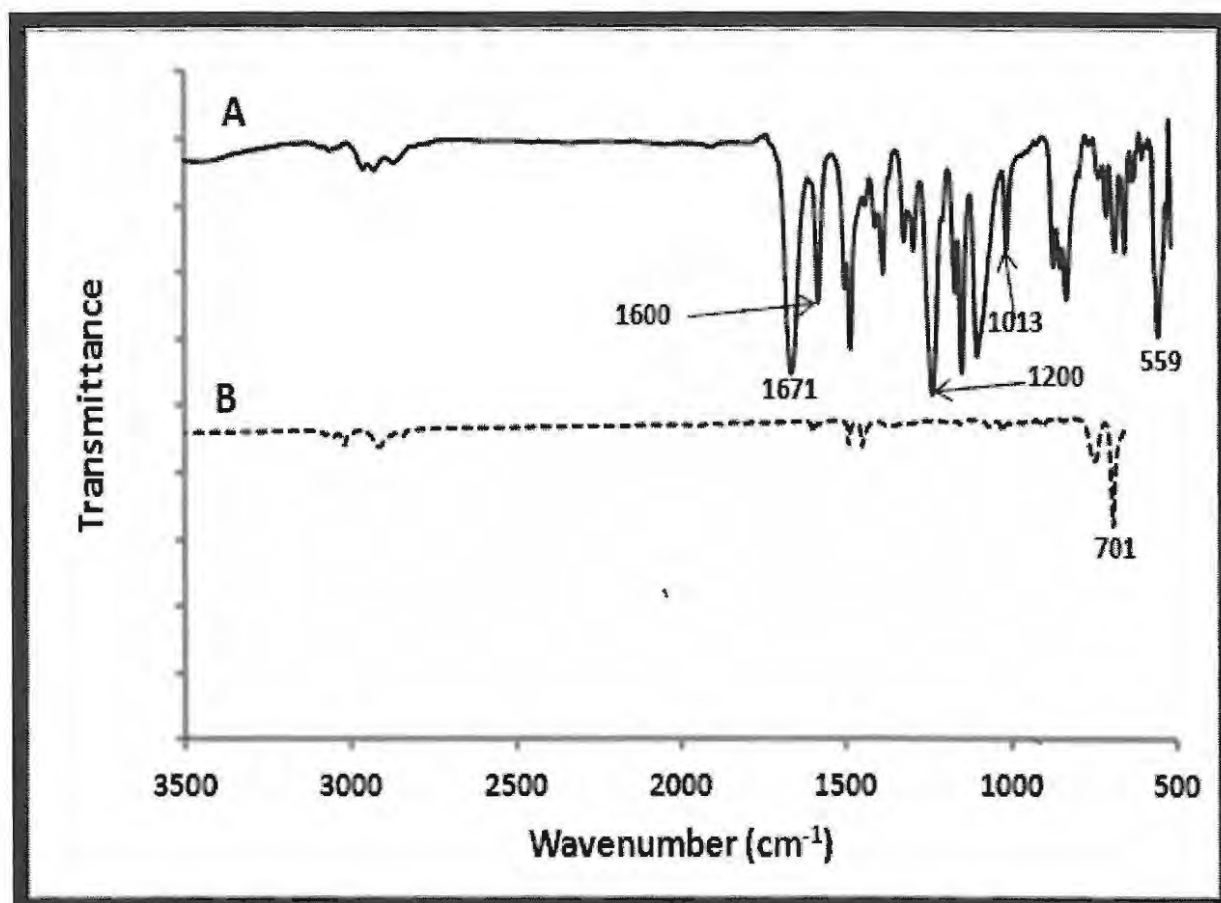
Figure 5.4.3.2: FT-IR spectra of imprinted fiber (A) NVMIN (B) NV removed-MIN

FTIR spectra of both NVMIN and NV removed-MIN are shown in Figure 5.4.3.2. FTIR can be used to qualitatively identify functional groups that are present in fiber structures. The NVMIN imprinted fiber spectrum showed absorption bands at 559, 1013, 1200, 1600 and 1671 cm^{-1} that were assigned to Ni–N, V=O, C–N, conjugated C=N, and C=C systems,

respectively, and indicated the success of the imprinting process. The spectrum for the NV removed-MIN showed a distinct characteristic peak at 701 cm^{-1} which could be attributed to C-H vibration and the peaks of the NTPP and VTPP molecules at 559, 1013 and 1200 cm^{-1} disappeared after excessive washing. The observed spectral absorptions implied that all template molecules had been completely removed.

5.4.4 Effect of extraction solvent on adsorption

There are several variables, such as the type of monomer or the nature of the cross-linker and the choice of solvent that affect the adsorption efficacy in terms of capacity, affinity and selectivity for the target analytes. Acetonitrile, ethyl acetate, dichloromethane and chloroform were selected as solvents to optimize extraction by using 50 mgL^{-1} NTPP standard solution.

As shown in Figure 5.4.4, the effect of the solvent nature on the adsorption is obvious. NTPP adsorbs strongly in chloroform and dichloromethane because both solvents contained more oxidizing species with chloroform being the best. However, in ethyl acetate the strength decreased and in acetonitrile the adsorption strength was the weakest. In addition, the highest extraction percentage achieved in chloroform could be attributed to its low dipole moment (μ=1.04), compared to other solvents which have higher dipole moments (dichloromethane μ=1.60, ethyl acetate μ=1.78, and acetonitrile μ=3.92).

119
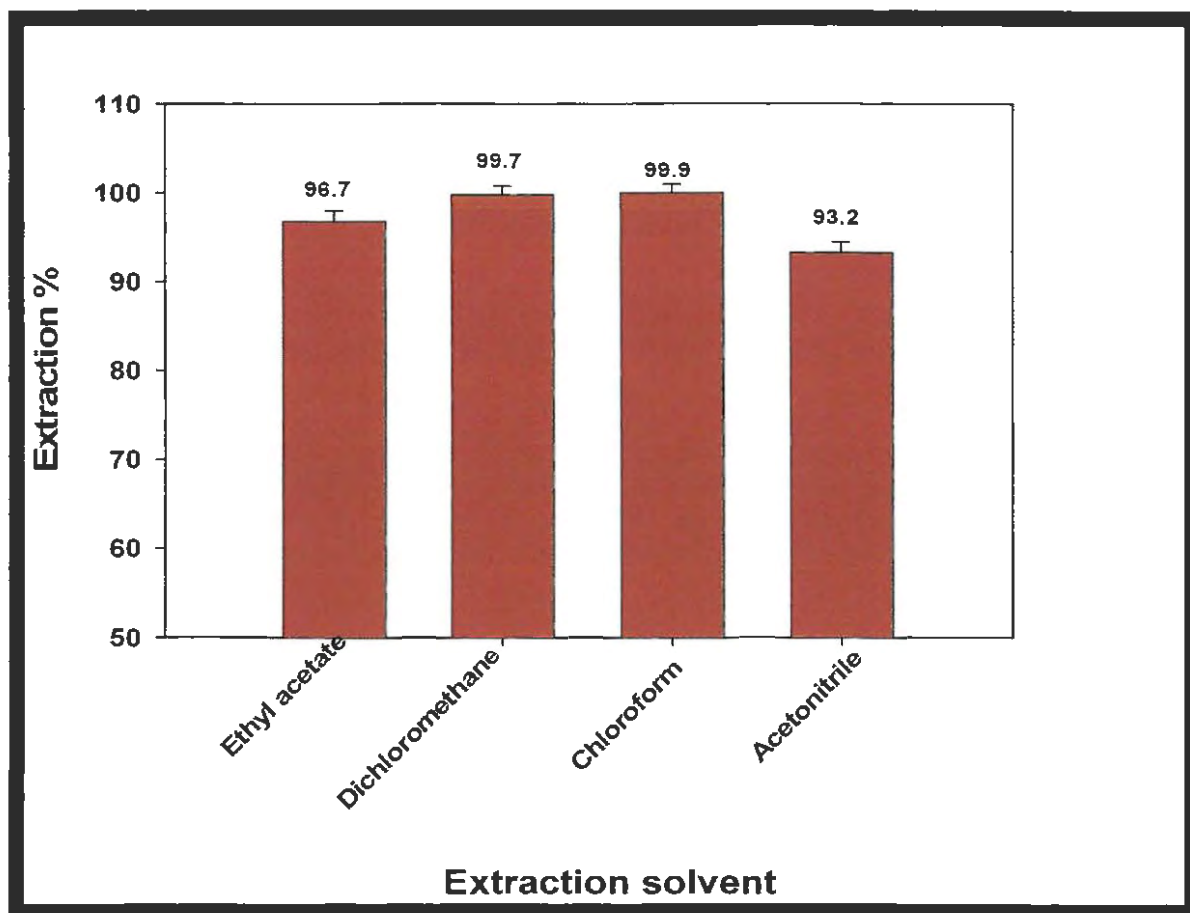
Figure 5.4.4: Percentage of NTPP adsorption from extraction solvents

5.4.5 Adsorption of NTPP onto imprinted nanofibers

The successful application of imprinted fibers necessitates the availability of materials with appropriate physical properties and selectivity. NTPP binding was studied in an organic environment at low concentration level. Figure 5.4.5 showed that the binding capacity was varied from 99.3 to 99.9 % at a concentration range from 10 to 50 mgL^{-1}. The result

illustrated that the NVMIN showed higher affinity (99 % higher) for NTPP than NIN which indicated that the NVMIN contains a lot of specific binding sites.
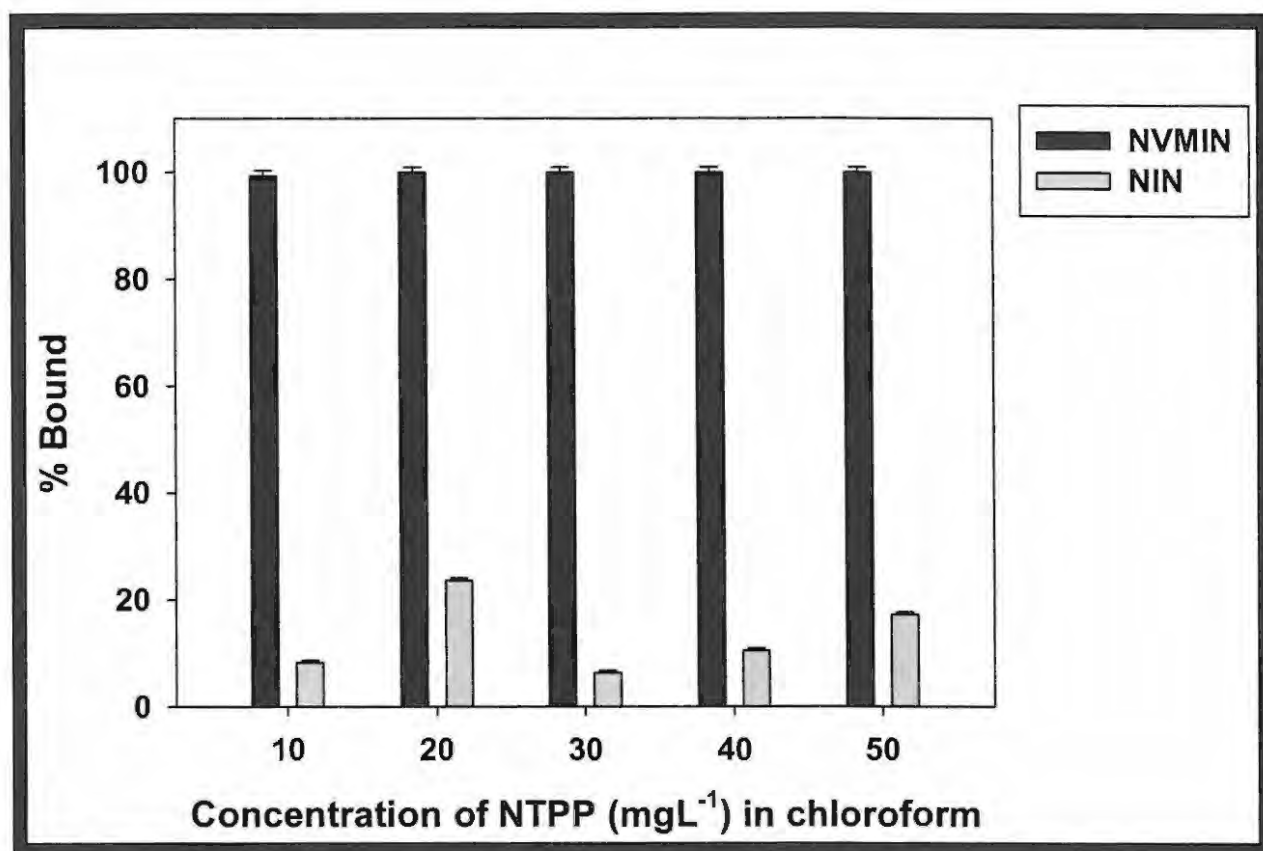
Figure 5.4.5: Percentage of rebinding capacity of NVMIN and NIN at different NTPP concentrations

5.4.6 Adsorption selectivity

Competitive adsorption experiments on NVMIN and NIN were conducted in chloroform solution containing NTPP and VTPP, respectively. As shown in Figure 5.4.6, the adsorption capacities of NTPP and VTPP to the NVMIN were both 33.3 mgg^{-1}, whereas those to the NIN were about 0.8 and 0.8 mgg^{-1}, respectively. Obviously, the adsorption capacities of NTPP

and VTPP on the NVMIN were higher than those on the NIN. The recognition coefficients (α) of NTPP and VTPP were both 41.6 , according to Eq. 4.4. It can be demonstrated that NVMIN synthesized for both NTPP and VTPP had the same selectivity specialism for these molecules.
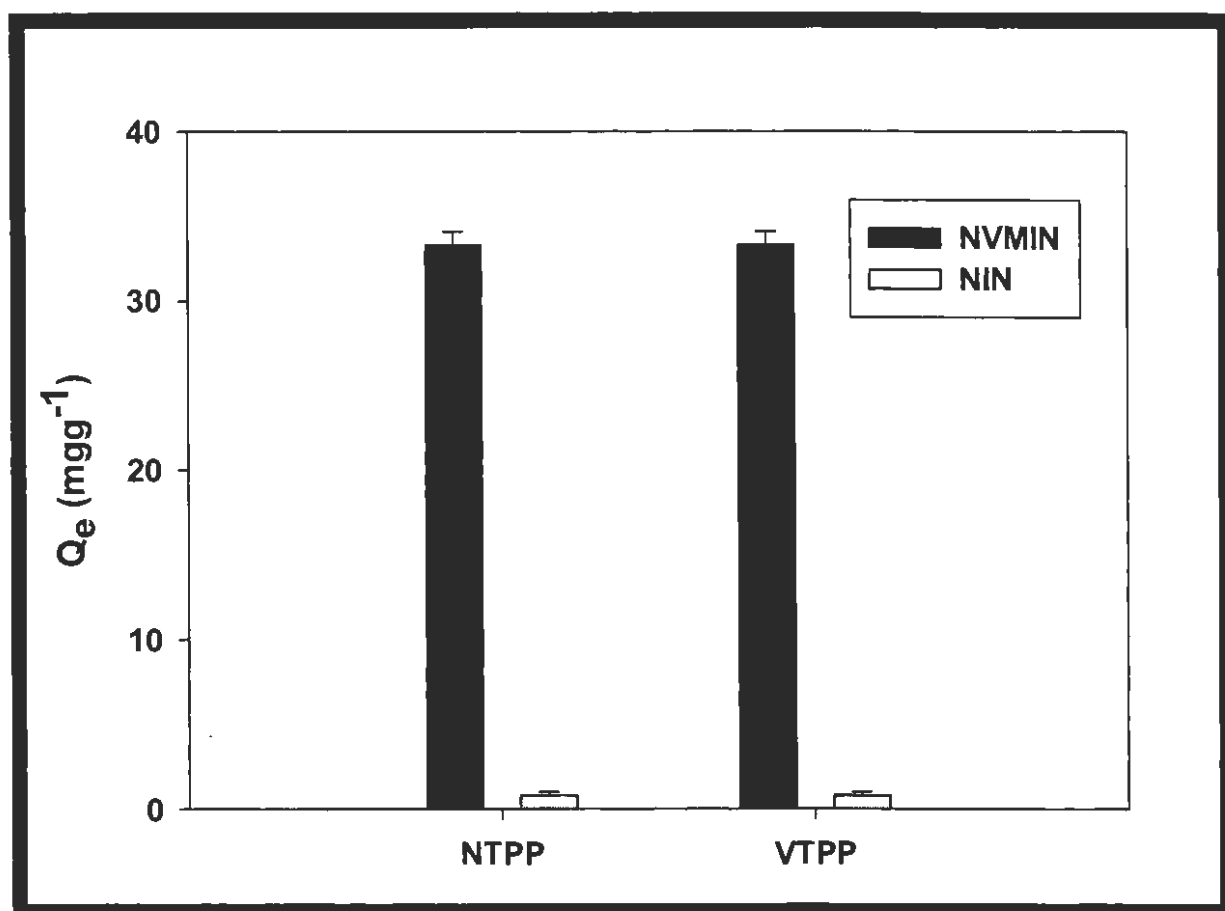
Figure 5.4.6: Competitive adsorption of NTPP and VTPP onto NVMIN and NIN

5.4.7 Conclusion

The feasibility of preparing NVMINs using NTPP and VTPP as the mixed-templates for the recognition and selective removal of a group of metalloporphyrins from organic media was successfully demonstrated. The sorbent exhibited outstanding selectivity and adsorption ability for metalloporphyrin group. Solvent effects and their properties on electro-spinnability of the polymer solutions were investigated. The spinnable concentration of the polymers in the single solvent system was around 20 % and solution concentrations higher than 24 % favoured the formation of nanofibers without any beads.

Among the three modifiers, DCM and PEN helped improve the electrospinnability of the polymer solution with PEN being the best modifier, specifically, at all the solvent mixture ratios the nanofibers were continuous and smooth without any beads or droplets on the surface of the electrospun nanofiber. Adsorption was found to be strongly dependent on the extraction solvent.

It could be concluded that imprinting mixtures of templates simultaneously is a plausible approach for producing multi-analyte molecular recognition in complicated samples.

6

Concluding remarks

6 Concluding remarks

The studies conducted in this thesis dealt with development of a new method for selective clean-up of metalloporphyrins from organic media through the application of molecular imprinting and electrospinning technologies. These technologies have been known for years and have vast applications in water and wastewater treatment, as well as many other different industries. However, to my knowledge they have never been applied to remove heavy metal compounds from fuel oil. The method developed overcomes disadvantages of other technologies currently available, with regard to simplicity, selectivity, and affordability.

Based on the studies reported in this work, MIP materials particularly in the form of imprinted electrospun nanofibers were shown to be potential competitors to the traditional particle based solid phase extraction sorbents for selectivity. It has also been shown that a chemical cross-linker could be successfully incorporated into an imprinted nanofibers. In all cases, both the MIP and imprinted nanofibers sorbents exhibited outstanding adsorption ability for metalloporphyrin group. The imprinted nanofibers could be regenerated and re-used up to nine times without incurring any significant loss in removal efficiency. Regarding the extraction of the NTPP, the choice of solvent had a crucial impact on adsorption. It was demonstrated that the quantity of template and the type of spinnable polymer used are of considerable importance to the success of the imprinted nanofibers.

The performance of the multiply templated imprinted nanofibers to selectively remove both VTPP and NTPP was found to be novel and remarkable. It can be concluded that electrospinning-imprinting method is a viable approach based on its simple operation and high efficiency.

Furthermore, it is recommended that the research results reported in this thesis be used as ground information for subsequent research in which styrene based imprinted sorbent will be employed in the pilot/full-scale applications.

This thesis has established that the knowledge and the success of the reactive electrospinning technology to produce an imprinted nanofibers provides a new and versatile opportunity for the process and application of functional nanomaterials.

References

[1] A.S. Pepper, P.J. Corvi, Mar. Pet. Geol. 12 (1995) 417–452.

[2] L.C. Price, J.L. Clayton, Geochim Cosmochim Acta 56 (1992) 1213–1222.

[3] L.F. Baker, J.J.H. Ciborowski, M.D. Mackinnon, Sci. Total Environ. 414 (2012) 177–186.

[4] C.R. Evans, M.A. Rogers, N.J.I. Baily, Chem. Geol. 8 (1971) 147–170.

[5] A. Narve, K. Harald, E.J. Einar, S. Johan, Energy Fuels 16 (2002) 1287–1295.

[6] J.G. Speight (4Ed.) (2007) The Chemistry and Technology of Petroleum. CRC Press, Boca Raton.

[7] M.F. Ali, A. Bukhari, M. Saleem, Ind. Eng. Chem. 22 (1983) 691–694.

[8] W.D. Walls, Energy Policy 38 (2010) 2110–2115.

[9] J.G. Speight (Ed.) (2001) Handbook of Petroleum Analysis. John Wiley and Sons Inc, New Jersey.

[10] S. Matar (Ed.) (2000) Chemistry of Petrochemical Process. Gulf Published Company, Houston.

[11] R.M.S. Souza, A.L.S. Meliande, C.L.P. da Silveira, R.Q. Aucélio, Microchem Journal 82 (2006) 137–141.

[12] B. Skrbic, J. Novakovic, N. Miljevic, J. Environ. Sci. Health A 37 (2002) 7–16.

[13] T.F. Yen (Ed.) (1975) The Role of Trace Metals in Petroleum. Ann Arbor Science Publishers, Ann Arbor, Michigan.

[14] L. Zychlinski, J.Z. Byczkowski, A.P. Kulkarni, Arch Environ. Con. Tox. 20 (1991) 295–298.

[15] R.G. Cooper, Indian J. Occup. Environ. Med. 11 (2007) 97–102.

[16] M.F. Ali, S. Abbas, Fuel Processing Tech. 87 (2006) 573–584.

[17] N.A. Yong, Oil and Gas J. 30 (1931) 22–25.

[18] US Patent, 15, 506, (1856).

[19] US Patent, 176, 423, (1876).

[20] US Patent, 4, 522, 702, (1985).

[21] J.R. Maxwell, C.T. Pillinger, G. Eglinton, Chem. Soc. J. 25 (1971) 571–628.

[22] C. Ovalles, I. Rojas, S. Acevedo, G. Escobar, G. Jorge, L.B. Gutierrez, A. Rincón, B. Scharifker, Fuel Proc. Technol. 48 (1996) 159–172.

[23] J.M. Sugihara, T. Okada, J.F. Branthaven, J. Chem. Eng. Data 10 (1965) 190–194.

[24] W. Zhao, W. Xu, S. Zhong, Z. Zong, J. of China Univer. Of Mining and Technol. 18 (2008) S71–574.

[25] M. Ashtari, M. Bayat, M. Sattarin, Energy Fuels 25 (2011) 300–306.

[26] S.I. Anderson, E.H. Stenby, Fuel Sci. Technol. Int. 14 (1996) 261–287.

[27] J.S. Buckley, G.J. Hirasaki, Y. Liu, S. Von Drasek, J.X. Wang, B.S. Gill, Pet. Sci. Technol. 16 (1998) 251–285.

[28] S.A. Mousavi-Dehghani, M.R. Riazi, M. Vafaie Sefti, G.A. Mansoori, Pet. Sci. Eng. 42 (2003) 145–156.

[29] S. Ashoori, M. Jamialahmadi, H. Müller Steinhagen, K. Ahmadi, Iran J. Chem. Eng. 25 (2006) 41–47.

[30] S.L. Chen, S.S. Jia, Y.H. Luo, S.Q. Zhao, Fuel 73 (1994) 439–442.

[31] V.A. Adewusi, B. Ademodi, T. Oshinowo, Fuel Proc. Technol. 27 (1991) 21–34.

[32] C.W. Curtis, K.J. Tsai, J.A. Guin, Fuel Proc. Technol. 16 (1987) 71–87.

[33] M.S. Rana, V. Sámano, J. Ancheyta, J.A.I. Diaz, Fuel 86 (2007) 1216–1231.

[34] Japanese Patent, 54110206, (1979).

[35] A.L. Hines, R.N. Maddox (Ed.) (1985) Mass Transfer: Fundamental and Application. Upper Saddle River, New Jersey.

[36] M. Tymchyshn, PhD Thesis, Lakehead University (2008).

[37] US Patent, 0114569 A1, (2009).

[38] A.A. Adeyi, F. Aberuagba, Res. J. of Chem. Sci. 2 (2012) 14–20.

[39] H. Zhang, Y. Wang, X. Liu, J. Kong, C. Nie, Talanta 93 (2012) 172–181.

[40] P.S. Sharma, F. D'Souza, W. Kutner, Anal. Chem. 34 (2012) 59–77.

[41] K. Yoshimatsu, L. Ye, J. Lindberg, I.S. Chronakis, Biosens. and Bioelectr. 23 (2008) 1208–1215.

[42] C. He, Y. Long, J. Pan, K. Li, F. Liu, J. Biochem. Biophys. Methods 70 (2007) 133–150.

[43] N. Pérez-Moral, A.G. Mayes, Anal. Chim. Acta 504 (2004) 15–21.

[44] J. Haginaka, J. Chromatogr. B 866 (2008) 3–13.

[45] A.G. Mayes, K. Mosbach, Anal. Chem. 68 (1996) 3769–3774.

[46] A. Beltran, F. Borrull, P.G.A. Cormack, R.M. Marcé, Trends in Anal. Chem. 29 (2010) 1363–1375.

[47] L. Ye, O. Ramström, K. Mosbach, Anal. Chem. 70 (1998) 2789–2792.

[48] L. Ye, P.A.G. Cormack, K. Mosbach, Anal. Communi. 36 (1999) 35–38.

[49] L. Ye, P.A.G. Cormack, K. Mosbach, Anal. Chim. Acta 435 (2001) 187–196.

[50] C. Cacho, E. Turiel, C. Pérez-Conde, Talanta 78 (2009) 1029–1035.

[51] K. Hosoya, K. Yoshizako, Y. Shirasu, K. Kimata, T. Araki, N. Tanaka, J. Haginaka, J. Chromatogr. A 728 (1996) 139–147.

[52] S. Ashraf, A. Cluley, C. Mercado, A. Mueller, Water Sci. Technol. 64 (2011) 1325–1332.

[53] J.S. Ach, N. Jömann (Ed.) (2006) Size matters: Ethical and Social Challenges of Nanobiotechnology. LIT, Münster.

[54] S. Ramakrishna, K. Fujihara, W.E. Teo, T.C. Lim, Z. Ma (Ed.) (2005) An Introduction to Electrospinning and Nanofibers. World Scientific, Singapore.

[55] M. Delvaux, J. Duchet, P.Y. Stavaux, R. Legras, S. Demonstier-Champagne, Synth. Metals 113 (2000) 275–280.

[56] C.R. Martin, Science 266 (1994) 1961–1966.

[57] M. Steinhart, J.H. Wendoff, A. Greiner, R.B. Wehrspohn, K. Nielsch, U. Gosele, Science 296 (2002) 1997–2008.

[58] J.G. Park, S.H. Lee, B. Kim, Y.M. Park, Appl.Phys. Lett. 81 (2002) 4625–4633.

[59] US Patent, 1, 975, 504, (1934).

[60] J. Kayser, R.L. Shambaugh, Polym. Eng. Sci. 30 (1990) 1237–1251.

[61] US Patent, 5, 476, 616, (1995).

[62] J.G. McCulloch, Nonwoven J. 8 (1999) 139–149.

[63] R. Nayak, R. Padhye, I.L. Kyratzis, Y.B. Truong, L. Arnold, Text. Res. J 82 (2012) 129–147.

[64] D.H. Tan, C. Zhou, C.J. Ellison, S. Kumar, C.W. Macosko, F.S. Bates, J. Non-Newt. Fluid Mech. 165 (2010) 892–900.

[65] N. Fedorova, B. Pourdeyhimi, J. Appl. Polym. Sci. 104 (2007) 3434–3442.

[66] J.D. Hartgerink, E. Beniash, S.I. 5tupp, Science 294 (2001) 1684–1688.

[67] G. Liu, L. Qiao, A. Guo, Macromol. 29 (1996) 5508–5510.

[68] X. Yan, G. Lin, F. Liu, Angew. Chem. Int. Ed. 40 (2001) 3593–3596.

[69] H.E. Jeong, S.H. Lee, P. Kim, K.Y. Shuh, Nano Lett. 6 (2006) 1508–1513.

[70] X. Xing, Y. Wang, B. Li, Opt. Express 16 (2008) 10815–10822.

[71] P.X. Ma, R. Zhang, J. Biomed. Mater Res. 46 (1999) 60–72.

[72] V.J. Chen, L.A. Smith, P.X. Ma, Biomaterials 27 (2006) 3973–3979.

[73] K. Haupt, A.V. Linare, M. Bompart, B.T.S. Bui, Top Curr. Chem. 325 (2012) 1–28.

[74] B. Sellergren, M. Lepisto, K. Mosbach, J. Am. Chem. Soc. 117 (1988) 7105–7111.

[75] G. Wulff, S. Schauhoff, J. Org. Chem 56 (1991) 395–400.

[76] K.J. Shea, D.A. Spivak, B. Sellergren, J. Am. Chem. Soc. 115 (1993) 3368–3369.

[77] J. Matsui, Y. Miyoshi, O. Doblhoff-Dier, T. Takeuchi, Anal. Chem. 67 (1995) 4404–4408.

[78] J. Matsui, O. Doblhoff-Dier, T. Takeuchi, Chem. Lett. 6 (1995) 489–492.

[79] J. Matsui, Y. Miyoshi, R. Matsui, T. Takeuchi, Anal. Sci. 11 (1995) 1017–1019.

[80] G. Wulff, Angew. Chem. Int. Ed. Engl. 34 (1995) 1812–1832.

[81] K. Haupt, K. Mosbach, Treads in Biotechnol. 16 (1998) 468–475.

[82] B. Sellergren (Ed.) (2001) Molecularly Imprinted Polymer-Man-Made Mimic of Antibodies and Their Applications in Analytical Chemistry. Amsterdam Elsevier.

[83] M. Komiyama, T. Takeuchi, T. Mukawa, H. Asanuma (Ed.) (2003) Molecular Imprinting: From Fundamentals to Applications. Wiley-VCH Verlang GmbH & Co. KGaA, Weinheim.

[84] R.J. Umpleby, S.C. Baxter, A.M. Rampey, G.T. Rushton, Y. Chen, K.D. Shimizu, J. of Chromagr. B 804 (2004) 141–149.

[85] D.A. Spivak (Ed.) (2005) "Selectivity in Molecularly Imprinted Matrices" Molecularly Imprinted Materials: Science and Technology. Marcel Dekker, New York.

[86] G. Wulff, R. Grobeeinsler, W. Vesper, A. 5arhan, Makromol. Chem. 178 (1977) 2817–2825.

[87] G. Wulff, W. Vesper, R. Grobeeinsler, A. Sarhan, Makromol. Chem. 178 (1977) 2799–2816.

[88] G. Wulff, A. 5arhan, Angew. Chem. Int. Ed. Engl. 11 (1972) 341–343.

[89] C.J. Tan, H.G. Chua, K.H. Ker, Y.W. Tong, Anal. Chem. 80 (2008) 683–692.

[90] C.J. Tan, Y.W. Tong, Anal. Chem. 79 (2007) 299–306.

[91] A. Martin-Esteban, Trends in Anal. Chem. 45 (2013) 169–181.

[92] P.G.A. Cormack, A.Z. Elorza, J. of Chromatogr. B 804 (2004) 173–182.

[93] W.M. Mullett, M.F. Dirie, E.P.C. Lai, H. Guo, X. He, Anal. Chim. Acta 414 (2000) 123–131.

[94] C. Yu, K. Mosbach, J. Org. Chem. 62 (1997) 4025–4028.

[95] O. Ramström, L.I. Anderson, K. Mosbach, J. Org. Chem. 58 (1993) 7562–7570.

[96] G. Wulff, J. Vietmeier, H.G. Poll, Makromol. Chem. 188 (1987) 731–740.

[97] M. Sibrian-Vazquez, D.A. Spivak, J. Polym. Sci. A, Polym. Chem. 42 (2004) 3668–3675.

[98] W.M. Mullett, PhD Thesis, University of Ottawa (2000).

[99] B. Sellergren, K.J. Shea, J. Chromatogr. 635 (1993) 31–49.

[100] M. Randhawa, I. Gartner, C. Becker, J. Student, M. Chai, A. Mueller, J. Appl. Polym. Sci. 106 (2007) 3321–3326.

[101] M. Shamsipur, J. Fasihi, K. Ashtari, Anal. Chem. 79 (2007) 7116–7123.

[102] I.A. Nicholls, K. Adbo, H.S. Anderson, J. Ankarbo, J. Hedin-Dahlstrom, P. Jokela, J.G. Karlson, L. Olofsson, J. Rosengren, S. Shorvi, J. Svenson, S. Wikman, Anal. Chim. Acta 435 (2001) 9-15.

[103] M. Kempe, K. Mosbach, Anal. Lett. 24 (1991) 1137–1145.

[104] D.J. O'Shannessy, B. Ekberg, K. Mosbach, Anal. Biochem. 177 (1989) 144–149.

[105] B. Sellergren, M. Lepisto, K. Mosbach, J. Am. Chem. Soc. 110 (1988) 5853–5860.

[106] H.S. Andersson, I.A. Nicholls, Bioorg. Chem. 25 (1997) 203–211.

[107] S. Striegler, E. Tewes, Eur. J. Inorg. Chem. 15 (2002) 487–495.

[108] H. Guo, X. He, J. Anal. Chem. 368 (2000) 461–465.

[109] A. Molinelli, J. O'Mahony, K. Nolan, M.R. Smyth, M. Jakusch, B. Mizaikoff, Anal. Chem. 77 (2005) 5196–5204.

[110] D.J. Duffy, K. Das, S.L. Hsu, J. Penelle, V.M. Rotello, H.D. Stidham, J. Am. Chem. Soc. 124 (2002) 8290–8296.

[111] A. Katz, M.E. Davis, Macromol. 32 (1999) 4113–4121.

[112] F. Lanza, M. Ruther, A.J. Hall, C. Dauwe, B. Sellergren, Mater. Res. Soc. Symp. Proc. 723 (2002) 93–103.

[113] C. Lübke, M. Lübke, M.J. Whitcombe, E.N. Vulfson, Macromol. 33 (2000) 5098–5105.

[114] J. Svenson, J.G. Karlsson, I.A. Nicholls, J. Chromatogr. A 1024 (2004) 39–44.

[115] B. Sellergren, K.J. Shea, J. Chromatogr. 635 (1993) 31–49.

[116] D.A. Spivak, Advanc. Drug Deliv. 57 (2005) 1779–1794.

[117] F.W. Billmeyer (Jr) (Ed.) (2005) Polymer Science. John Wiley and Sons Inc. New York.

[118] M. Manzer, E. Trommsdroff (Ed.) (1977) Polymerization Processes. Wiley Interscience, New York.

[119] V.K. Sarin, S.B.H. Kent, R.B. Merrifield, J. Am. Chem. Soc. 102 (1980) 5463–5470.

[120] S.A. Piletsky, K. Karim, E.V. Piletska, C.J. Day, K.W. Freebairn, C. Legge, A.P.F. Turner, Analyst 126 (2001) 1826–1830.

[121] I. Chianella, M. Lotierzo, S.A. Piletsky, I.E. Tothill, B.N. Chen, K. Karim, A.P.F. Turner, Anal. Chem. 74 (2002) 1288–1293.

[122] L.Q. Wu, B.W. Sun, Y.Z. Li, W.B. Chang, Analyst 128 (2003) 944–949.

[123] L.Q. Wu, Y.Z. Li, J. Mol. Recognit. 17 (2004) 567–574.

[124] I. Chianella, K. Karim, E.V. Piletska, C. Preston, S.A. Piletsky, Anal. Chim. Acta 559 (2006) 73–78.

[125] Y. Li, C. Huang, J. Zheng, H. Qi, Talanta 103 (2013) 8–13.

[126] I.S. Chronakis, J. Mater. Proc. Technol. 167 (2005) 283–293.

[127] J.H. He, Polymer 45 (2004) 9067–9070.

[128] "On the 100th anniversary of the birth of I.V. Petrysnov-Sokolov". Izvestiya, Atomospheric and Oceanic Physics 43(2007) 395–412.

[129] S. Ramakrishna, K. Fujihara, W.E. Teo, T. Yong, Z. Ma, R. Ramaseshan, Materials today 9 (2006) 40–50.

[130] G.I. Taylor, Proc. Roy. Soc. A 313 (1969) 453–475.

[131] L. Rayleigh, Philos. Mag. 14 (1882) 184–186.

[132] J. Zeleny, Phys. Rev. 10 (1917) 1–6.

[133] Y.M. Shin, M.M. Hohman, M.P. Brenner, G.C. Rutledge, Polymer 42 (2001) 9955-9967.

[134] G. Taylor, Proceedings of the Royal society of London A: Mathematical, Physical and Engineering Sciences 313 (1969) 453-475.

[135] L. Larrondo, M.S.J. Manley, J. Polym. Sci. Polym. Phys. 19 (1981) 909–920.

[136] L. Larrondo, M.S.J. Manley, J. Polym. Sci. Polym. Phys. 19 (1981) 921–932.

[137] L. Larrondo, M.S.J. Manley, J. Polym. Sci. Polym. Phys. 19 (1981) 933–40.

[138] A.L Yarin, S. Koombhongse, D.H. Reneker, J. Appl. Phys. 90 (2001) 4836–4840.

[139] J.M. Deitzel, C. Krauthauser, D. Harris, P.C. Kleinmeyer, J. Kleinmeyer (Ed.) (2006) ACS Symposium Series in Polymeric Nanofibers. Washington, DC.

[140] P.K. Baumgarten, J. Colloid Inter. Sci. 36 (1971) 1–9.

[141] J. Doshi, D.H. Reneker, J. Electrost. 35 (1995) 151–160.

[142] S. Koombhongse, W. Liu, D.H. Reneker, J. Polym. Sci. 39 (2001) 2598–2606.

[143] M.M. Hohman, M. Shin, G.C. Rutledge, M.O. Brenner, Phys. Fluids 13 (2001) 2221–2236.

[144] M.M. Hohman, M. Shin, G.C. Rutledge, M.O. Brenner, Phys. Fluids 13 (2001) 2201–2220.

[145] M. Shin, M.M. Hohman, M.P. Brenner, G.C. Rutledge, Polymer 42 (2001) 3303–3309.

[146] A.L Yarin, S. Koombhongse, D.H. Reneker, J. Appl. Phys. 89 (2001) 3018-3026.

[147] D.H. Reneker, W. Kataphinan, A. Theron, E. Zussman, A.L. Yarin, Polymer 43 (2002) 6785-6794.

[148] A. Greiner, J.H. Wendoeff, Angew. Chem. Int. Ed. Engl. 46 (2007) 5670-5703.

[149] Z. Sun, E. Zussman, A.L. Yarin, J.H. Wendorff, A. Greiner, Adv. Mater. 15 (2003) 1929-1932.

[150] Y. Zhang, Z.M. Huang, X. Xu, C.T. Lim, S. Ramakrishna, Chem. Mater. 16 (2004) 3406-3409.

[151] S. Kidoaki, I.K. Kwon, T. Matsuda, Biomater. 26 (2005) 37-46.

[152] M.J. Smith, M.J. McClure, S.A. Sell, C.P. Barnes, B.H. Walpoth, D.G. Simpson, G.L. Bowlin, Acta Biomater. 4 (2008) 58-66.

[153] X. Yang, J.D. Shah, H. Wang, Tissue Eng. Part A 15 (2009) 945-956.

[154] V. Thomas, X. Zhang, S.A. Catledge, Y.K. Vohra, Biomed. Mater. 2 (2007) 224-232.

[155] T.A. Telemesco, C. Ayres, G.L. Bowlin, G.E. Wnek, E.D. Boland, N. Cohan, C.M. Baumgarten, J. Mattews, D.G. Simpson, Acta Biomater. 1 (2005) 377-385.

[156] M.J. McClure, S.A. Sell, D.G. Simpson, B.H. Walpoth, G.L. Bowlin, Acta Biomater. 6 (2010) 2422-2433.

[157] I.C. Um, D. Fang, B.S. Hsiao, A. Okamoto, B. Chu, Biomacromol. 5 (2004) 1428-1436.

[158] Z.M. Huang, Y.Z. Zhang, M. Kotai, S. Ramakrishna, Compos. Sci. Technol. 63 (2003) 2223-2232.

[159] S.A. Sell, M.J. McClure, C.E. Ayres, D.G. Simpson, G.L. Bowlin, J. Biomater. Sci. Polym. Ed. 22 (2010) 1253-1273.

[160] B.S. Jha, R.J. Colello, J.R. Bowman, S.A. Sell, K.D. Lee, J.N. Bigbee, G.L. Bowlin, W.N. Chow, B.E. Mathern, D.G. Simpson, Acta Biomater. 7 (2010) 203-215.

[161] I.S. Chronakis, A. Jakob, B. Hagström, L. Ye, Langmuir 22 (2006a) 8960-8965.

[162] K. Yoshimatsu, L. Ye, J. Lindberg, I.S. Chronakis, Biosens. Bioelectr. 23 (2008) 1208–1215.

[163] P. Silvia, T.S.B. Bernadette, H. Karsten, A.G. Levi, Langmuir 27 (2011) 1547–1550.

[164] I.S. Chronakis, B. Milosevic, A. Frenot, L. Ye, Macromol. 39 (2006b) 357–361.

[165] C. Xie, Z. Zhang, D. Wang, G. Guan, D. Gao, J. Liu, Anal. Chem. 78 (2006) 8339–8346.

[166] C. Xie, B. Liu, Z. Wang, D. Gao, G. Guan, Z. Zhang, Anal. Chem. 80 (2008) 437–443.

[167] J.Y. Chang, W.J. Kim, Mater. Lett. 65 (2011) 1388–1391.

[168] J.G. Speight (Ed.) (1980) The Chemistry of Technology of Petroleum. Marcel Dekker, New York.

[169] R.J. Quann, R.A. Ware, C.W. Hung, J. Wei, Adv. Chem. Eng. 14 (1988) 95–259.

[170] K. Qian, A.S. Mennito, K.E. Edwards, D.T. Ferrugheli, Analyst 133 (2008) 1064–1071.

[171] C.D. Ford, S.A. Holmes, L.F. Thompson, D.R. Latham, Anal. Chem. 53 (1981) 831–836.

[172] V.P. Joshi, M.G. Kulkarni, R.A. Mashelker, J. Chromatogr. A 849 (1999) 319–330.

[173] 5.A. Piletsky, E.V. Piletska, A. Guerreiro, I. Chianella, K. Karim, A.P.F. Turner, Macromol. 37 (2004) 5018–5022.

[174] K.G. Yang, Z.B. Liu, M. Mao, X.H. Zhang, C.S. Zhao, Anal. Chim. Acta 546 (2005) 30–36.

[175] Y. Liu, F. Wang, T. Tan, M. Lei, Anal. Chim. Acta 581 (2007) 137–146.

[176] W. Dong, M. Yan, M. Zhang, Z. Liu, Y. Li, Anal. Chim. Acta. 542 (2005) 186–192.

[177] E. Yilmaz, K. Haupt, K. Mosbach, Angew. Chem. Int. Ed. Engl. 39 (2000) 2115–2118.

[178] M. Damirel, S.B. Sevin, R. Say, Y. Yazan, Pharm. Sci. 32 (2007) 147–157.

[179] D.K. Singh, S. Mishra, Desalination 257 (2010) 177–183.

[180] Y.C. Wong, Y.S. Szeto, W.H. Cheung, G. McKay, Langmuir 19 (2003) 7888–7894.

[181] Y.Q. Xia, T.Y. Guo, M.D. Song, B.H. Zhang, B.L. Zhang, React. Funct. Polym. 68 (2008) 63–69.

[182] J. Aburto, A. Mendez-Orozco, S.L. Borgne, Chem. Eng. Proc. 43 (2004) 1587–1595.

[183] R. Nirmala, D. Kalpana, J.W. Jeong, H.J. Oh, J.H. Lee, R. Navamathavan, Y.S. Lee, H.Y. Kim, Colloids Surf. A 384 (2011) 605–611.

[184] L.A. Tom, N.A. Schneck, C. Walter, J. Chromatogr. B 909 (2012) 61–64.

[185] J. Schmidt, R. Prignitz, D. Peschka, A. Münch, B. Wagner, E. Bänsch, W. Peukert, J. of Colloid and Interf. Sci. 386 (2012) 240–251.

[186] W. Gilbert (1600) Price D.J, editor. London: The Chiswick Press.